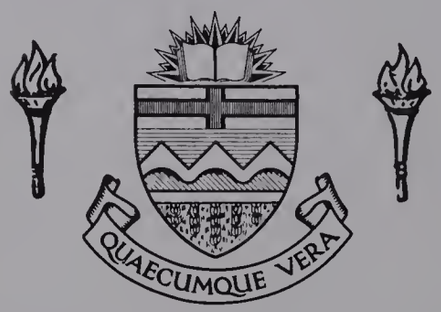

THE UNIVERSITY OF ALBERTA

RELEASE FORM

NAME OF AUTHOR MARK R. LOEWEN

TITLE OF THESIS A STUDY OF A VERTICAL PLANE JET-PLUME IN SHALLOW WATER

DEGREE FOR WHICH THESIS WAS PRESENTED MASTER OF SCIENCE

YEAR THIS DEGREE GRANTED FALL, 1984

DATED September 24, 1984

THE UNIVERSITY OF ALBERTA

A STUDY OF A VERTICAL PLANE JET-PLUME IN SHALLOW WATER

by

MARK R. LOEWEN

A THESIS

SUBMITTED TO THE FACULTY OF GRADUATE STUDIES AND RESEARCH

IN PARTIAL FULFILMENT OF THE REQUIREMENTS FOR THE DEGREE

OF MASTER OF SCIENCE

DEPARTMENT OF CIVIL ENGINEERING

EDMONTON, ALBERTA

FALL, 1984

THE UNIVERSITY OF ALBERTA

FACULTY OF GRADUATE STUDIES AND RESEARCH

The undersigned certify that they have read, and recommend to the Faculty of Graduate Studies and Research, for acceptance, a thesis entitled A STUDY OF A VERTICAL PLANE JET-PLUME IN SHALLOW WATER submitted by MARK R. LOEWEN in partial fulfilment of the requirements for the degree of MASTER OF SCIENCE.

ABSTRACT

The problem of a vertical plane jet-plume in shallow water was investigated experimentally and analytically. The four distinct regions of flow are the jet-plume region, surface impingement region, internal hydraulic jump region and the stratified counterflow region. Only the first three were studied in detail.

The experiments concentrated on the surface impingement and internal hydraulic jump regions. Velocity profiles and dye photographs were compiled for six runs. An additional 13 runs were done in which only dye photographs were taken. The velocity profiles and scale data were then analyzed and plotted.

The analytical portion of the study consisted of three parts. The first was the development of the plane jet-plume equations. The second part was a control volume type of analysis of the surface impingement region. This yielded an equation for the impingement depth of the surface layer. The third part was a momentum analysis of the internal hydraulic jump region. Two distinct equations were developed.

The experimental data was compared to the predictions of the theoretical equations. The variations of the velocity and length scales were compared to the case of a plane non-buoyant surface discharge.

ACKNOWLEDGEMENTS

The author would like to thank Dr. N. Rajaratnam for his enthusiastic support and guidance in this study. The assistance of the staff of the T. Blench Hydraulics Laboratory is greatly appreciated. Financial support for this study was provided by the Natural Sciences and Engineering Research Council by means of a Postgraduate Scholarship awarded to the author and a grant to Dr. N. Rajaratnam. This support is gratefully acknowledged.

The author would like to thank his wife, Cheryl, for her support, assistance and encouragement throughout his Master's program.

Table of Contents

List of Tables

List of Figures

List of Plates

List of Symbols

A	constant for a given jet-plume
A_1	constant of integration
b	velocity half-width
b_o	outlet half-width
$\overline{b}_u$	velocity width
$\overline{b}_c$	pollutant width
b_T	temperature half width
B_o	outlet buoyancy flux
c	tracer concentration at a point
c_m	maximum value of c at a cross-section
F_1	densimetric Froude number at section 1
F_o	outlet densimetric Froude number
g	acceleration due to gravity
h	depth of lower layer before the jump
h'	depth of lower layer after the jump
h_L	head loss in the surface impingement region
H	total depth of flow

I_i	constant of integration
K	ratio of the spreading rates
K_2	velocity spreading rate coefficient
K_L	loss coefficient
P	mean pressure at a point
P_o	pressure at point B
P_w	wall pressure
P_s	stagnation pressure
q_1	layer 1 specific discharge
q_2	layer 2 specific discharge
q_o	outlet specific discharge
$\bar{q}_i$	dimensionless specific discharge
r	density ratio
Ri_o	outlet Richardson number
$\bar{S}$	scale factor
S	dilution ratio
s	dimensionless density difference
$\bar{T}$	period of pulses

ΔT	temperature difference
u	mean velocity in x direction
u_m	maximum value of u at a cross-section
u_{mo}	maximum value of u at x=10cm
u_1	mean velocity in layer 1
u_2	mean velocity in layer 2
U_o	oulet velocity
v	mean velocity in the y direction
v_e	entrainment velocity
V_2	mean velocity at section 2
x	longitudinal coordinate
y	lateral coordinate
y_1	supercritical upstream depth
y_2	conjugate subcritical depth
y_3	lower layer upstream depth
y_4	lower layer downstream depth
Δy	height of surface disturbance
Δy_m	height of the surface disturbance at the centerline

u', v'	fluctuating components of velocity
a	dimensionless depth
a_e	entrainment coefficient
a_1 , a_2	constants of integration
β	momentum coefficient
β_1	momentum coefficient for lower layer
β_2	momentum coefficient for the upper layer
ϵ_x	turbulent diffusion coefficient in x direction
ϵ_y	turbulent diffusion coefficient in y direction
η	dimensionless y coordinate
ν	kinematic viscosity
ρ	mass density at a point
ρ_a	mass density of ambient fluid
$\Delta\rho_o$	mass density difference at outlet
$\Delta\rho_m$	maximum value of density difference at a cross-section
τ	turbulent shear stress
ψ	dimensionless lower layer depth

I. INTRODUCTION

A. GENERAL

The case of the vertical jet-plume in shallow water is a complex problem in the field of fluid mechanics. There have been several studies of this particular flow configuration but few conclusive results have been obtained. This is due to the complicated interactions and couplings of the different regions of flow and because of the difficulty in establishing the far field boundary conditions. This study explores both experimentally and analytically the behavior of a vertical plane jet-plume in shallow water.

B. PRACTICAL SIGNIFICANCE

The study of a jet-plume impinging on a free surface has practical application to several engineering problems. One application is to the discharge of cooling water from electric generation plants. A convenient method of disposing of the cooling water is to discharge it through a pipe into the ocean. The pipe is constructed out from the shore along the bed and, when a suitable depth is reached, the cooling water is discharged through ports in the top or side of the pipe. The individual jet-plumes merge to form a plane jet-plume which impinges on the free surface and then spreads out along the surface.

Another practical application is the discharge of sewage into coastal waters. For coastal cities, the most economical method of sewage disposal is to perform only a primary treatment and then to pipe the sewage out into the ocean. This discharge scheme is similar to the one described previously for the cooling water except that the sewage must be discharged at much greater depths for environmental reasons.

A third application is to the flow induced by air bubblers which control ice formation in reservoirs and the spread of oil slicks. A perforated rubber hose is weighted down on the bed and compressed air is pumped through the hose producing a row of bubbles. As the bubbles rise to the surface they induce flow which impinges on the free surface and then spreads. This flow at the surface will keep reservoir gates free from ice and can also be used to contain an oil slick.

C. FLOW REGIONS AND FIELDS

To simplify the analysis of the vertical plane jet-plume in shallow water Jirka and Harleman (1979) defined four regions of flow. The four regions are: jet-plume region, surface impingement region, internal hydraulic jump region and stratified counterflow region. Figure 1 shows the four regions and some of the nomenclature used.

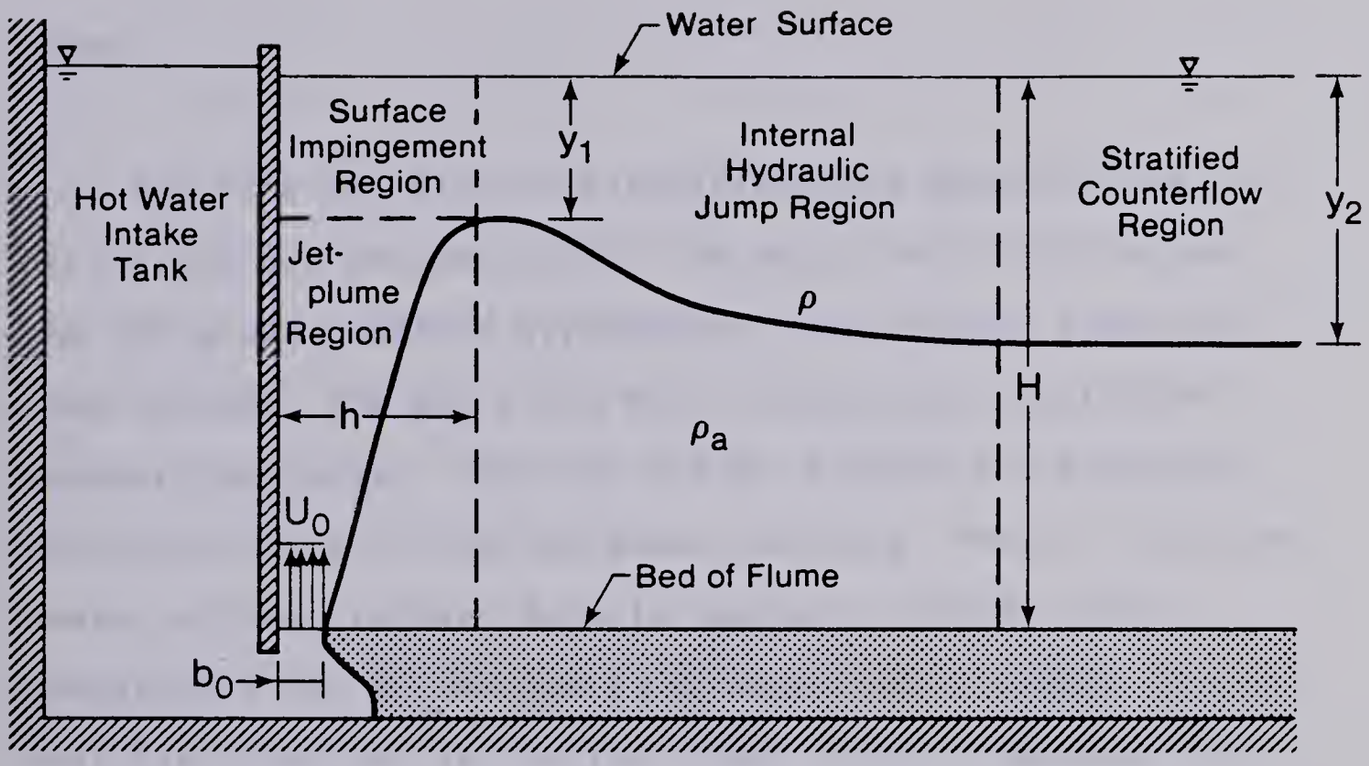

FIGURE 1. Flow regions and nomenclature.

The flow near the nozzle up to the point where the potential core ends is called the zone of flow establishment. In this zone the shear layer caused by the shearing at the interface of the high velocity jet-plume and the stagnant ambient fluid has not penetrated to the center line. At the point where the shear layer has penetrated to the center line, the center line velocity and temperature begin to decay. Beyond this point the region is called the zone of established flow. The length of the zone of flow establishment is approximately 10 b_o as determined by Albertson et al (1950). Therefore the neglect of this zone can only be justified if the submergence ratio H/b_o is

large.

The flow can also be classified more generally as the near field and the far field. The near field will include the jet-plume, surface impingement and internal hydraulic jump regions. The far field will include the stratified counterflow region. The near field is where the momentum characteristics of the jet-plume dominate. The far field is where surface transfer aspects dominate, (Pande 1975). Temperature can be treated as a conservative tracer in the near field but not in the far field. This is because the surface transfer of heat within the far field determines the boundary conditions.

D. LITERATURE REVIEW

PLANE JET-PLUMES

Many studies have been done on the subject of plane jet-plumes or plane buoyant jets, as they are also called. The work of Rouse et al (1952) on free convection from a line source and point source was one of the first. Many other investigators have studied the problem since but the most complete and definitive study was carried out by Kotsovinos (1975).

He studied the plane jet-plume in great detail using a laser Doppler velocimeter for velocity measurements and small bead thermistors for temperature measurements. The main conclusion of his study was that the turbulent structure of jets and plumes are quite different reflecting the different nature of the forces which propel each of them. The pure jet is propelled by inertia forces and the jet-plume by buoyancy forces.

Jets and plumes were found to have dissimilar turbulence characteristics but the shape and spreading rate of their mean velocity profiles were found to be approximately equal. The spread of b, the velocity half-width for jet-plumes, was observed to be:

$$\frac{db}{dx} = 0.1 \tag{1}$$

A constant spreading rate for jet-plumes proves that earlier theories which assumed a constant entrainment coefficient were incorrect. Kotsovinos gives the following entrainment coefficients for jets and plumes.

$$\alpha_e(\text{jet}) = 0.055 \tag{2}$$

$$\alpha_e(\text{plume}) = 0.110 \tag{3}$$

Kotsovinos observed that the virtual origin for the mean velocity profiles was sometimes upstream and sometimes downstream of the nozzle. It varied in location from 6 b_o downstream to 13 b_o upstream from the nozzle and there was no correlation with the outlet Richardson number. Kotsovinos explains that this is due to the fact that a plane jet is non-self-preserving in character.

SURFACE DISCHARGES

Rajaratnam and Humphries (1984) studied the behavior of plane non-buoyant surface discharges. They found that the longitudinal velocity profiles were similar. The exponential equation:

$$\frac{u}{u_m} = \exp\left[-0.693\left(\frac{y}{b}\right)^2\right] \tag{4}$$

was found to describe the experimental results reasonably well up to y/b equal to 1.4. Above this value the equation underestimated the data. The variation of the velocity scale was found to be given by the following semi-empirical equation:

$$\frac{u_m}{U_o} = \frac{3.1}{\sqrt{x/b_o}} \tag{5}$$

where u_m is the maximum value of u at a cross-section and U_0 is the outlet velocity.
This gives a value for the velocity scale which is about 0.9 times the corresponding value for the plane free jet. They also determined that the variation of the length scale was linear and given by:

$$\frac{db}{dx} = 0.07 \tag{6}$$

Chu and Vanvari (1976) investigated the case of a two-dimensional buoyant surface discharge. Their study was primarily experimental in nature and concentrated on the supercritical jet region upstream of the internal hydraulic jump. A series of four tests were run in which fresh water was discharged at the surface over a layer of saline water. Velocity and temperature measurements were gathered and analyzed.

Chu and Vanvari found that the velocity length scale b tended to vary linearly near the nozzle and be described by:

$$\frac{db}{dx} = 0.0678 \tag{7}$$

but further downstream the expansion rate decreased. The longitudinal velocity profiles were found to be similar and

described by a standard exponential equation, similar to equation 4. They also found that the buoyancy profiles were linear with the maximum occuring at the free surface and the minimum equal to zero at the jet boundary. The entrainment velocity was found to be proportional to the longitudinal turbulent intensity $\sqrt{u'^2}$ with the constant of proportionality equal to 0.18.

Rajaratnam and Subramanyan (1983) studied both buoyant surface jets and jumps. They found that in surface jets the growth of the jet thickness followed the non-buoyant surface jet curve given by equation 6 up to some value of x/b_o and then deviated from it to approach asymptotically a horizontal line. This agrees with the findings of Chu and Vanvari (1976). The growth of the jet thickness for surface jumps also follows the non-buoyant surface jet curve up to some x/b_o value and then falls below the curve approaching asymptotically a horizontal line. However, the asymptotic value approached by the surface jump is always greater than the corresponding value for the buoyant surface jet.

Rajaratnam and Subramanyan (1983) also determined that for both buoyant surface jets and jumps the longitudinal velocity profiles at different x stations were approximately similar. Equation 4 describes the profiles reasonably well up to values of y/b of 1.5. Temperature measurements were

obtained in the surface jet experiments and it was found that the temperature profiles at different x stations were similar. The equation

$$\frac{\Delta T}{\Delta T_m} = \exp\left[-0.693\left(\frac{y}{b_T}\right)^2\right] \qquad (8)$$

was found to describe the profiles well for Ri_o equal to 0.002, 0.003 and 0.004 but for Ri_o equal to 0.4 the profile is very different. This is explained by the reduced mixing at the interface at high Ri_o. In equation 8 b_T is the distance from the point of maximum temperature to the point where it is half the maximum, ΔT is the temperature difference and ΔT_m is the maximum of ΔT at a given cross-section.

Rajaratnam and Subramanyan, through careful injection of dye near the interface, determined that for buoyant surface jets there is vertical entrainment of ambient fluid but for internal hydraulic jumps there is hardly any. The small velocities in the reverse roller are said to be too weak to induce turbulent entrainment in this region. Using this fact and their experimental results they developed a diagram which can be used to differentiate between buoyant surface jets, surface jumps and drowned surface jumps.

IMPINGING JET-PLUMES

Notable studies on the subject of vertical plane jet-plumes in shallow water are those of Jirka and Harleman (1979), Pryputniewicz and Bowley (1975), and Lee and Jirka (1981). The investigation by Pryputniewicz and Bowley (1975) was for a round jet-plume and concentrated on the vertical jet-plume region. The studies by Jirka and Harleman (1979) and Lee and Jirka (1981) dealt with plane and round jet-plumes respectively. Both studies investigate thouroughly the near field characteristics of these flows. This study is concerned specifically with plane jet-plumes and as a result only Jirka and Harleman's (1979) work will be reviewed in detail here.

Jirka and Harleman (1979) analyzed the jet-plume region of flow using an integral analysis. A variable entrainment coefficient was assumed in a form which corresponds to an approximately constant spreading rate. The entrainment velocity was assumed to be proportional to the maximum velocity at a cross section following Morton et al (1956). The normalized profiles for velocity and density were assumed similar and were approximated by the familiar exponential equations. These assumptions reduced the governing equations to a solvable form and the solution obtained is similar to one which will be developed in the following chapter.

The surface impingement region was analyzed by Jirka and Harleman using a control volume type of analysis. They made the following assumptions:

1. The inflow has the characteristics of the buoyant jet region , that is fully established profiles and zero dynamic pressure.
2. Negligible entrainment occurs into the control volume.
3. The horizontal outflow has uniform velocity and density profiles.

The energy losses through the region were estimated using the following formula:

$$gh_L = \frac{1}{2} K_L \bar{u}_1^2 \qquad (9)$$

where h_L is the energy loss in meters, $\bar{u}_1$ is the average outflow velocity and K_L is a loss coefficient. Estimates for K_L were obtained from data on 90 degree elbows in closed conduit flow. An energy equation, a continuity equation and a buoyancy conservation equation were then used to obtain a solution for y_1, the outflow depth.

Jirka and Harleman (1979) made the following assumptions in analyzing the internal hydraulic jump region:

1. Shear stresses at the surface, interface and bed were negligible.

2. Hydrostatic pressure occurred throughout.
3. The velocity distributions were uniform.
4. The entrainment into the jump region was negligible.
5. Equal counterflow, that is, the discharge in the lower layer was equal to that in the upper layer.
6. Boussinesq approximation was valid.

Following Yih and Guha (1955) the momentum conservation equations were written for the upper and lower layers. Manipulation of these equations provided an equation for the change in height of the upper layer. A solution was presented graphically which for a given supercritical depth and densimetric Froude number gives the corresponding conjugate depth.

For high upstream densimetric Froude numbers there was no solution to the equation. Jirka and Harleman interpreted this as indicating a downstream flow instability. An unstable flow or discharge being defined as one in which the flow in the upper layer mixes with the flow in the lower layer and is re-entrained into the jet-plume region. The discharge instability occurs because as the densimetric Froude number increases the outlet densimetric Froude number has also increased. From this it follows that the entrainment into the jet-plume region has increased and thus the discharge in the lower layer has also increased. An increase in the upstream densimetric Froude number also

implies an increase in the upper layer discharge. With the discharges and velocities increasing in both layers, the interfacial shear between the two layers also increases and at some critical point mixing begins to occur between the two layers. Thus an unstable discharge configuration is formed. A recirculation eddy approximately 2.5H in length forms at the outlet and a build-up of heat occurs until some steady state is achieved. A stability diagram was presented which for a given submergence and outlet densimetric Froude number predicts a stable or unstable discharge configuration.

The mixing characteristics of this type of flow were also examined by Jirka and Harleman (1979). For a stable discharge the dilution ratio defined as:

$$S = \frac{\text{upper layer discharge}}{\text{outlet discharge}} \qquad (10)$$

was directly predicted from the jet-plume theory. For an unstable discharge the analysis was more complex. Following Schijf and Schonfeld (1953) the horizontal momentum equations for both layers in the statified counterflow region were written. Using Boussinesq approximation and the assumption of constant total depth the two equations reduced to a single differential equation. This equation was integrated to give a solution for the height of the

interface above a datum and the layer densimetric Froude number. The integrated equation was then used to calculate the height of the interface at the point 2.5H from the outlet where the recirculating eddy ends. Then knowing the height of the interface and the layer densimetric Froude number at this point the dilution ratio was calculated.

An experimental investigation was included in the study by Jirka and Harleman (1979) in an attempt to validate their theoretical work. A total of 19 experiments were run in which the submergence ratio was varied from 60 to 1300 and the densimetric Froude number at the outlet from 13 to 312. Extensive temperature measurements were taken as well as photographs of the dyed flow. Limited velocity measurements were obtained by taking time lapse photographs of falling dye crystals. The experimental tank was closed, that is, it had no overflow and no ambient water recharge system, so the flow could not be maintained in a steady state for long periods of time.

It was observed that the stability criterion correctly predicted the stability of the 19 runs. It was also found that the dilution ratios were predicted reasonably well by the theory, within approximately 25% for all 19 runs. The height of the interface was predicted quite closely by the theory. It was discovered that entrainment into the jump

region was negligible as assummed.

Some of the main conclusions reached by Jirka and Harleman were as follows:

1. The discharge stability depends only on the behavior of the near field.
2. The discharge stability is dependent on 2 parameters, the submergence and the outlet densimetric Froude number.
3. The far-field boundary conditions have a significant effect on the mixing characteristics of the flow.

E. PROPOSED WORK

EXPERIMENTAL WORK

This experimental investigation was proposed because the behavior of jet-plumes in shallow water is not well understood. Previous investigators such as Jirka and Harleman (1979) and Pryputniewicz and Bowley (1975) have studied this problem with emphasis on the engineering aspects. In this study a more fundamental approach to the problem was taken. The emphasis was placed on velocity measurements. It was thought that a better understanding of the physics of the problem could be achieved by compiling a complete set of velocity profiles.

The experimental work was done in three parts. The first was a preliminary investigation to provide some qualitative information and to smooth out any problems with the experimental equipment. Dye photographs were taken and analyzed but no useable data were obtained.

The second part consisted of six complete runs, velocity profiles and dye photographs were taken. The velocity profiles were taken at distances up to 200 times the outlet half-width downstream to ensure that any trends in the data were clearly observed, and not limited by inadequate data. No data were gathered in the vertical jet-plume region because it was assumed that the present jet-plume theory adequately described this region.

The third part of the experimental work consisted of thirteen supplementary runs. Velocity profiles were taken only at x=10 cm. These profiles were used to obtain the depth of the surface layer y_1. Dye photographs were also taken and analyzed for the thirteen supplementary runs.

THEORETICAL AND ANALYTICAL WORK

To supplement the experimental work some theoretical analysis was carried out. The theoretical analysis was also done in three parts. The first was the derivation of the equations for the jet-plume region. These equations describe

the behavior of the flow within this region and also provide the initial conditions for the surface impingement region.

The second section was a control volume type of analysis used to describe the flow in the surface impingement region. The flow in this region is not readily analyzed because none of the slender flow approximations are applicable. Therefore a cruder type of control volume analysis had to be used in order to obtain a useable solution.

The third section of analysis dealt with the internal hydraulic region. One method of analysis used for investigation of this region involved many simplifying assumptions and produced a Belanger type equation. A second method with less resrictive assumptions produced a more complex equation, a fourth order polynomial. The predictions of the conjugate depths from both equations were then compared to the experimental data to verify the theory.

II. THEORETICAL DEVELOPMENTS

A. JET-PLUME REGION

EQUATIONS OF MOTION

The Reynold's equations of motion for a plane steady flow in cartesian coordinates can be written as:

$$u \frac{\partial u}{\partial x} + v \frac{\partial u}{\partial y} = - \frac{1}{\rho} \frac{\partial P}{\partial x} + \nu \nabla^2 u - \left[\frac{\partial \overline{u'^2}}{\partial x} + \frac{\partial \overline{u'v'}}{\partial y} \right] - g\rho \qquad (11)$$

$$u \frac{\partial v}{\partial x} + v \frac{\partial v}{\partial y} = - \frac{1}{\rho} \frac{\partial P}{\partial y} + \nu \nabla^2 v - \left[\frac{\partial \overline{u'v'}}{\partial x} + \frac{\partial \overline{v'^2}}{\partial y} \right] \qquad (12)$$

$$\left[\frac{\partial u}{\partial x} + \frac{\partial v}{\partial y} \right] + \frac{1}{\rho} \left[u \frac{\partial \rho}{\partial x} + v \frac{\partial \rho}{\partial y} \right] = - \frac{1}{\rho} \left[\frac{\partial}{\partial x} \overline{\rho' u'} + \frac{\partial}{\partial y} \overline{\rho' v'} \right] \qquad (13)$$

where x and y are as shown in Figure 2

u and v are the turbulent mean velocity components in the x and y directions respectively

u' and v' are the fluctuating components of velocity

P is the mean pressure at a point

ρ is the mean mass density of the fluid at a point

ν is the kinematic viscosity of the fluid

and the bars denote time averaging.

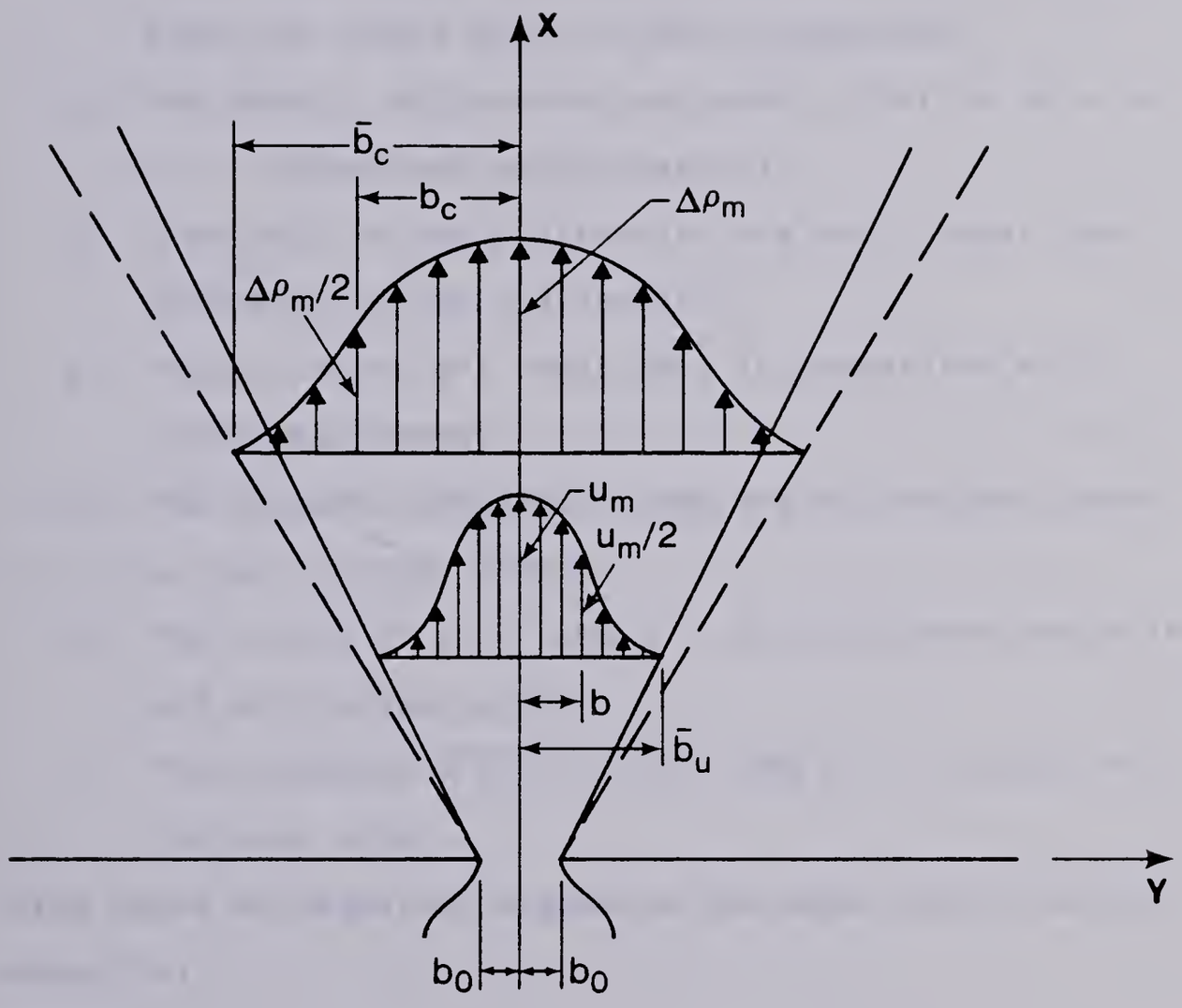

FIGURE 2. Definition sketch for the jet-plume region

The following assumptions were made in this analysis:

1. The length scale in the x direction is much larger than the length scale in the y direction.
2. The density differences are small, that is $\Delta\rho_o / \rho << 1$ (Boussinesq approximation).
3. Gradients in the y direction are much larger than gradients in the x direction.
4. Viscous terms are negligible in comparison with turbulence terms.
5. The largest turbulence terms are of the same order as the inertial terms.
6. The values of u',v' and U_t, the turbulence scale are all of the same order.
7. The values of $\overline{u'v'}$, $\overline{u'^2}$, $\overline{v'^2}$ and U_t^2 are all of the same order.

Using order of magnitude arguments the equations of motion reduce to:

$$u \frac{\partial u}{\partial x} + v \frac{\partial u}{\partial y} = \frac{1}{\rho} \frac{\partial \tau}{\partial y} + g \frac{\Delta\rho}{\rho_a} \qquad (14)$$

$$\frac{\partial u}{\partial x} + \frac{\partial v}{\partial y} = 0 \qquad (15)$$

The buoyancy conservation equation can be reduced to:

$$\frac{\partial(uc)}{\partial x} + \frac{\partial(vc)}{\partial y} = -\left[\frac{\partial}{\partial x}\left(\overline{u'c'}\right) + \frac{\partial}{\partial y}\left(\overline{v'c'}\right)\right] \qquad (16)$$

where $c=g\,\Delta\rho$ and c' is the fluctuating component of the modified gravity term c.

Letting:

$$-\overline{u'c'} = \varepsilon_x \frac{\partial c}{\partial x} \qquad -\overline{v'c'} = \varepsilon_y \frac{\partial c}{\partial y} \qquad (17)$$

where ϵ_x and ϵ_y are the turbulent diffusion coefficients for buoyancy in the x and y directions respectively. Assuming ϵ_x is of the same order as ϵ_y and using the assumptions listed earlier equation 16 reduces to:

$$\frac{\partial(uc)}{\partial x} + \frac{\partial(vc)}{\partial y} = \frac{\partial}{\partial y}\left(\varepsilon_y \frac{\partial c}{\partial y}\right) \qquad (18)$$

If ϵ_y is assumed constant across the plume the result is the final buoyancy conservation equation:

$$\frac{\partial(uc)}{\partial x} + \frac{\partial(vc)}{\partial y} = \varepsilon_y \frac{\partial^2 c}{\partial y^2} \qquad (19)$$

INTEGRAL ANALYSIS

Equation 15 is integrated from y=0 to a large value of y outside the jet-plume denoted as ∞. Using Liebnitz's rule and denoting the entrainment velocity by v_e the equation obtained is:

$$\frac{d}{dx} \int_0^\infty u \, dy = - v_e \qquad (20)$$

Following Morton et al (1956) it is assumed that the entrainment velocity is proportional to the maximum longitudinal velocity at a given cross-section. Using this assumption equation 20 becomes:

$$\frac{d}{dx} \int_0^\infty u \, dy = \alpha_e \, u_m \qquad (21)$$

where α_e is the entrainment coefficient and u_m is the maximum value of u at a given cross-section.

Integrating the momentum equation (equation 16) from y=0 to y=∞ and using both the continuity equation and Liebnitz's rule, the result is:

$$\frac{d}{dx} \rho \, u^2 \, dy = \int_0^\infty c \, dy \qquad (22)$$

Equation 22 states that the rate of increase of axial momentum in the jet-plume is equal to the buoyant force per unit length of jet-plume.

Integrating the buoyancy conservation equation (equation 19) from y=0 to y=∞ and applying Liebnitz's rule gives:

$$\frac{d}{dx} \int_o^\infty u\ c\ dy = 0 \qquad (23)$$

This equation indicates that the buoyancy flux is constant along the jet-plume. If B_o the buoyancy flux at the nozzle is given by:

$$B_o = 2\ b_o\ U_o\ g\ \Delta\rho_o \qquad (24)$$

then equation 23 can be rewritten as:

$$2 \int_o^\infty u\ c\ dy = B_o = 2\ b_o\ U_o\ g\ \Delta\rho_o \qquad (25)$$

Multiplying equation 14 by u and integrating from y=0 to y=∞ and applying Liebnitz's rule gives the integral energy equation.

$$\frac{d}{dx} \int_o^\infty \frac{\rho u^2}{2}\ u\ dy = \int_o^\infty u\ c\ dy - \int_o^\infty \tau\ \frac{\partial u}{\partial y}\ dy \qquad (26)$$

This equation states that the increase in energy (LHS) equals the energy production by buoyancy (first term on the RHS) minus turbulence production (second term on RHS).

The u(y) velocity profiles and c(y) density deficiency profiles have been shown to be similar at different cross-sections (Kotsovinos 1975). This can be stated

mathematically as:

$$\frac{u}{u_m} = f(\eta) \tag{27}$$

$$\frac{c}{c_m} = h(\eta) \tag{28}$$

where b is the velocity half-width, the distance from the centerline of the jet-plume to where $u=u_m/2$ and where $\eta = y/b$. The integral continuity equation (equation 20) can now be rewritten as:

$$\frac{d}{dx}(u_m b) = \frac{\alpha_e}{I_1} u_m \tag{29}$$

where $I_1 = \int_0^\infty f \, d\eta$

The integral momentum equation (equation 22) upon substitution becomes:

$$\frac{d}{dx}(b\, u_m^2) = \frac{I_3}{\rho_a I_2} b\, c_m \tag{30}$$

where $I_2 = \int_0^\infty f^2 d\eta$ $\qquad$ $I_3 = \int_0^\infty h \, d\eta$

The integral buoyancy conservation equation (equation 25) can be rewritten as:

$$u_m \, c_m \, b = \frac{B_o}{2 I_4} \tag{31}$$

where $I_4 = \int_o^\infty f \, h \, d\eta$

The integral energy equation (equation 26) becomes:

$$\frac{\rho_a I_6}{2} \frac{d}{dx} b \, u_m^3 = - \rho_a \, u_m^3 \, I_7 + u_m \, c_m \, b \, I_4 \tag{32}$$

where $I_6 = \int_o^\infty f^3 \, d\eta$ $\qquad$ $I_7 = \int_o^\infty G \, f' \, d\eta$

$f' = \frac{df}{d\eta}$ $\qquad$ $G = \frac{\tau}{\rho u_m^2}$

The behavior of jet-plumes is very jet like near the nozzle where momentum flux dominates. Further away from the nozzle, the behavior becomes more plume-like as the buoyancy starts to dominate. Kotsovinos has established that the spreading rates for plane jets and plumes are approxiamately equal. However the entrainment coefficient for a plane plume is much greater than that for a plane jet. Given this fact, the integral continuity, momentum, buoyancy and energy equations can be used to show that:

$$\alpha_e = 2 \frac{I_1 I_7}{I_6} + \frac{1}{F^2} \left[2 \frac{I_1 I_3}{I_2} - 2 \frac{I_1 I_4}{I_6} \right] \tag{33}$$

where $F^2 = \dfrac{u_m^2}{g \frac{\Delta \rho_m}{\rho_a} b}$

Rewriting equation 33 as:

$$\alpha_e = \alpha_1 + \frac{\alpha_2}{F^2} \tag{34}$$

where $\alpha_1 = 2\,\frac{I_1 I_7}{I_6}$ $\qquad$ $\alpha_2 = \left[2\,\frac{I_1 I_3}{I_2} - 2\,\frac{I_1 I_4}{I_6}\right]$

For a pure jet $F^2=\infty$ and therefore:

$$\alpha_1 = \alpha_e \text{ (jet)} \tag{35}$$

where α_e (jet) is the entrainment coefficient for a pure jet.

For the pure plume F can be shown to be equal to 4.14 and if α_e (plume) is the entrainment coefficient for a plume, α_2 is given by:

$$\alpha_2 = (4.14)^2\,[\alpha_e \text{ (plume)} - \alpha_e \text{ (jet)}] \tag{36}$$

Therefore the entrainment coefficient for a plane jet-plume will be given as:

$$\alpha_e = \alpha_e \text{ (jet)} + \frac{17.14}{F^2}\,(\alpha_e \text{ (plume)} - \alpha_e \text{ (jet)}) \tag{37}$$

Using the integral momentum and buoyancy equations an equation of the form shown below can be developed.

$$u_m^3 + 2\, u_m^2 \left(\frac{d}{dx}\, u_m\right) = A \tag{38}$$

where $A = \dfrac{I_3}{2\, K_2\, I_2\, I_4}\, \dfrac{B_o}{\rho_a}$ $\qquad b = K_2\, x$

The solution of equation 38 is:

$$u_m = \left[A + \frac{A_1}{x^{3/2}}\right]^{1/3} \tag{39}$$

where A_1 is a constant of integration.

In the case of a plane jet $B_o=0$, and therefore $A=0$, equation 39 reduces to:

$$u_m = \frac{A_1^{1/3}}{\sqrt{x}} \tag{40}$$

In the case of the plane plume $A_1=0$, because u_m is invariant with x and therefore:

$$u_m = A^{1/3} \tag{41}$$

it can be shown that A_1 is given by:

$$A_1 = U_o^3 \left[\frac{b_o}{K_2\, I_2}\right]^{3/2} \tag{42}$$

With these results equation 39 may be rewritten as:

$$\frac{u_m}{U_o} = \left[\frac{I_3}{K_2\, I_2\, I_4\, F_o^{\,2}} + \frac{1}{K_2^{\,3/2}\, I_2^{\,3/2} (x/b_o)^{3/2}}\right]^{1/3} \qquad (43)$$

Substituting equation 39 into equation 31 and rearranging gives:

$$\frac{\Delta\rho_m}{\Delta\rho_o} = \frac{1}{K_2 I_4}\left[\frac{I_3}{K_2\, I_2\, I_4}\,\frac{1}{F_o^{\,2}} + \frac{1}{(K_2\, I_2)^{3/2}\,(x/b_o)^{3/2}}\right]^{-1/3} \frac{1}{x/b_o} \qquad (44)$$

Now substituting equations 43 and 44 into the expression for F and reducing:

$$F = \left[\frac{I_3}{K_2 I_2} + \frac{I_4\, F_o^{\,2}}{K_2^{\,3/2}\, I_2^{\,3/2}\,(x/b_o)^{3/2}}\right]^{1/2} \qquad (45)$$

then substituting for F in equation 37 yields:

$$\alpha_e = \alpha_e\,(\text{jet}) + \frac{17.14\,\left(\alpha_e\,(\text{plume}) - \alpha_e\,(\text{jet})\right)}{\left[\frac{I_3}{K_2 I_2} + \frac{I_4\, F_o^{\,2}}{(K_2 I_2)^{3/2}\,(x/b_o)^{3/2}}\right]} \qquad (46)$$

Kotsovinos found that the u velocity profiles were similar and that they were well represented by the following expression:

$$\frac{u}{u_m} = \exp\,(-\,0.693\,\eta^2) \qquad (47)$$

He also found that the density defect profiles were similar

and well represented by:

$$\frac{c}{c_m} = \exp\left(-0.693\left(\frac{\eta}{K}\right)^2\right) \tag{48}$$

where K is the ratio of the spreading rate of density to the spreading rate of velocity.

Using the exponential equations it was found that:

$$I_1 = 1.065 \quad I_2 = 0.753 \quad I_3 = 1.065\ K \quad I_4 = \frac{1.065\ K}{\sqrt{1 + K^2}} \tag{49}$$

Kotsovinos also determined that the value of K_2 is equal to 0.097. From the experimental work of Rouse et al (1956) and Kotsovinos (1975) a value of 1.18 is assigned to K. With these values for the constants equations 43 to 46 become:

$$\frac{u_m}{U_o} = \left[\frac{21.2}{F_o^2} + \frac{50.7}{(x/b_o)^{3/2}}\right]^{1/3} \tag{50}$$

$$\frac{\Delta\rho_m}{\Delta\rho_o} = \frac{12.75}{\left[\frac{21.2}{F_o^2} + \frac{50.7}{(x/b_o)^{3/2}}\right]^{1/3}} \frac{1}{(x/b_o)} \tag{51}$$

$$F = \left[17.1 + \frac{41.4\ F_o^2}{(x/b_o)^{3/2}}\right]^{1/2} \tag{52}$$

$$\alpha_e = \alpha_e \text{ (jet)} + \frac{17.1\ (\alpha_e \text{ (plume)} - \alpha_e \text{ (jet)})}{\left[17.1 + \frac{41.4\ F_o^2}{(x/b_o)^{3/2}}\right]} \tag{53}$$

If α_e (jet)=0.53 and α_e (plume)=0.103 equation 52 becomes:

$$\alpha_e = 0.053 + \frac{0.855}{\left[17.1 + \frac{41.4\ F_o^2}{(x/b_o)^{3/2}}\right]} \tag{54}$$

Equations 50,51,52 and 54 are plotted in Figures 3, 4,5 and 6 respectively.

B. SURFACE IMPINGEMENT REGION

Within the surface impingement region the flow changes direction by 90° and therefore the usual slender flow approximations are not valid. Without these simplifying assumptions the equations of motion do not reduce to a manageable form. Therefore a control volume type of analysis was used to to investigate this region. Figure 7 is a definition sketch of the surface impingement region.

CONTROL VOLUME ANALYSIS

The unknowns in the surface impingement region are the velocity,density and depth at section 1. All quantities are known at section 2 from the equations for the jet-plume. The following assumptions were made in the analysis.

1. Half Gaussian profiles for velocity and density profiles at section 1.
2. Inflow q_2 equals outflow q_1, that is, there is no

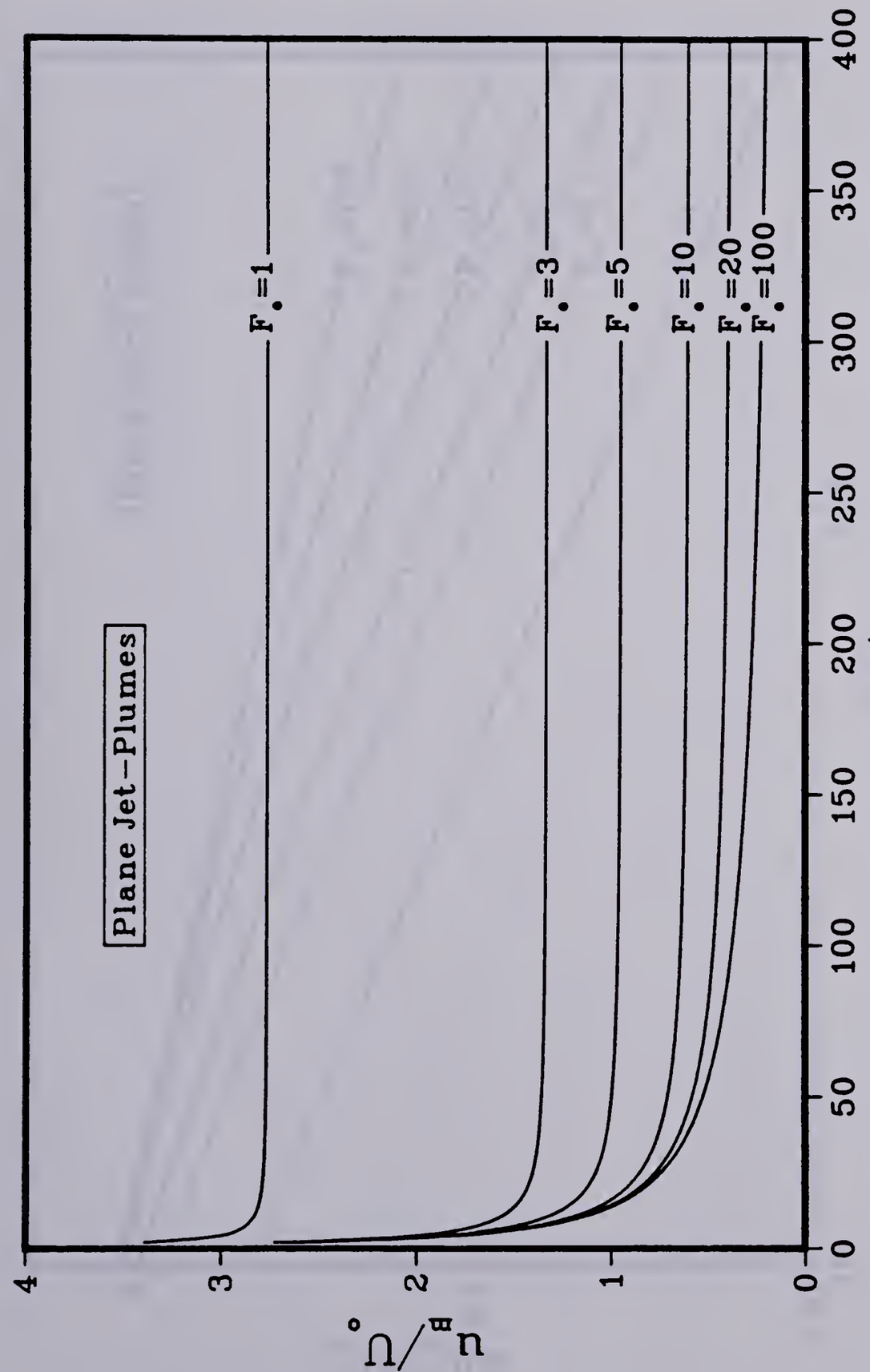

FIGURE 3. Equation for the dimensionless maximum velocity of a plane jet-plume.

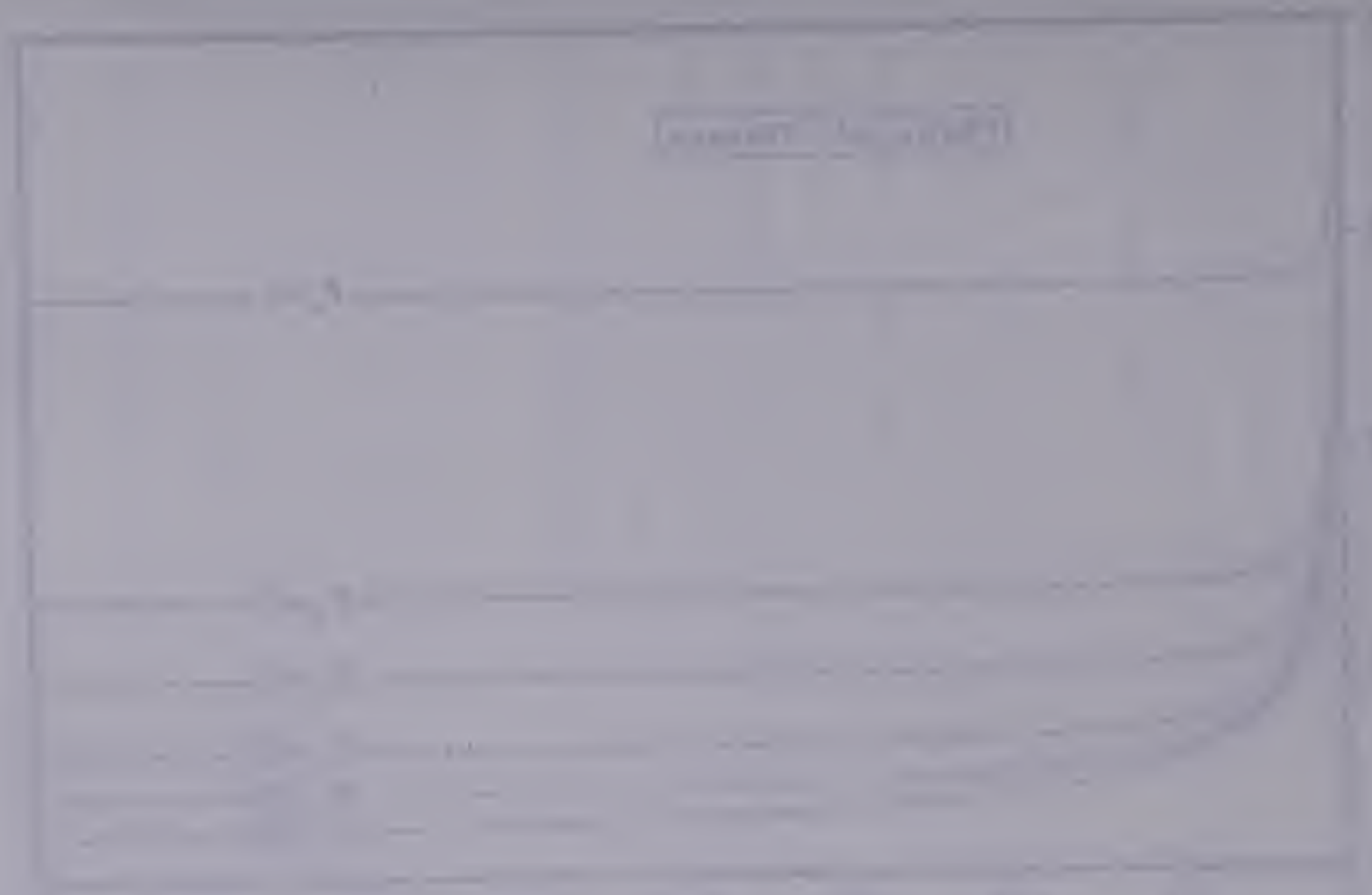

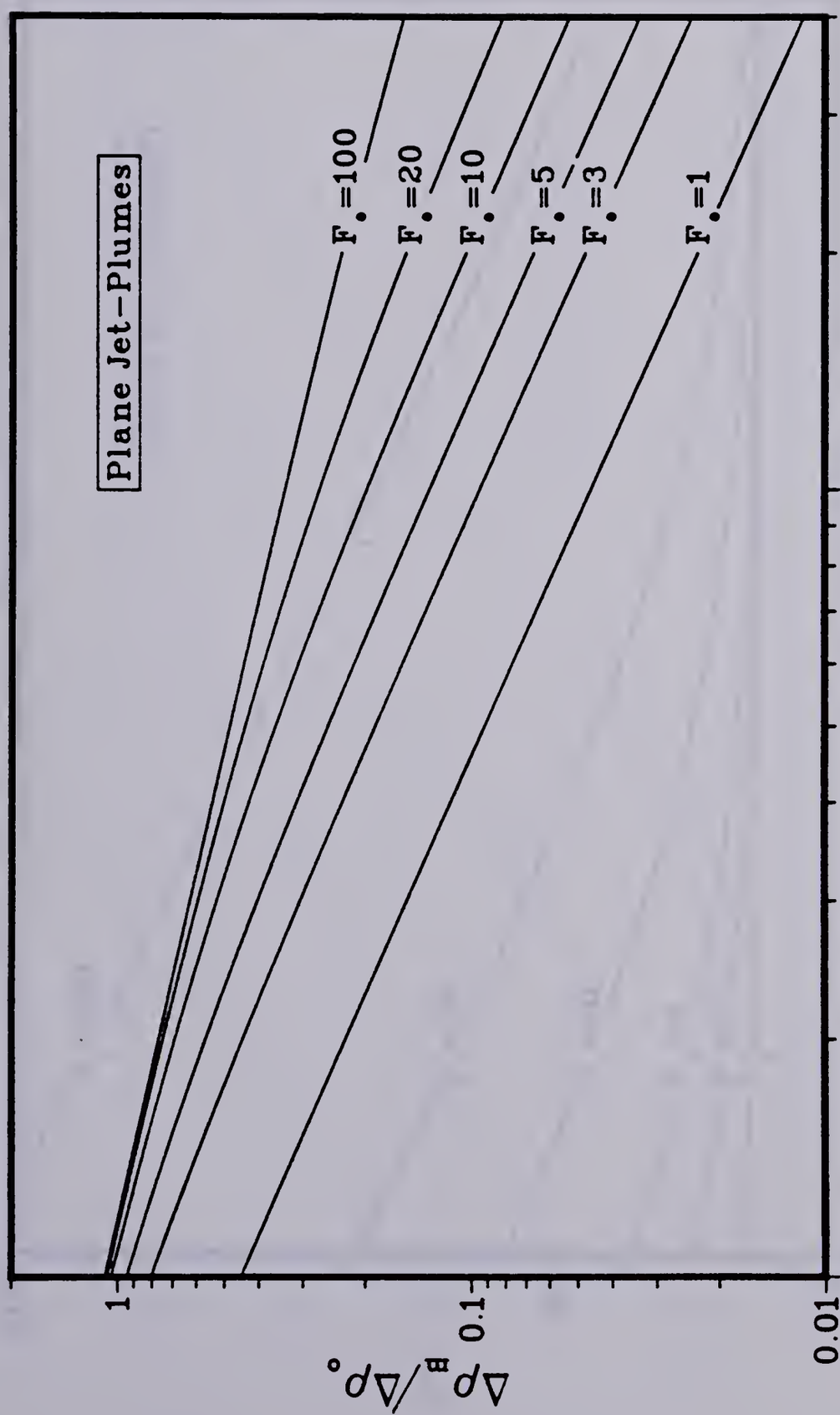

FIGURE 4. Equation for the dimensionless density deficiency of a plane jet-plume.

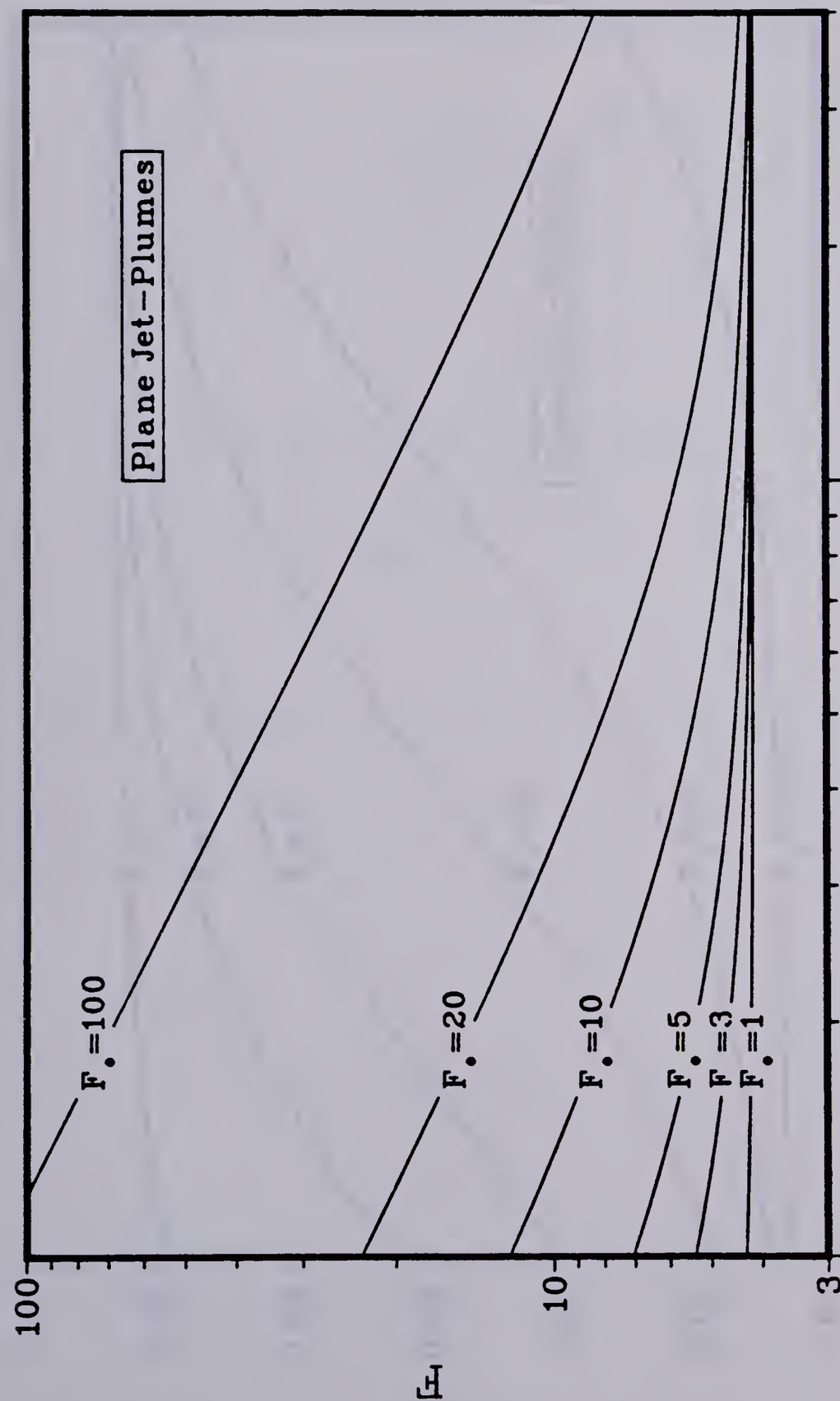

FIGURE 5. Equation for the densimetric Froude number of a plane jet-plume.

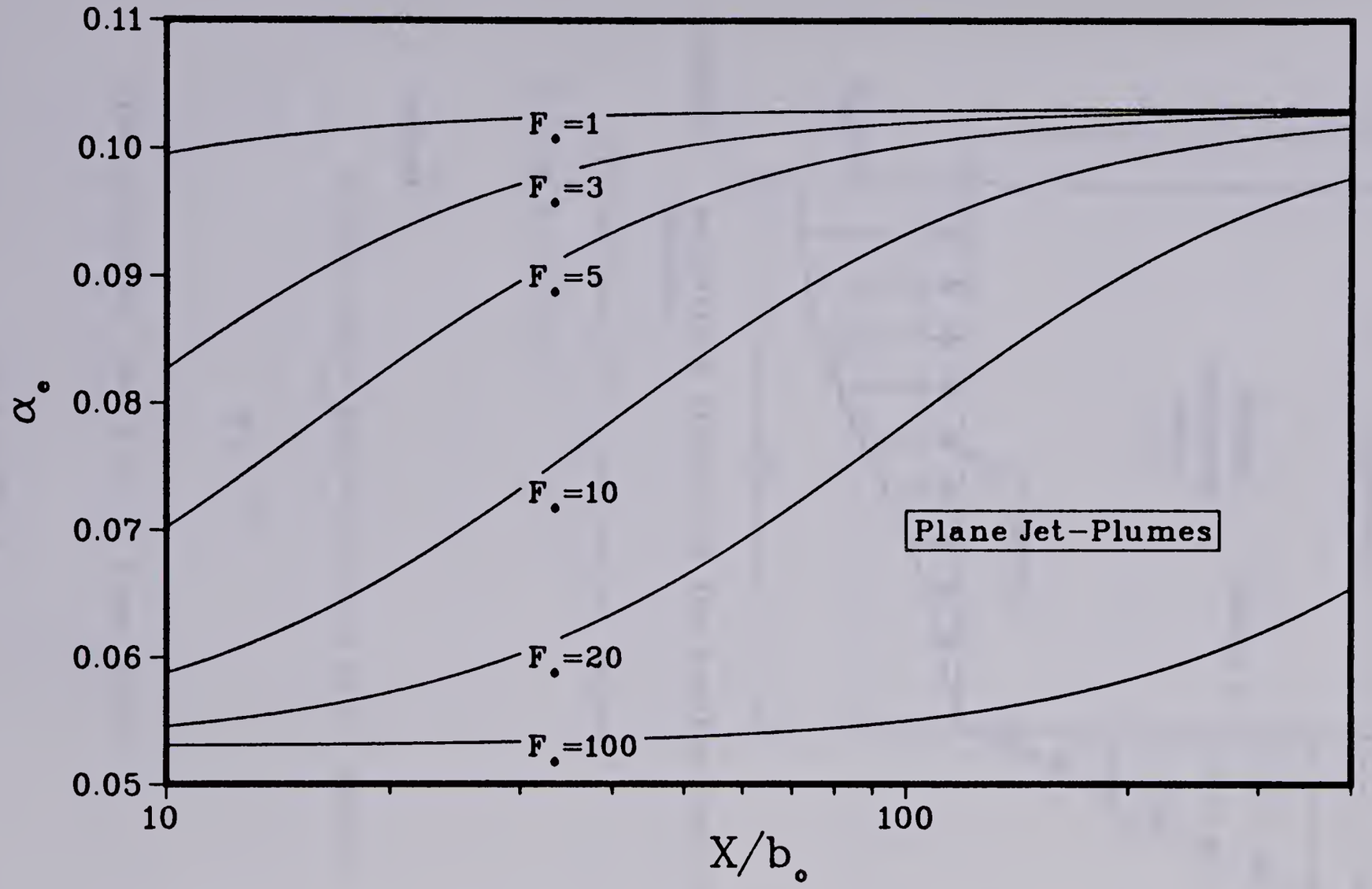

FIGURE 6. Equation for the entrainment coefficient of a plane jet-plume.

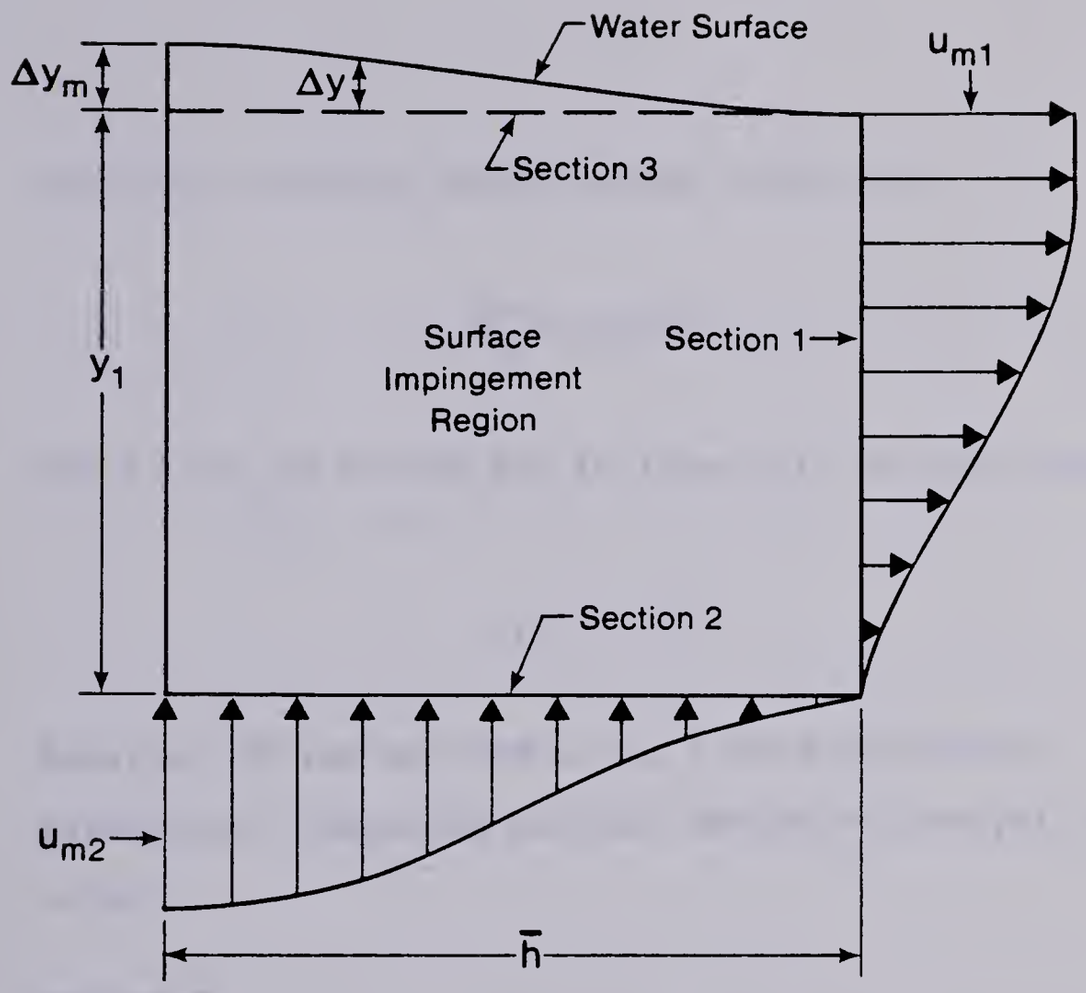

FIGURE 7. Definition sketch for the surface impingement region.

entrainment into the control volume.

3. $\Delta\rho_{m2} = \Delta\rho_{m1}$

Method 1

A very simple approach would be to assume:

$$y_1 = \bar{h} \tag{55}$$

From jet-plume theory it is known that:

$$b = 0.097\ x \tag{56}$$

The total velocity width can be taken as:

$$\overline{b_u} = 2.5\ b \tag{57}$$

Now y_1 can be solved for in terms of the total depth H.

$$y_1 = 0.20\ H \tag{58}$$

Equation 58 was derived using a very arbitrary assumption ,therefore another method of analysis was tried.

Method 2

From the work of Beltaos (1972) an equation for the pressure distribution caused by a plane jet impinging on a smooth wall could be found:

$$\frac{P_w}{P_s} = \exp\left[-38.5\ (x/H)^2\right] \tag{59}$$

where P_w is the pressure on the wall
and P_s is the stagnation pressure at the centerline, on the wall.
Assuming that the disturbance to the free surface caused by a plane jet-plume in shallow water is directly analagous to this pressure, an equation of the following form could be written:

$$\frac{\Delta y}{\Delta y_m} = \exp\left[-38.5\ (x/H)^2\right] \tag{60}$$

Recalling that $h=0.2425(H-y_1)$ equation 60 could be rewritten as:

$$\frac{\Delta y}{\Delta y_m} = \exp\left[-38.5\left(\frac{x}{4.12\ h + y_1}\right)^2\right] \tag{61}$$

If y_1 is taken as 2.5b then the average velocity at section 1 equals $0.426u_{m1}$. Writing the momentum equation in the x direction and simplifying gives:

$$\Delta y_m = 0.037\ u_{m1}^2 \tag{62}$$

The pressure along section 2 is constant and equal to $\rho g y_1$ and the pressure along section 3 is equal to $\rho g \Delta y$. It follows then that the momentum equation in the vertical direction is:

$$\rho\ q_2\ V_2 = \rho\ g \int_0^\infty \Delta y\ dx \tag{63}$$

The term on the right is the weight of the water contained in the free surface disturbance for a unit width of jet-plume. Substituting and rearranging gives:

$$\Delta y_m = \frac{0.129\ u_{m2}^2\ h}{4.124\ h + y_1} \tag{64}$$

From the assumption that $q_2=q_1$ it follows that:

$$u_{m2}\, h = u_{m1}\, y_1 \tag{65}$$

Recalling from jet-plume theory that $h=0.2425(H-y_1)$, the final result is:

$$y_1 = 0.23\ H \tag{66}$$

The second method gives almost the same result as the simplistic first method. When the first method result is used the equations for velocity and density are considerably simplified. Therefore y_1 is assumed to equal h and the equation for u_{m1} is as follows:

$$u_{m1} = u_{m2} = U_o \left[\frac{21.2}{F_o^{\,2}} + \frac{70.8}{(H/b_o)^{3/2}}\right]^{1/3} \tag{67}$$

The equation for $\Delta\rho_{m1}$ will be:

$$\Delta\rho_{m1} = \Delta\rho_{m2} = \frac{15.94\ /\ (H/b_o)}{\left[\dfrac{21.2}{F_o^{\,2}} + \dfrac{70.8}{(H/b_o)^{3/2}}\right]^{1/3}} \tag{68}$$

C. INTERNAL HYDRAULIC JUMP REGION

MOMENTUM ANALYSIS

The analysis of a hydraulic jump in a fluid system of 2 layers was first carried out by Yih and Guha (1955). Following their analysis closely the following assumptions are made:

1. Hydrostatic pressure distribution throughout.
2. Interfacial and boundary shear stresses are negligible.
3. There is no entrainment between the layers.

Figure 8 shows a system of 2 layers with the relevant parameters labelled. By writing and rearranging the momentum equation for the upper and lower layers Yih and Guha obtained:

for the lower layer,

$$2\frac{q_2^2}{g}(y_3 - y_4) = y_3\, y_4\,(y_3 + y_4)\left[\frac{\rho}{\rho_a}(y_1 - y_2) + (y_3 - y_4)\right] \quad (69)$$

for the upper layer,

$$2\frac{q_1^2}{g}(y_1 - y_2) = y_1\, y_2\,(y_1 + y_2)\left[(y_1 - y_2) + (y_3 - y_4)\right] \quad (70)$$

Equations 69 and 70 are the equations when both layers are in motion. If the lower layer is stagnant, or can be approximated as such, the equations reduce to:

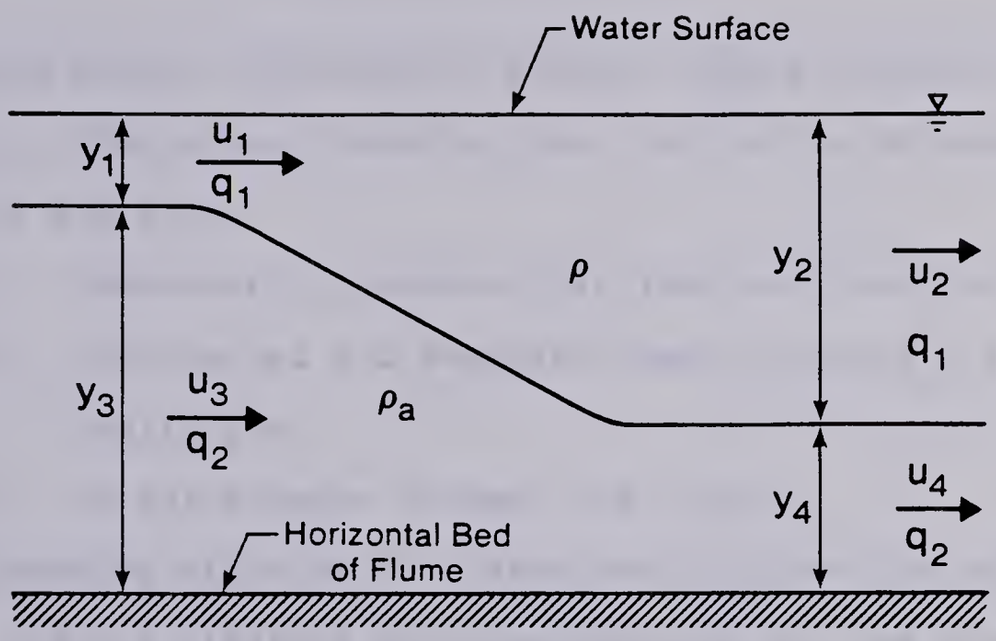

FIGURE 8. A two layered system following Yih and Guha.

$$\frac{y_2}{y_1} = \frac{\sqrt{1 + 8\ F_1^{\,2}} - 1}{2} \qquad (71)$$

where $$F_1 = \frac{u_1}{\sqrt{g\ y_1 \frac{\Delta\ \rho}{\rho_a}}} \qquad \Delta\ \rho = \rho_a - \rho$$

Equation 71 is exactly the same as the classic Belanger equation for open channel hydraulic jumps. The only difference is that in equation 71 the densimetric Froude number is used rather than the ordinary Froude number which contains no density terms.

Another approach to the problem was taken by Mehrotra (1973). He analyzed an internal hydraulic jump in a 2

layered system, enclosed in a duct. Figure 9 shows a sketch of his formulation. Mehrotra made the following assumptions in his analysis:

1. Hydrostatic pressure distribution throughout.
2. Interfacial and boundary shear stresses are negligible.
3. No entrainment between the layers.

The pressure at point A is arbitrarily given the value of zero and the pressure at B the value of P_o. The momentum equation for the upper layer can be reduced to the following form:

$$P_o = \frac{2 \rho_2 q_2 (u_2 - u_2')}{(2 H - h' - h)} \tag{72}$$

The momentum equation for the lower layer can similarly be reduced to:

$$P_o = \frac{2}{(h + h')} \left[\rho_1 q_1 (u_1' - u_1) + \frac{\rho_1 g}{2} (h^2 - h'^2) + \frac{\rho_2 g}{2} (h'^2 - h^2)\right] \tag{73}$$

If equations 72 and 73 are rearranged, simplified and like terms are grouped Mehrotra's final equation is obtained:

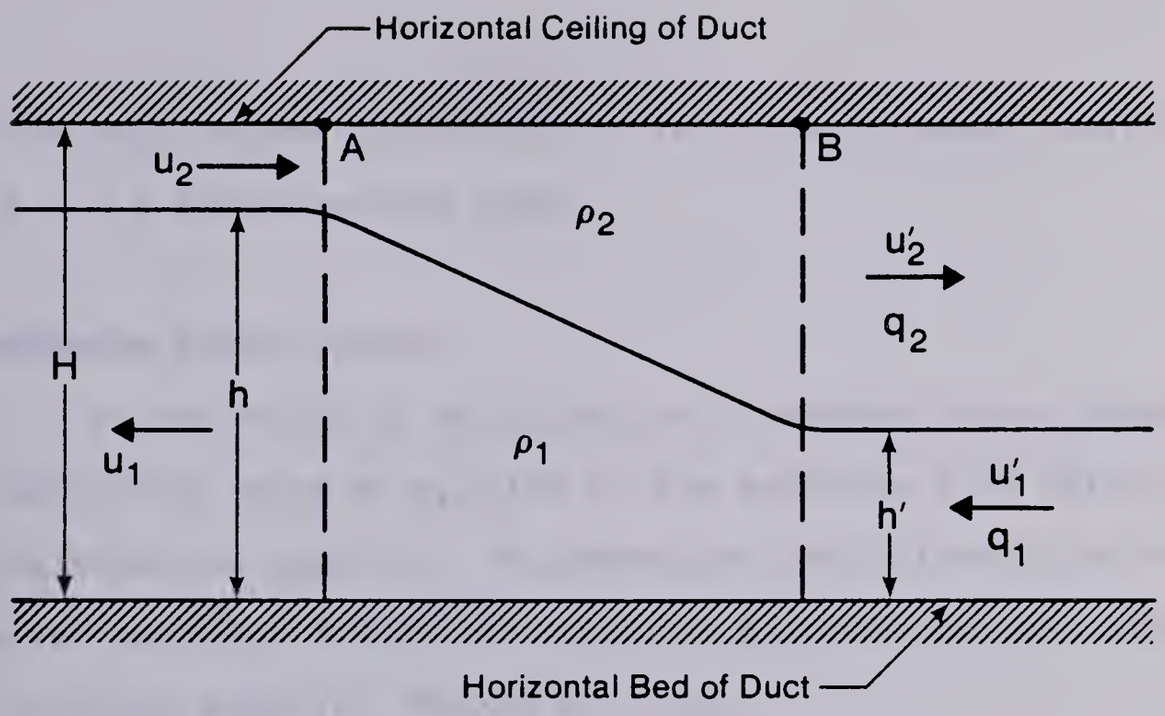

FIGURE 9. A two layered system following Mehrotra.

$$0 = \phi^4 - (3 - 2\alpha)\,\phi^3 + \left[\alpha^2 - 4\alpha + 2 + \frac{2\,\overline{q_1}^2}{\alpha\, s} - \frac{2\,r\,\overline{q_2}^2}{s(1-\alpha)}\right]\phi^2$$

$$- \left[\alpha^2 - 2\alpha - \frac{2\,\overline{q_1}^2}{s\,\alpha}\,(\alpha - 3) + \frac{2\,r\,\overline{q_2}^2\alpha}{s(1-\alpha)}\right]\phi \qquad (74)$$

$$+ \frac{4\,\overline{q_1}^2}{s\,\alpha} - \frac{2\,\overline{q_1}^2}{s}$$

where $\phi = \frac{h'}{H}$ $\alpha = \frac{h}{H}$ $r = \frac{\rho_2}{\rho_1}$ $\overline{q_i}^2 = \frac{q_i^2}{g\,H^3}$

$s = 1 - r$ $s = \frac{\rho_1 - \rho_2}{\rho_1}$

Equation 74 defines the conjugate depths of an internal hydraulic jump, in a system of 2 layers, enclosed in a duct

with both layers in motion. It is a fourth order ploynomial in ψ , a dimensionless depth.

MOMENTUM COEFFICIENTS

If the velocity distribution is non-uniform a momentum coefficient must be applied to the momentum flux terms in the momentum equation. The momentum coefficient β for a given velocity distribution may be calculated using the following equation (Henderson 1966).

$$\beta = \frac{\int_o^A v^2 \, dA}{V^2 \, A} \tag{75}$$

where V=average velocity A=area

v=velocity at a point

For a triangular velocity distribution β can be shown to equal 1.333. For an exponential velocity distribution of the form:

$$\frac{u}{u_m} = \exp\,(-\,0.693\,\eta^2) \tag{76}$$

β can be shown to equal 1.666.

If the momentum coefficient is applied to the analysis by Yih and Guha (1955) the following equation results:

$$\frac{y_2}{y_1} = \frac{\sqrt{1 + 8\beta F_1^2} - 1}{2} \tag{77}$$

If β is used in the derivation of Mehrotra's equation the result is:

$$0 = \phi^4 - (3 - 2\alpha)\phi^3 + \left[\alpha^2 + 2 - 4\alpha + \frac{2\beta_1 \bar{q}_1^2}{\alpha s} - \frac{2\beta_2 \bar{q}_2^2}{s(1-\alpha)}\right]\phi^2 \tag{78}$$

$$- \left[\alpha^2 - 2\alpha + \frac{6\beta_1 \bar{q}_1^2}{s\alpha} - \frac{2\beta_1 \bar{q}_1^2}{s} + \frac{2\beta_2 r \alpha \bar{q}_2^2}{s(1-\alpha)}\right]\phi$$

$$+ \frac{4\beta_1 \bar{q}_1^2}{s\alpha} - \frac{2\beta_1 \bar{q}_1^2}{s}$$

where β_1 = momentum coefficient for lower layer

β_2 = momentum coefficient for upper layer

III. EXPERIMENTAL INVESTIGATION

A. FLUME

All experiments were run in a flume located in the T. Blench Graduate Hydraulics Laboratory. The flume was 4.6 m long, 0.32 m wide and 0.5 m deep. A side view of the flume is shown in Figure 10 and a plan view in Figure 11. The actual test section was 3.7 m long, 0.1 m wide and 0.37 m deep. The test section had a wooden bed and plexi-glass sides.

The nozzle was streamlined and made of galvanized steel. The nozzle opening was 0.8 cm for the preliminary investigation and 0.5 cm thereafter. The flume slope could be adjusted but was kept level throughout the investigation.

B. CONSTANT HEAD ARRANGEMENT

To supply the hot water at a steady rate a constant head arrangement was used. Plate 1 shows the details of this arrangement. The water from the boiler was conveyed under city water pressure to a 200 liter mixing tank. From the mixing tank it was pumped up to a constant head overflow tank, by means of a small submersible pump. The constant head overflow tank was mounted about 3 m above the flume in order to provide the necessary head. From the constant head tank the hot water flowed through a flexible rubber hose to

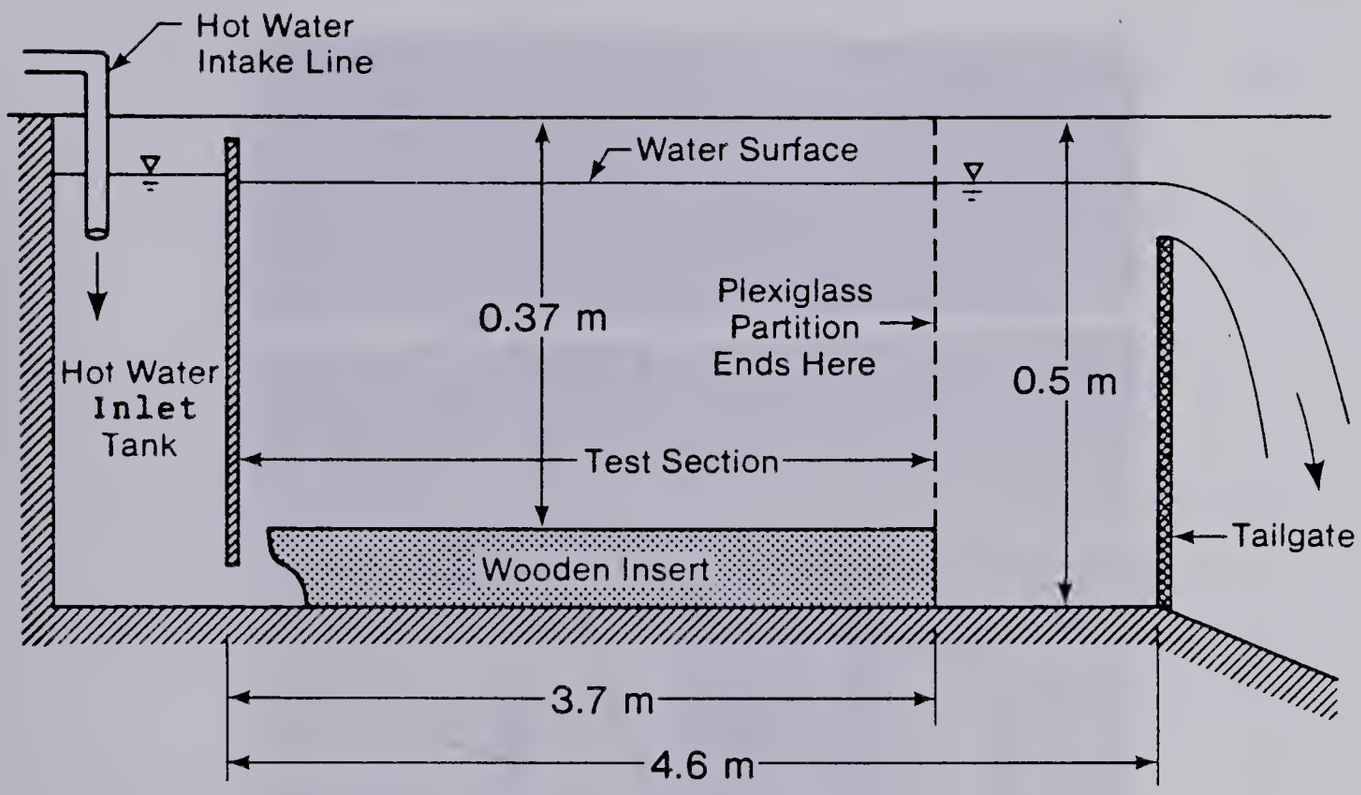

FIGURE 10. Side view of the testing flume.

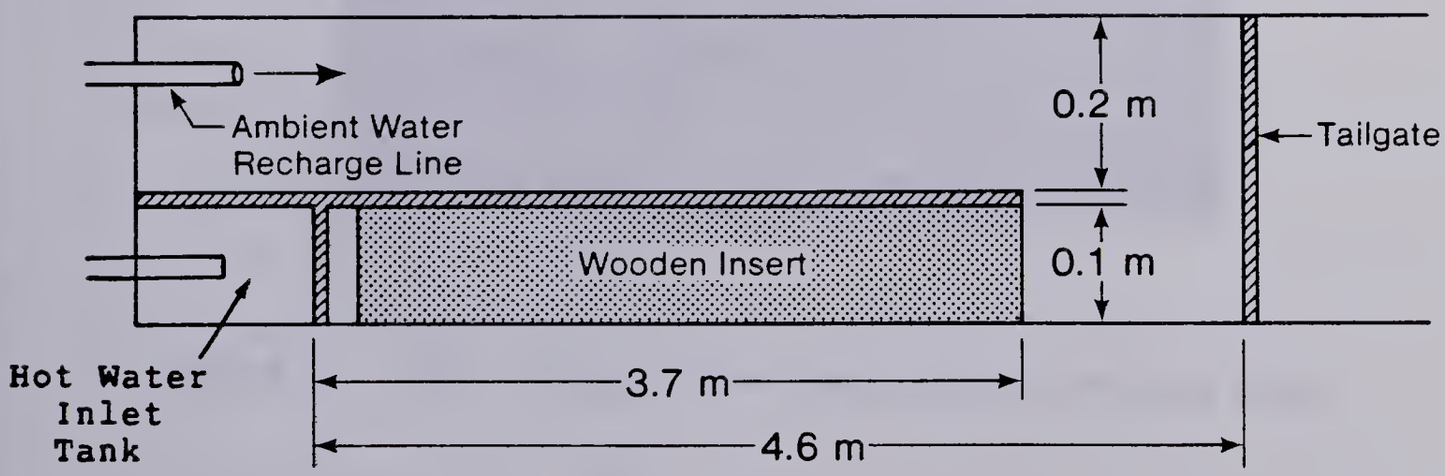

FIGURE 11. Plan view of the testing flume.

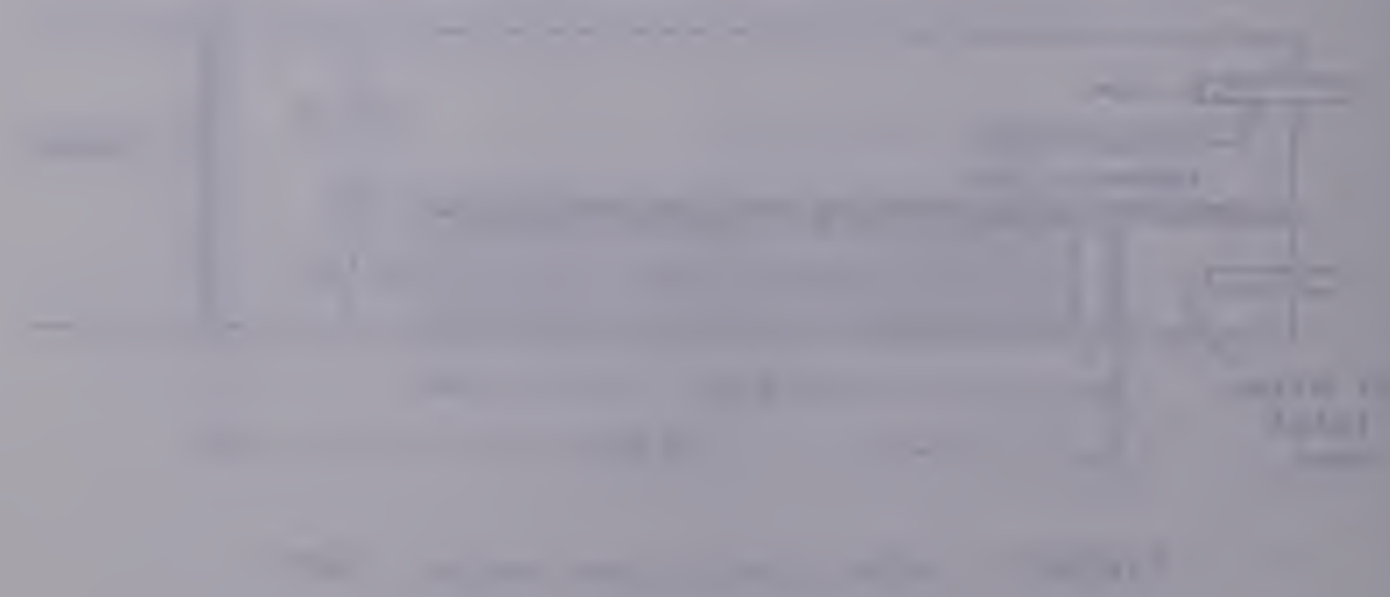

PLATE 1. The constant head tank and the mixing tank.

a rotameter and then into the hot water intake of the flume.

The mixing tank was installed after the first two runs because it was found that the boiler could not supply the hot water at a constant enough temperature. The first two runs were at high temperatures and the fluctuations in temperature were acceptable. However at lower temperatures the fluctuations increased and the mixing tank had to be installed to limit fluctuations to more acceptable levels.

C. ROTAMETER

The nozzle discharge was measured using a rotameter. It had a range of 0.015 liters/sec to 0.2 liters/sec (0.25 U.S. gal/min to 3.0 U.S. gal/min) and a scale which could be read to an accuracy of ±0.001 liters/sec (±0.02 U.S. gal/min). The rotameter was calibrated at three different temperatures, 60° C, 43° C and 21° C. The calibration chart is shown in Figure 12. The chart clearly indicates the rotameter has some sensitivity to temperature which follows from the fact that the dynamic viscosity varies from $1.81*10^{-5}$ N*sec/m at 20° C to $2.00*10^{-5}$ N*sec/m at 60° C (Roberson and Crowe, 1981). The calibration was carried out by volumetrically measuring the discharge over a set interval and then plotting the scale reading versus the measured discharge.

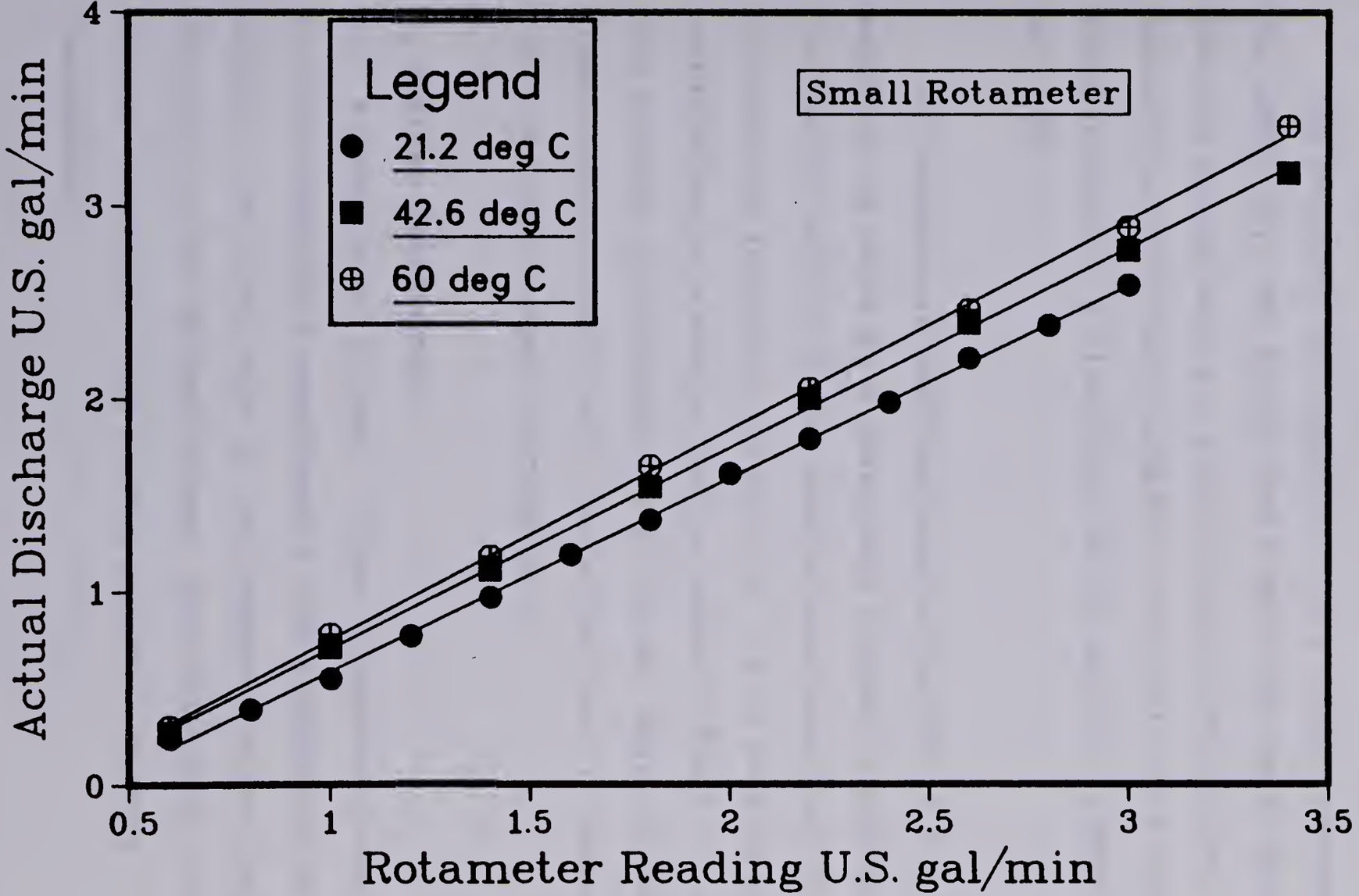

FIGURE 12. Rotameter calibration chart.

D. HOT WATER SUPPLY

The hot water was supplied from a boiler located within the laboratory. The boiler was a Delta Hot Water Blast Cleaning system having a burner input of 900,000 Btu. Operating at city water pressure, the boiler was capable of supplying up to 16 liters/min of hot water at temperatures up to 65° C.

At temperature settings greater than 35° C the boiler supplied the water at a reasonably constant temperature, fluctuating only 3° C. At temperatures lower than 35° C the fluctuations increased, to up to 8° C at a setting of 25° C. Installation of a mixing tank as shown in Plate 1 corrected this problem. The temperature in the hot water intake of the flume varied minimally with the mixing tank in operation, 0.6° C was the largest fluctuation.

E. DIGITAL THERMOMETER

A model 251A, Digitec, Digital Thermometer was used for all the temperature measurements. The thermometer had a range of -30° C to +100° C. The temperature was displayed digitally to two decimal places. The calibration of the digital thermometer was checked against a mercury thermometer.

F. PHOTOGRAPHIC EQUIPMENT

A Pentax MX camera was used for all the photography in the investigation. For the hydrogen bubble photographs the camera was mounted on a tripod and the shutter speed was 1/60 sec or 1/125 sec at an f-stop of 1.7. For the dye photographs the camera was handheld and the shutter speed was 1/30 sec at an f-stop of 1.7. Kodak VR100 film was used for all photographs. A tungsten 650 watt lamp was used for lighting in the hydrogen bubble photographs.

G. VELOCITY MEASUREMENTS

BACKGROUND

In this experimental investigation the velocities of interest were in the range from 1 cm/sec to 10 cm/sec. Several methods of measuring the velocity were attempted. A pitot tube with a pressure transducer to measure the difference between the static and dynamic heads was tried. This method was unsuccessful because the most sensitive transducer was not sensitive enough to pick up the small head differences at the low velocities. A pitot tube with a manometer filled partially with benzaldehyde, a substance which is 104.4% the density of water, which magnified the head difference by 22.7 times was also tried. This method was unsuccessful because the response time of the manometer was as long as one hour. Finally the hydrogen bubble method

was tried and found to be very successful.

BASIC DESCRIPTION

The hydrogen bubble method of velocity measurement is ideally suited for the measurement of very low velocities. In this method a fine wire is placed in the flow and subjected to an electrical impulse. The impulse causes electrolysis of water near the wire and small hydrogen bubbles to form on the wire. As each electrical impulse transmits through the wire a row of hydrogen bubbles forms on the wire and is swept off by the drag of the flowing water. The result is rows of small hydrogen bubbles downstream of the wire. To determine the velocity a photograph was taken similar to the one in Plate 2. From the photograph the distance between the rows of bubbles was measured. Knowing the appropriate scale factor for the photograph and the time between the impulses the velocity can be calculated. The longitudinal velocity u is given by:

$$u = \frac{\Delta x}{\bar{S}\,\bar{T}} \tag{79}$$

where Δx is the distance in cm between the rows of bubbles from the photograph, $\bar{T}$ is the time between pulses in seconds and $\bar{S}$ is the scale factor for the photograph. The scale factor was determined by photographing a scale at the same point in the water as where the wire was placed. $\bar{S}$ is the

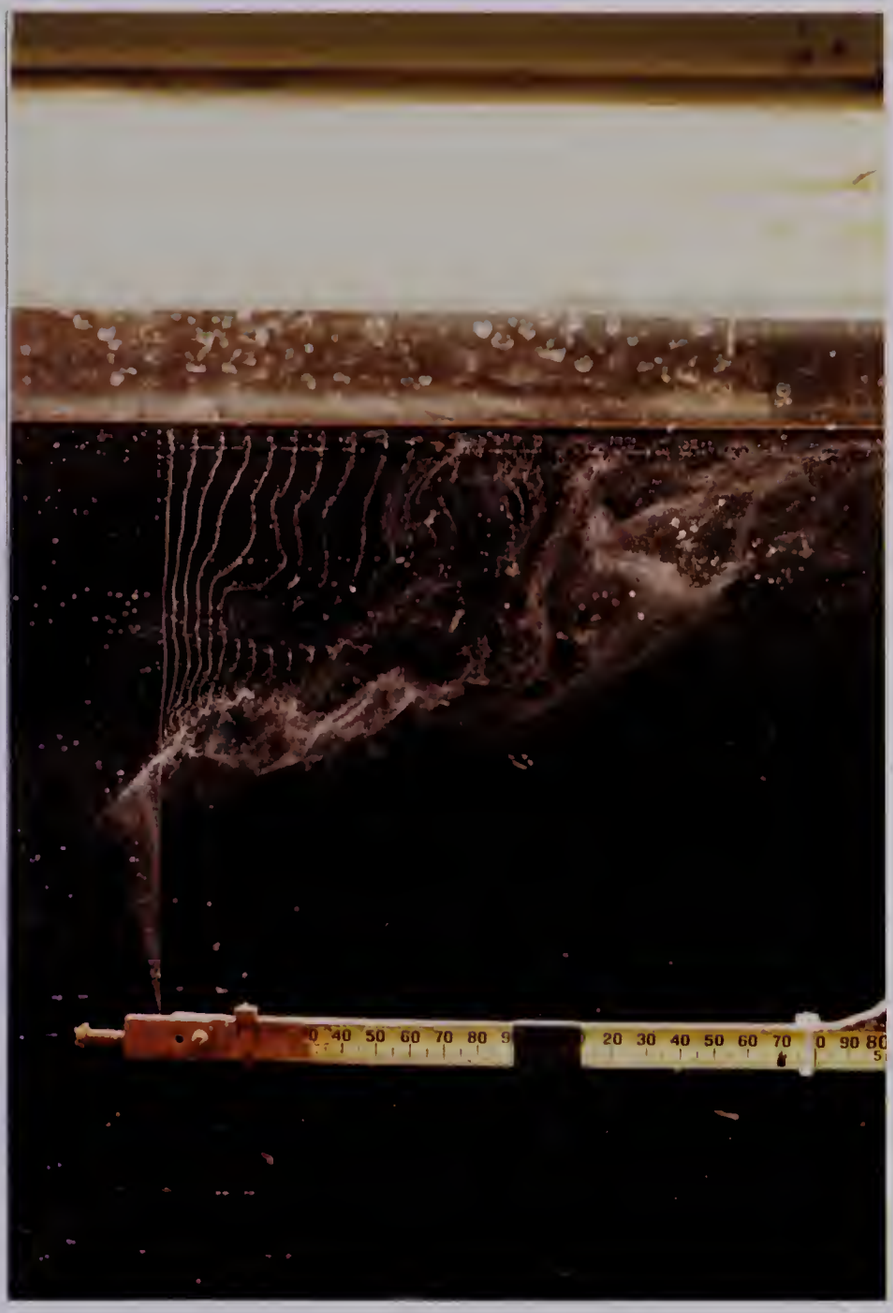

PLATE 2. A typical hydrogen bubble photograph.

ratio of the average distance between rows of bubbles on the photograph and the actual distance in the water. A more complete treatment of the hydrogen bubble method of velocity measurement can be found in Pande (1975).

HYDROGEN BUBBLE APPARATUS

A view of all the equipment used to produce the hydrogen bubbles is shown in Plate 3. The power supply was capable of providing up to 600 volts. The pulse generator could produce pulse frequencies from 0.5 Hz to 45 Hz and a pulse width from 0.6 msec to 8.5 m sec. An oscilloscope and digital frequency meter were used to determine the pulse period and width. As shown in Plate 4 the tungsten wire was mounted on a plastic frame. The wire used was 0.06 mm diameter and a 27 cm length was used to span the frame. A block diagram of the equipment set-up is illustrated in Figure 13.

OPERATIONAL CONSIDERATIONS

The clearest and strongest rows of bubbles were obtained at a voltage of 400 and at the widest pulse width of 8.5 msec. At narrower pulse widths and lower voltages the bubble rows tended to be easily broken up and more difficult to see in the photographs.

PLATE 3. The hydrogen bubble electronic equipment.

PLATE 4. Tungsten wire and plastic frame.

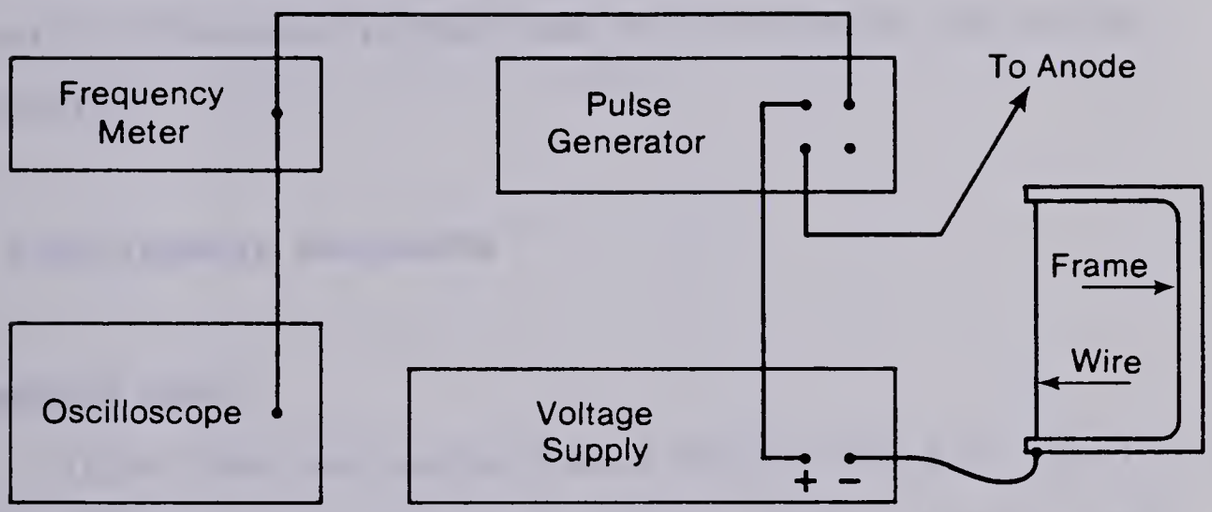

FIGURE 13. Block diagram of the hydrogen bubble equipment.

At discharges higher than 0.08 liters/sec, there were so many air bubbles in the hot water coming from the boiler that the rows of hydrogen bubbles were indistinguishable in the photographs. To circumvent this problem the higher densimetric Froude numbers were obtained by lowering the density difference rather than by increasing the outlet velocity.

H. EXPERIMENTAL PROCEDURE

COMPLETE RUNS

After some preliminary work which helped to clarify the problem, six detailed runs were done. The outlet F_o was varied from 0.85 to 13.82 and the submergence ratio H/b_o was varied from 43 to 68. Table 1 gives a complete listing of the relevant parameters. The outlet densimetric Froude number at the nozzle is defined as:

$$F_o = \frac{U_o}{\sqrt{g \frac{\Delta \rho_o}{\rho_a} b_o}} \tag{80}$$

and the outlet Richardson number is defined as:

$$R_{io} = \frac{g \frac{\Delta \rho_o}{\rho_a} b_o}{U_o^2} \tag{81}$$

The two are related by the following expression:

Run No.	F_o	Ri_o	T_o (°C)	T_a (°C)	H/b_o	U_o (cm/s)
1	13.82	0.00524	26.4	13.7	68	15.6
2	10.13	0.00975	25.3	14.5	68	10.6
3	9.05	0.0122	29.1	12.6	68	11.9
4	6.22	0.0258	29.2	14.2	68	8.0
5	2.83	0.125	41.4	14.6	43	7.0
6	0.85	1.384	36.1	14.7	43	1.8

TABLE 1. The relevant parameters for the 6 complete runs.

$$R_{io} = \frac{1}{F_o^2} \tag{82}$$

For each of the six runs, velocity profiles were taken downstream of the outlet at 10cm intervals, up to a distance of 100cm. The profiles were obtained by taking three photographs of the hydrogen bubbles at each cross-section. Approximately 7 data points were used to define a profile. Each data point was obtained by taking 2 measurements from each photograph for a total of six velocities which were then averaged to give the average longitudinal velocity at that point. The first measurement was obtained by taking the distance between the first and second rows of bubbles and dividing it by the period .The second measurement was obtained by taking the distance between the first and third rows and dividing it by twice the period. Figures 14-19 show all of the velocity profiles for the six runs. The data was connected by straight lines in Figures 14-19 to make it

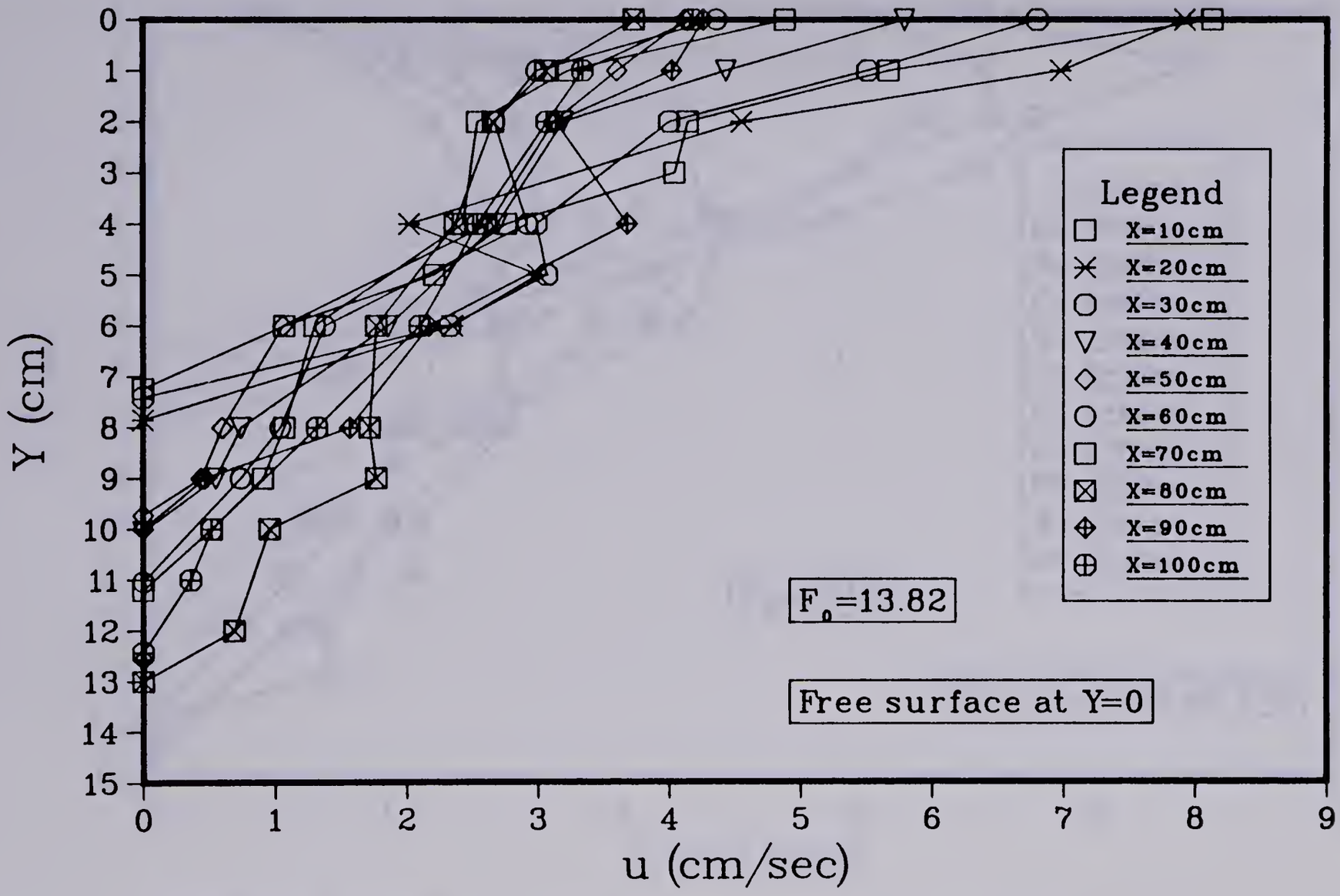

FIGURE 14. Dimensional velocity profiles for run where F_0=13.82.

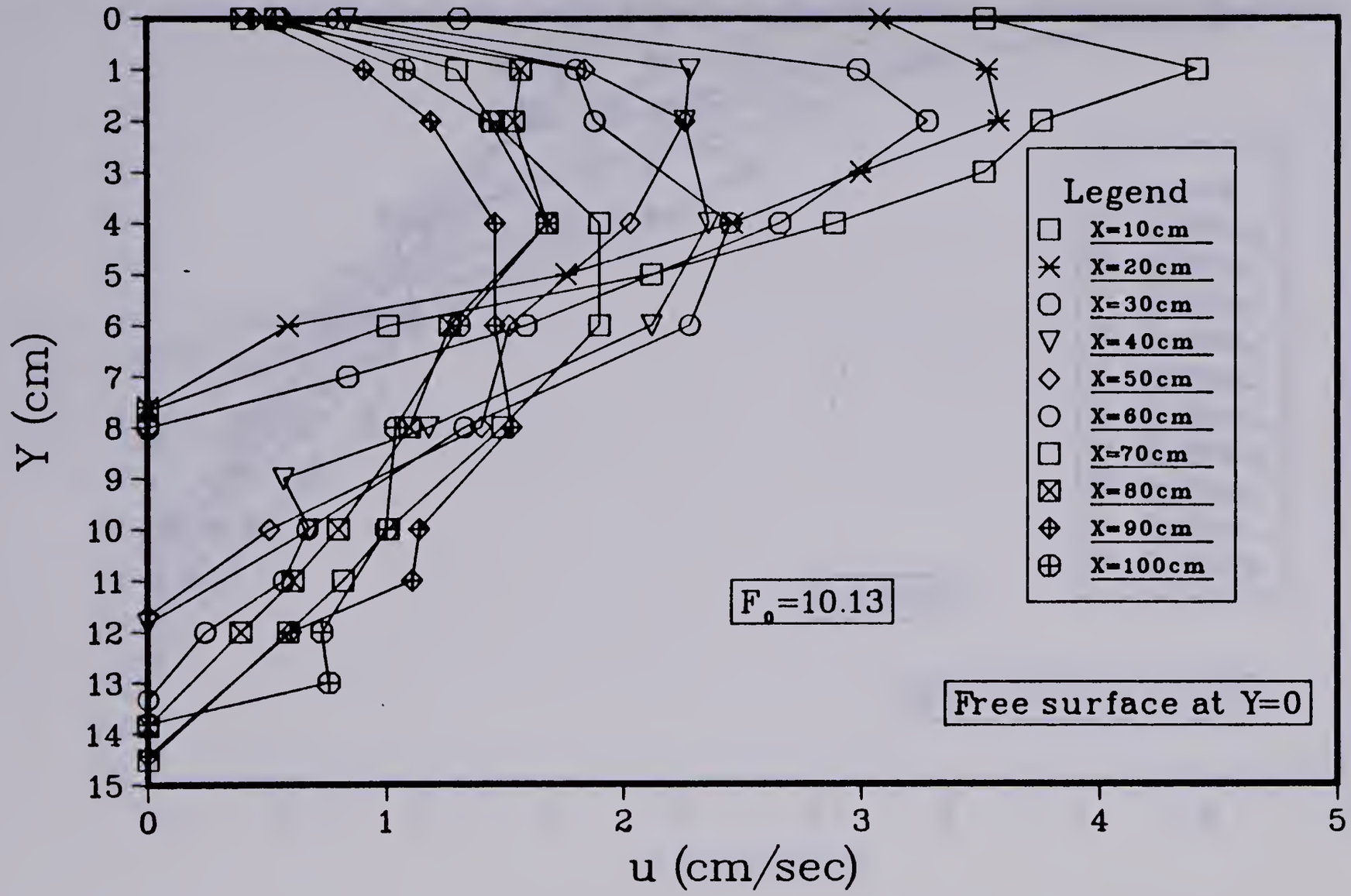

FIGURE 15. Dimensional velocity profiles for run where F_o=10.13.

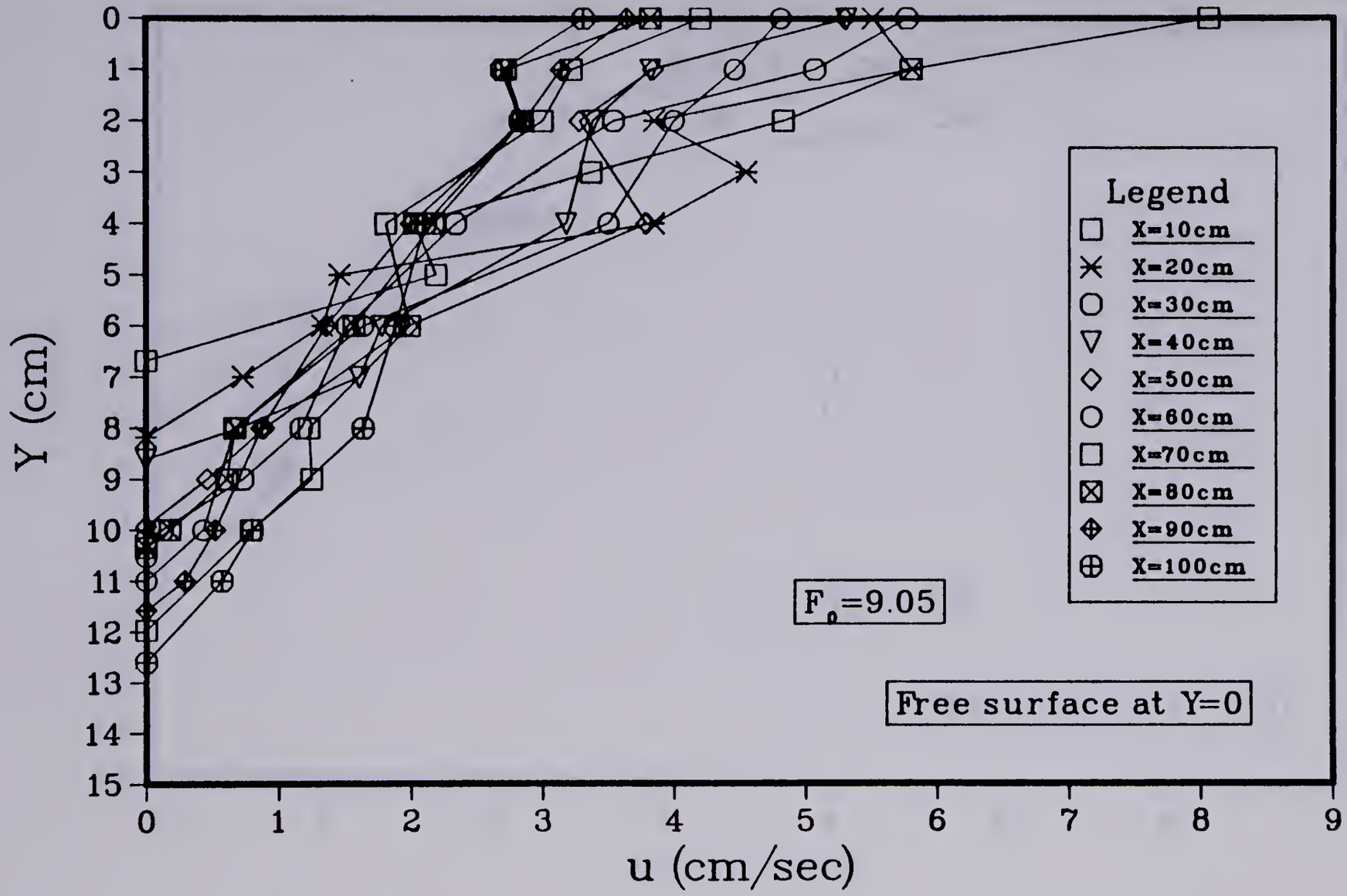

FIGURE 16. Dimensional velocity profiles for run where F_o=9.05.

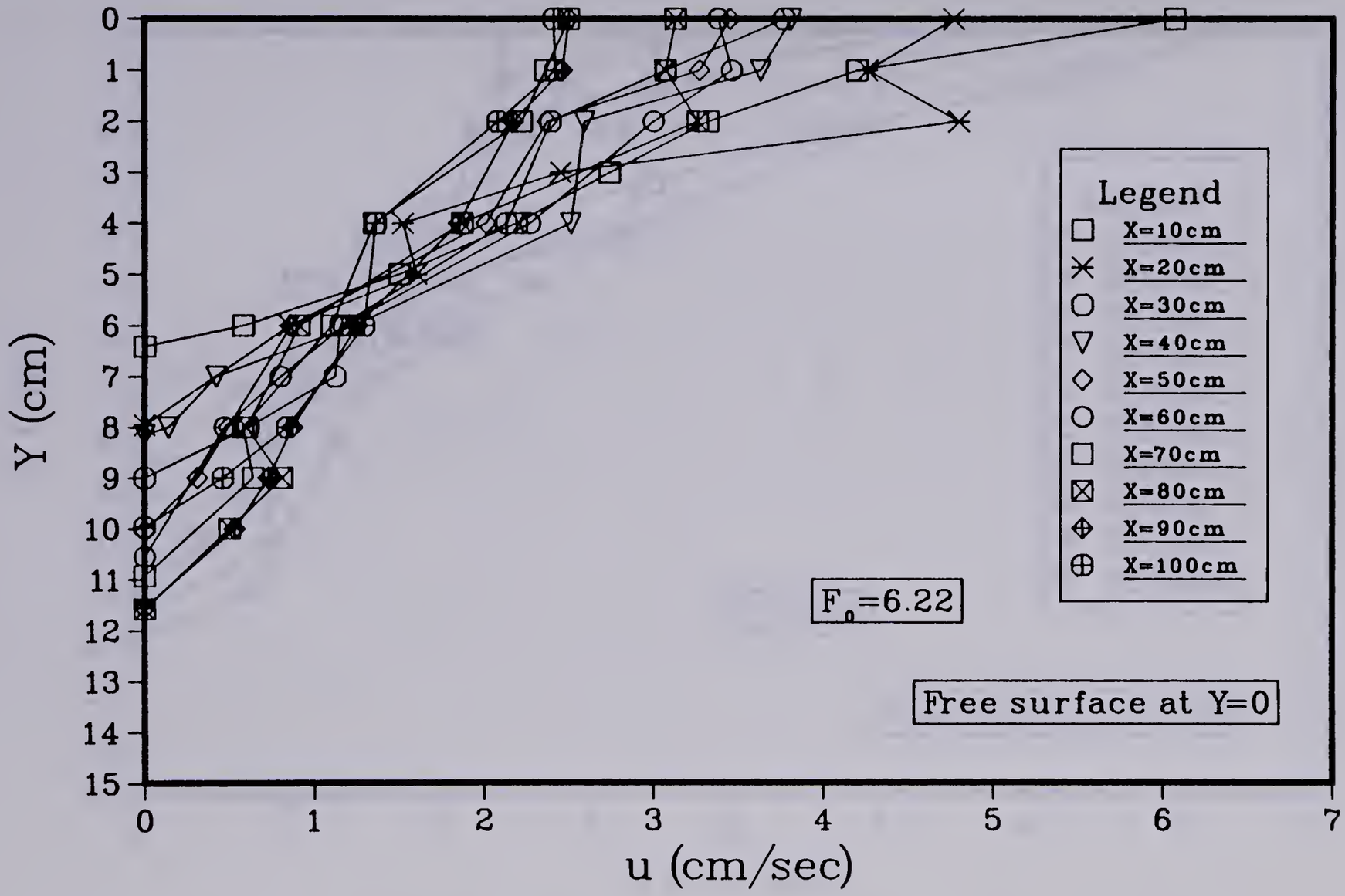

FIGURE 17. Dimensional velocity profiles for run where F_o=6.22.

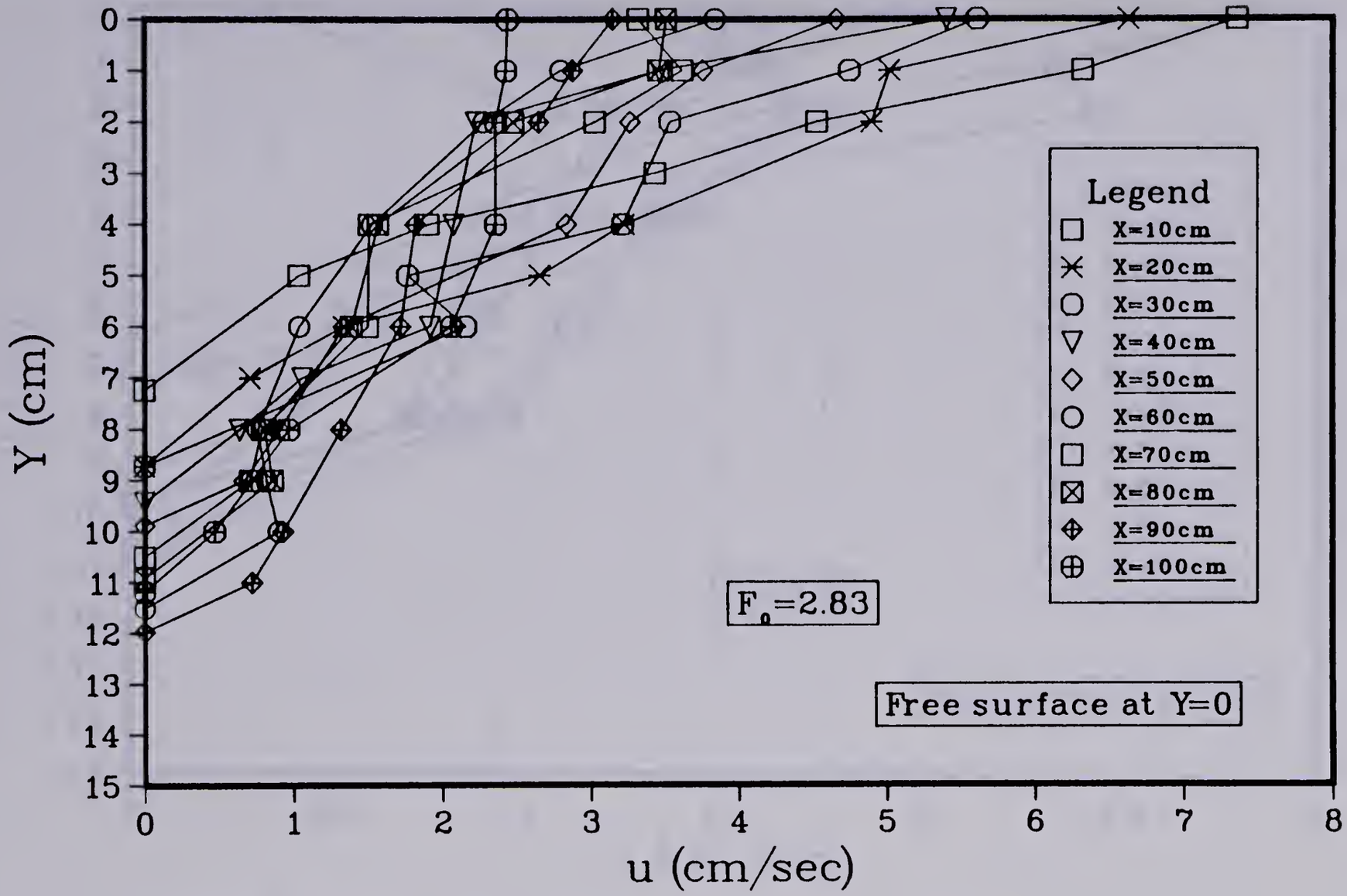

FIGURE 18. Dimensional velocity profiles for run where F_o=2.83.

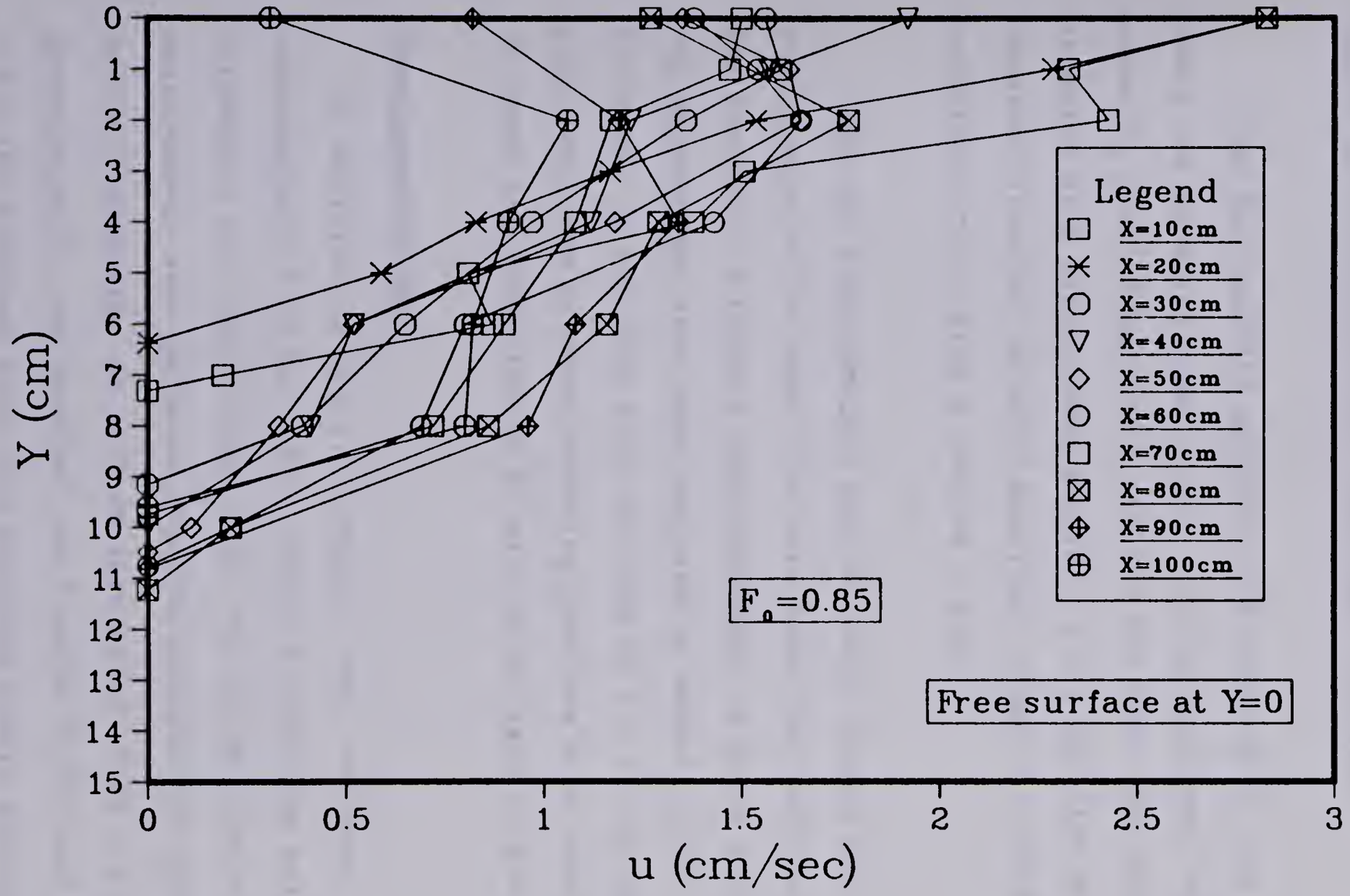

FIGURE 19. Dimensional velocity profiles for run where F_0=0.85.

easier to distinguish the individual profiles.

From the velocity profiles the value of $\bar{b}_u$ the point where the velocity goes to zero, can be obtained. Figure 20 shows $\bar{b}_u$ plotted against x for the six runs. The maximum velocity at a given cross-section, u_m, can also be readily obtained from the velocity profiles. Figure 21 shows the variation of u_m with x for the 6 runs.

Dye was injected into the hot water intake and photographs of the dyed flow were taken for each run (except for Fo=0.85). A typical dye photograph is shown in Plate 5. The photographs were then analyzed by measuring the thickness of the dyed flow, defined as $\bar{b}_c$, at the same cross-sections at which velocity profiles were taken. Figure 22 shows the variation of $\bar{b}_c$ with x for each of the 5 runs.

SUPPLEMENTARY RUNS

In addition to the six complete runs, thirteen supplementary runs were done. Table 2 lists the relevant parameters for the thirteen runs. For these runs no velocity measurements were gathered. Dye photographs and hydrogen bubble photographs at x=10 cm were taken. From the dye photographs $\bar{b}_c$ was obtained and Figures 23-25 show $\bar{b}_c$ versus x for the thirteen runs. The hydrogen bubble photographs at x=10 cm were used to determine $\bar{b}_u$ the distance from the free

surface to the point where the velocity goes to zero.

Run No.	F_o	Ri_o	T_o (°C)	T_a (°C)	H/b_o	U_o (cm/s)
sup1	6.70	0.022	25.2	11.1	28.6	7.60
sup2	2.96	0.144	24.8	11.1	28.6	3.30
sup3	8.22	0.015	25.3	11.1	37	9.30
sup4	4.70	0.045	25.2	11.2	37	5.30
sup5	13.45	0.0055	25.4	11.8	47	15.1
sup6	6.72	0.022	25.4	11.8	47	7.60
sup7	2.08	0.23	59	11.8	68	5.80
sup8	4.42	0.051	26.6	11.5	68	5.30
sup9	8.38	0.014	26.8	11.8	68	10.1
sup10	12.41	0.0065	27	11.9	68	15.1
sup11	16.72	0.0036	27.1	12.1	68	20.3
sup12	21.11	0.0022	27.1	12.4	68	25.5
sup13	26.78	0.0014	26.7	12.3	68	31.8

TABLE 2. The relevant parameters for the 13 supplementary runs.

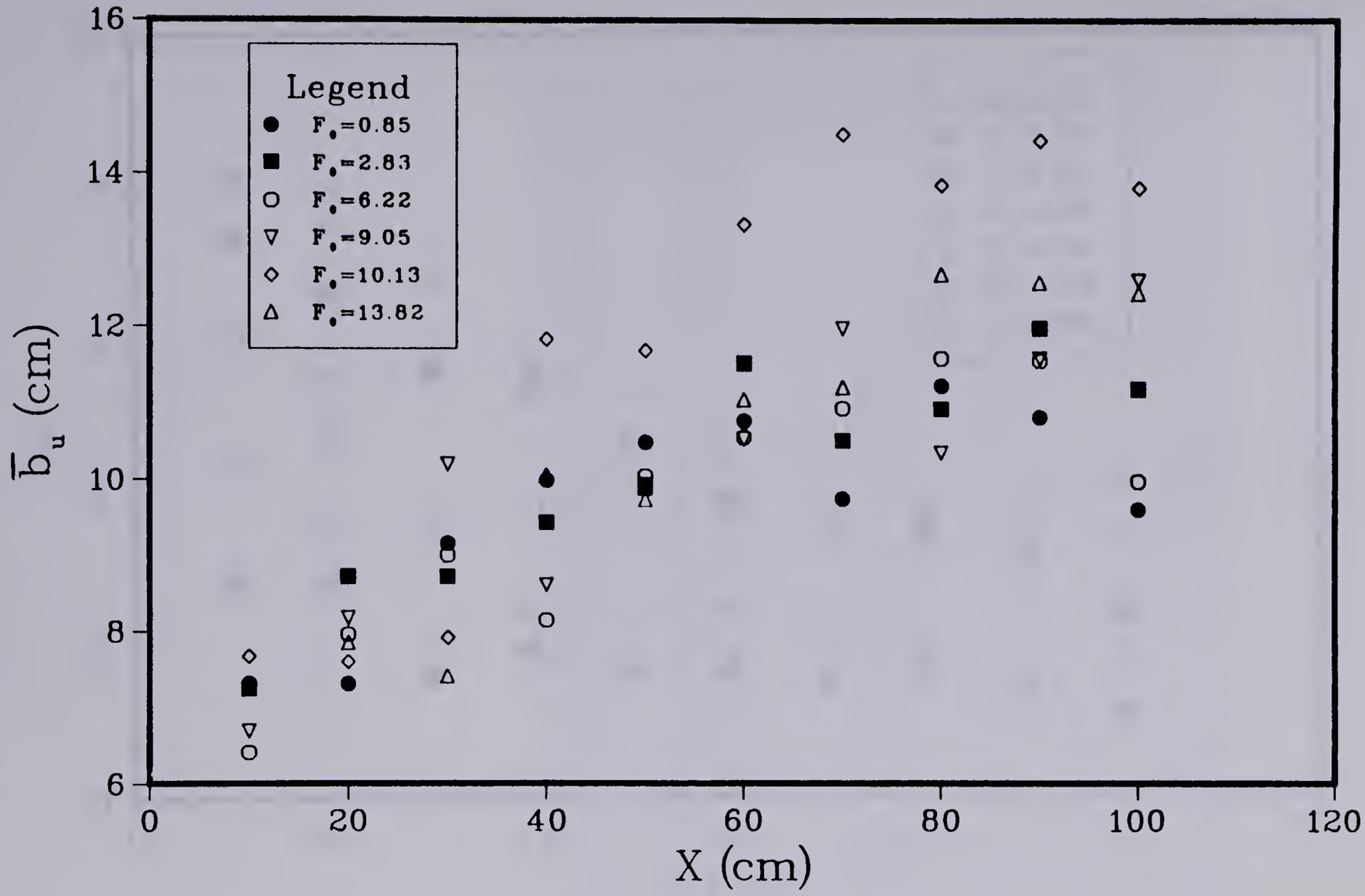

FIGURE 20. The variation of the velocity width for the 6 complete runs.

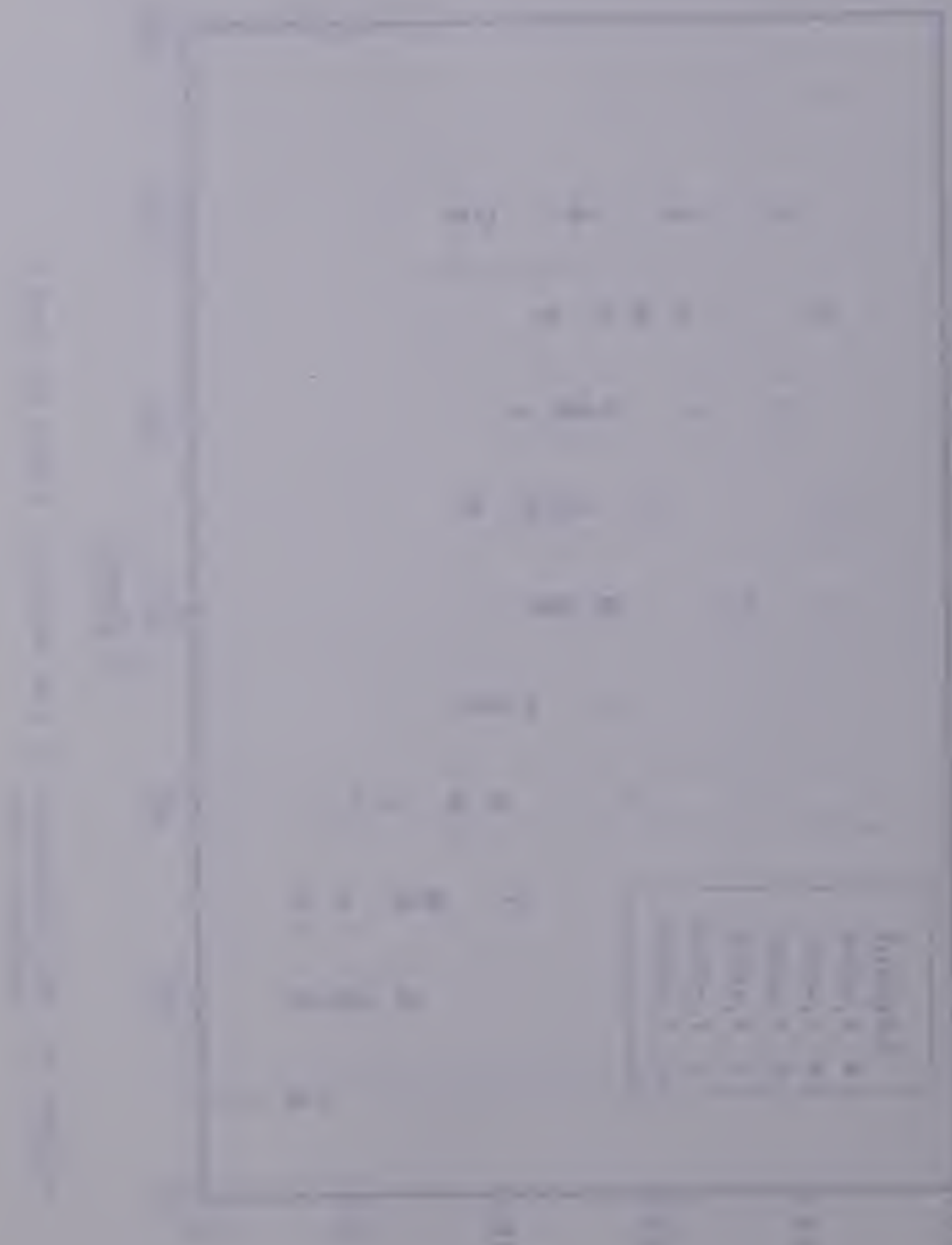

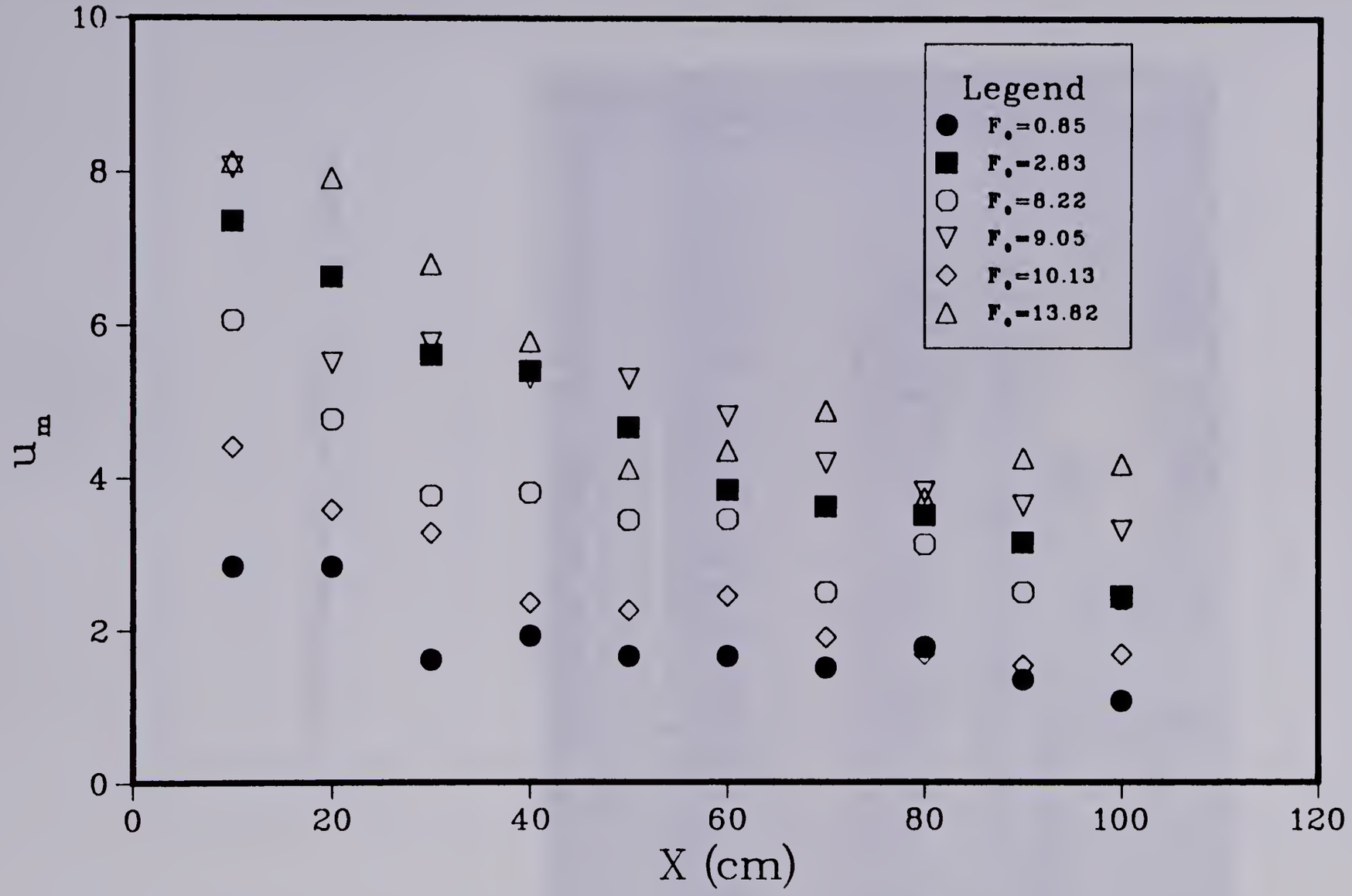

FIGURE 21. The variation of the maximum velocity for the 6 complete runs.

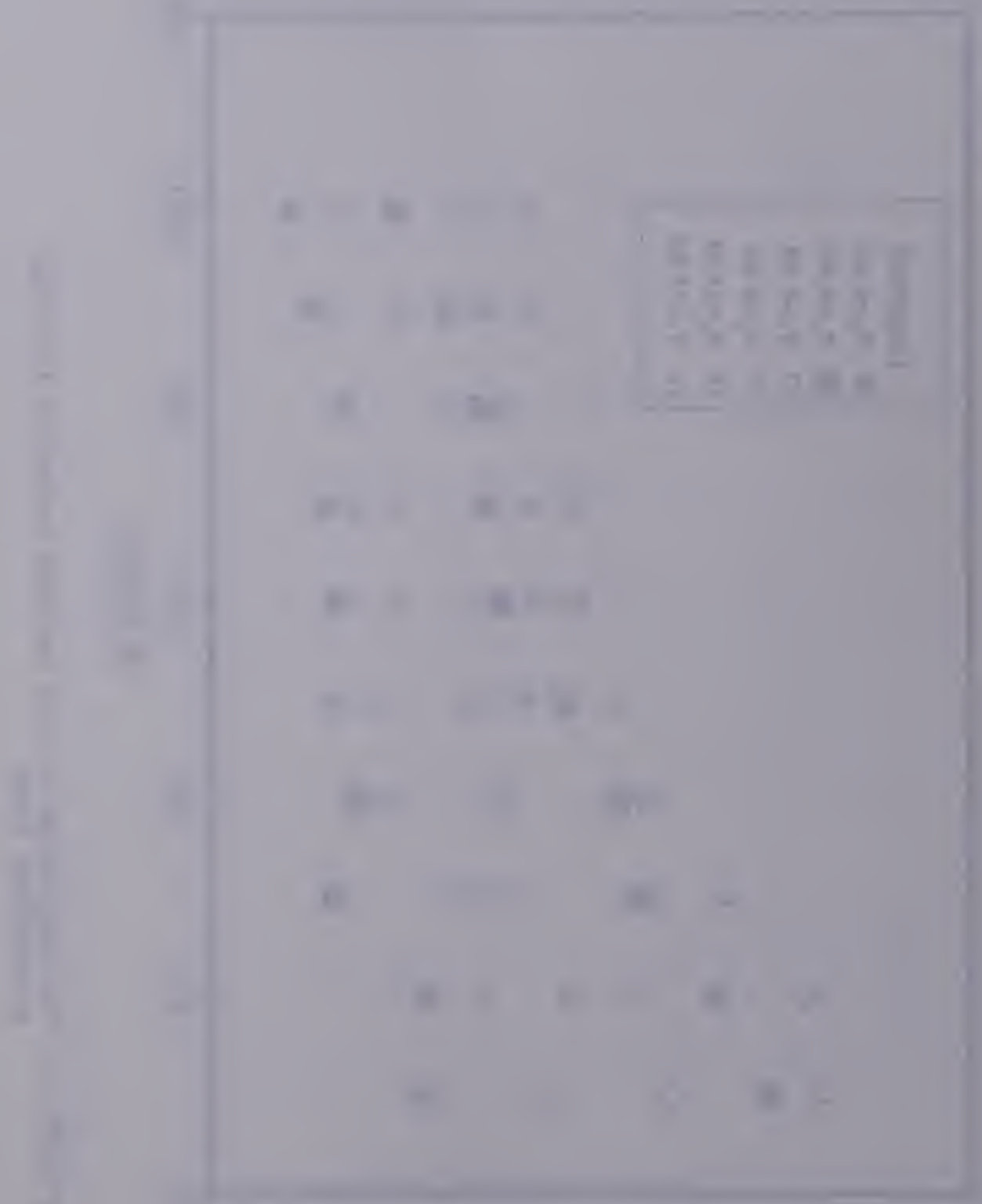

PLATE 5. A typical dye photograph.

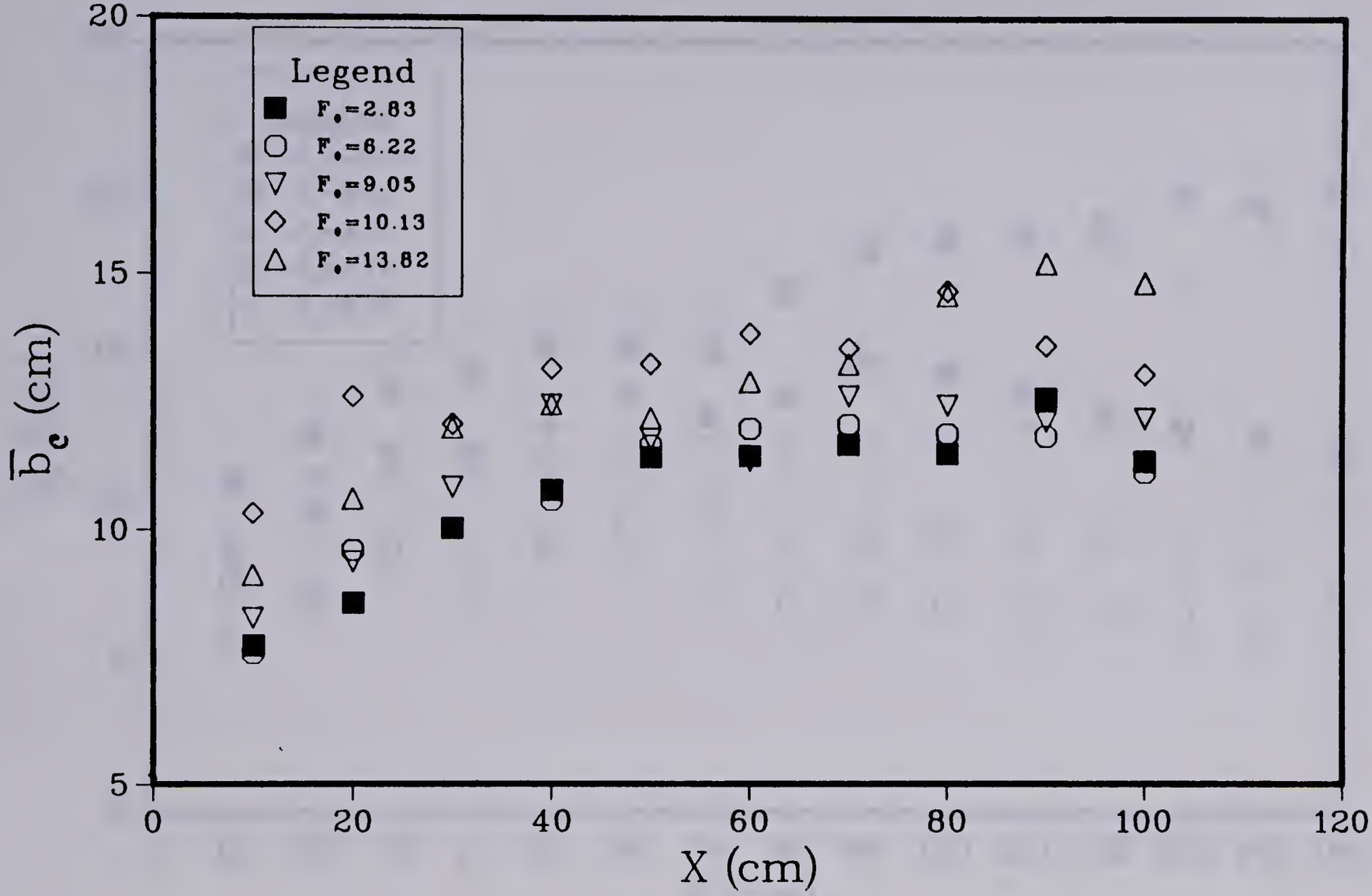

FIGURE 22. The variation of the pollutant width for the 6 complete runs.

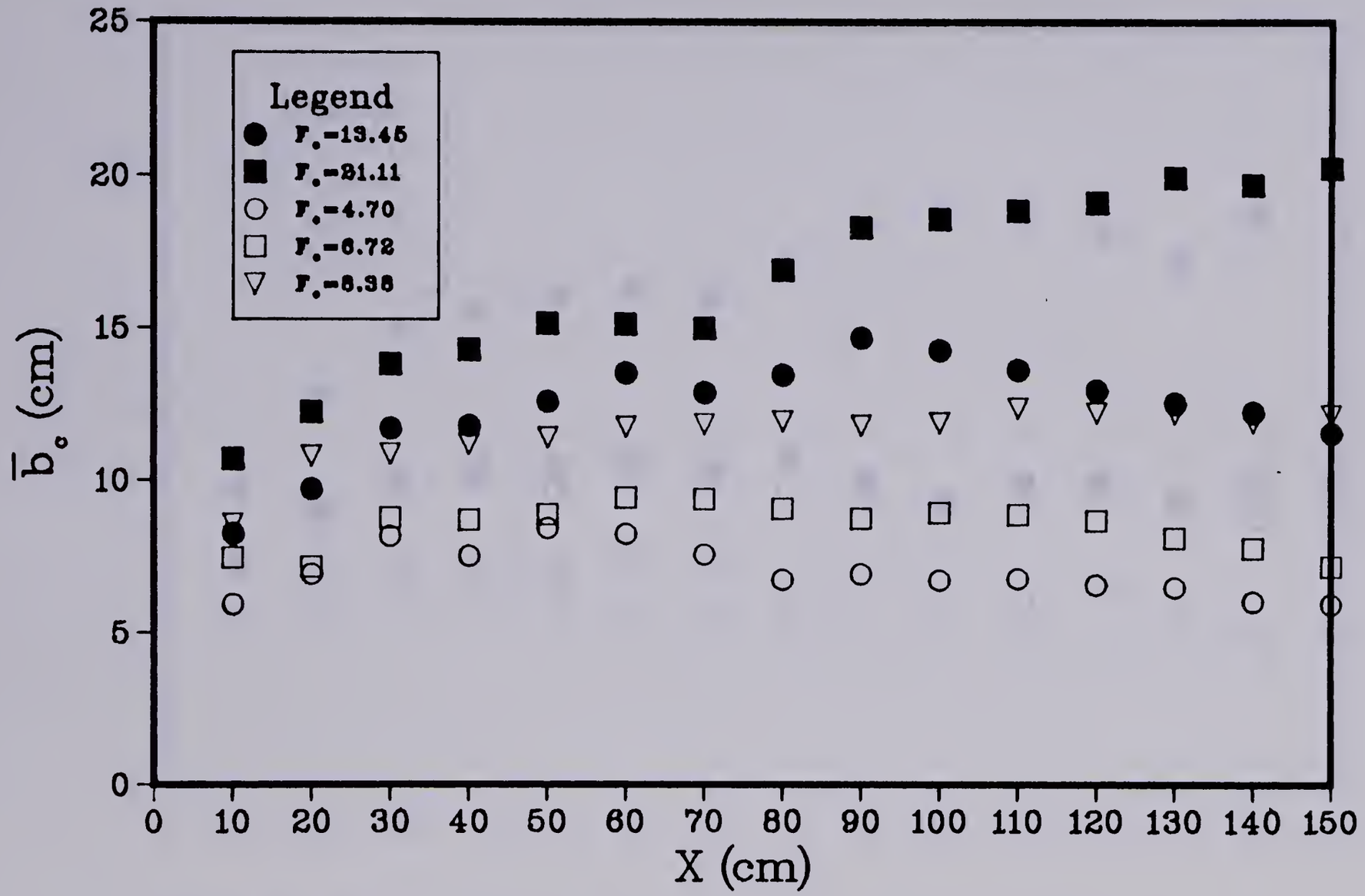

FIGURE 23. The variation of the pollutant width for 5 of the supplementary runs.

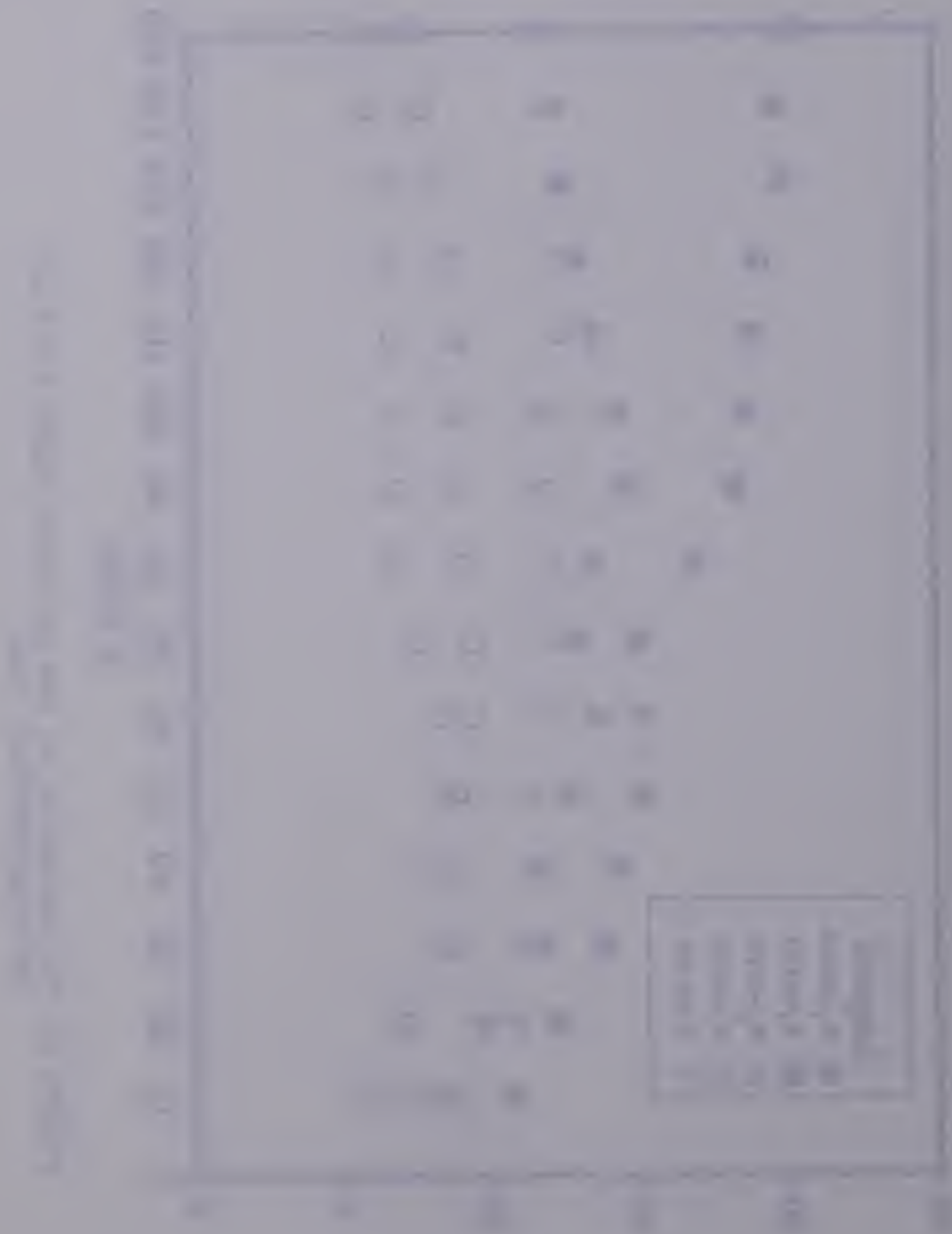

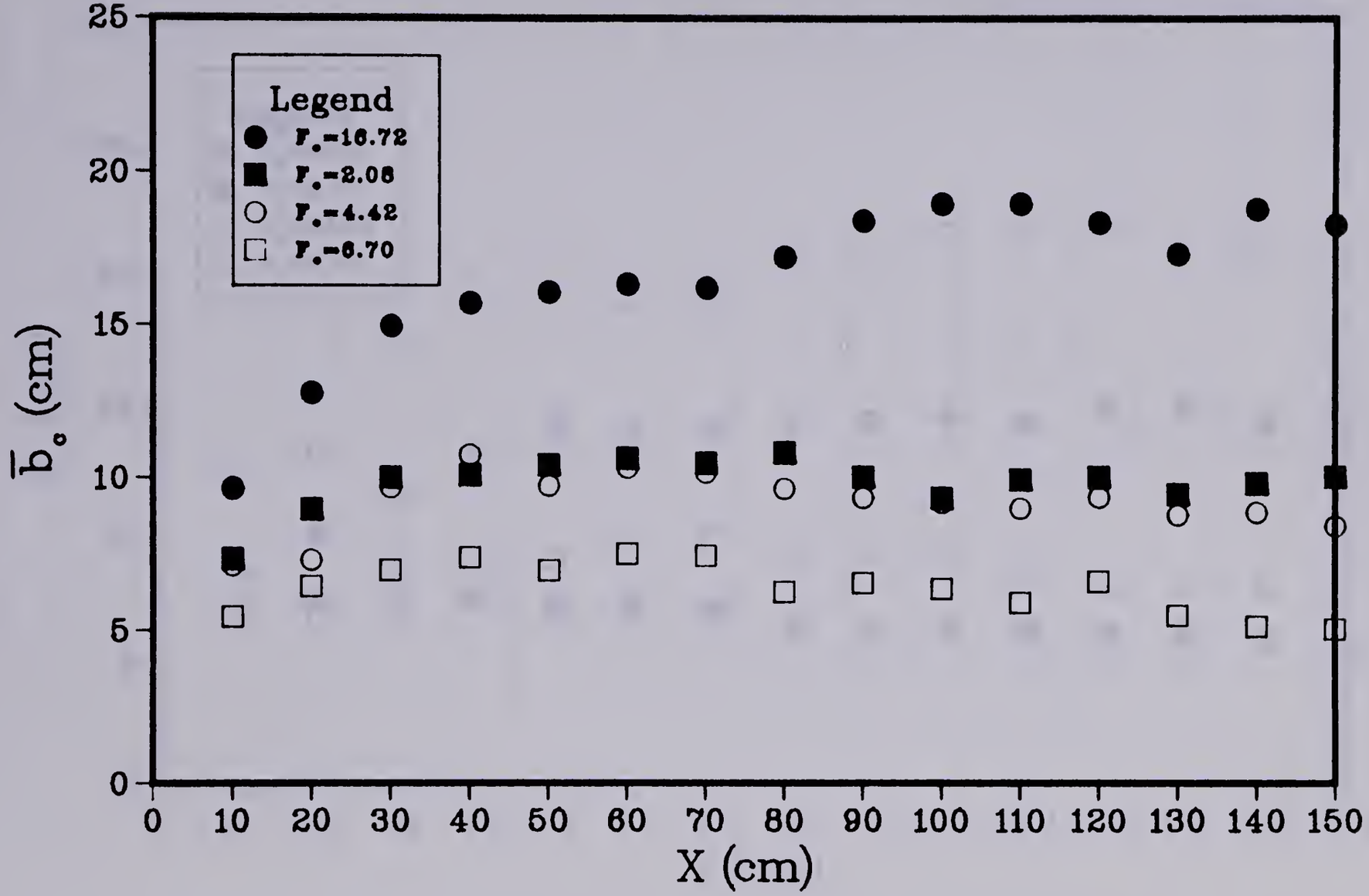

FIGURE 24. The variation of the pollutant width for 4 of the supplementary runs.

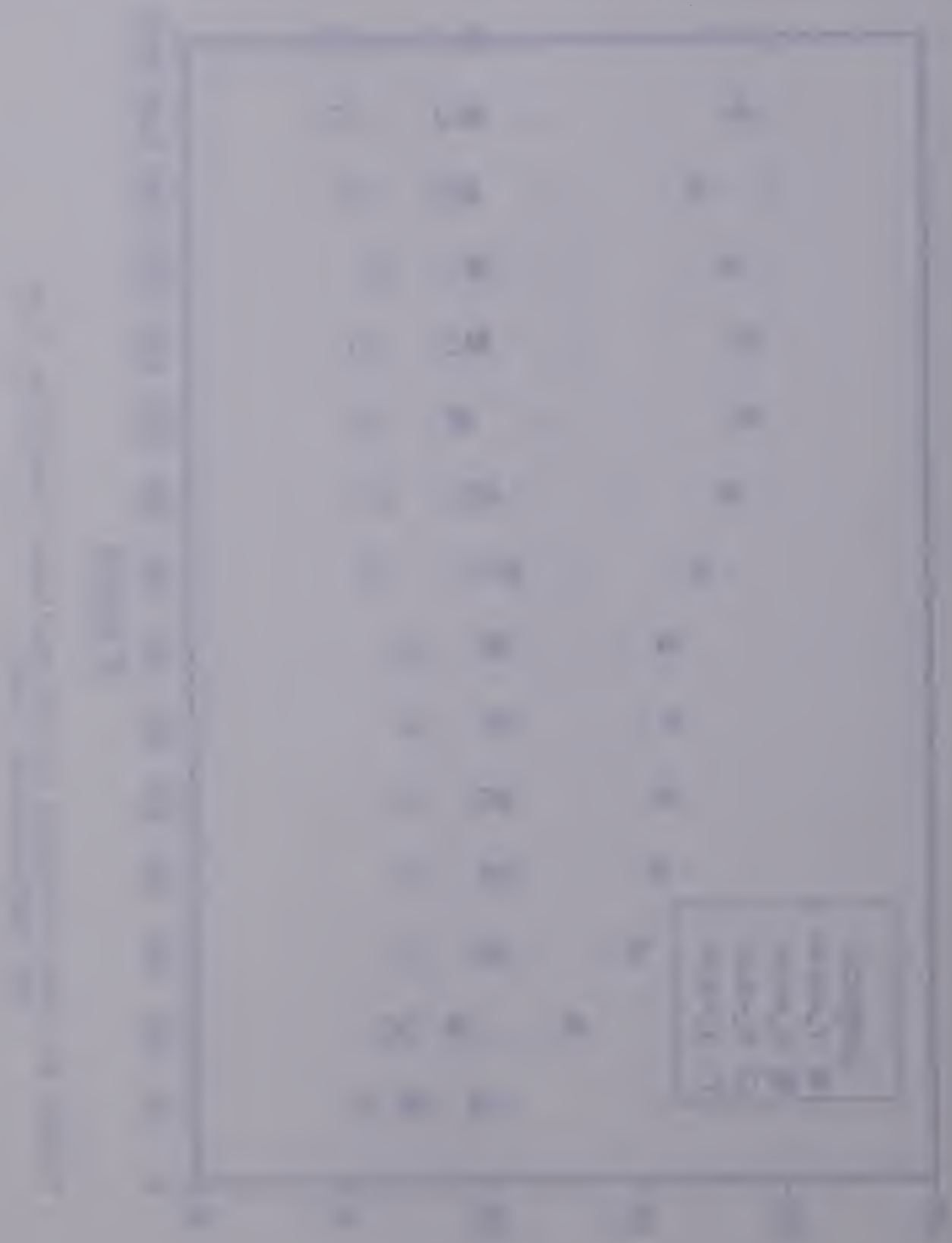

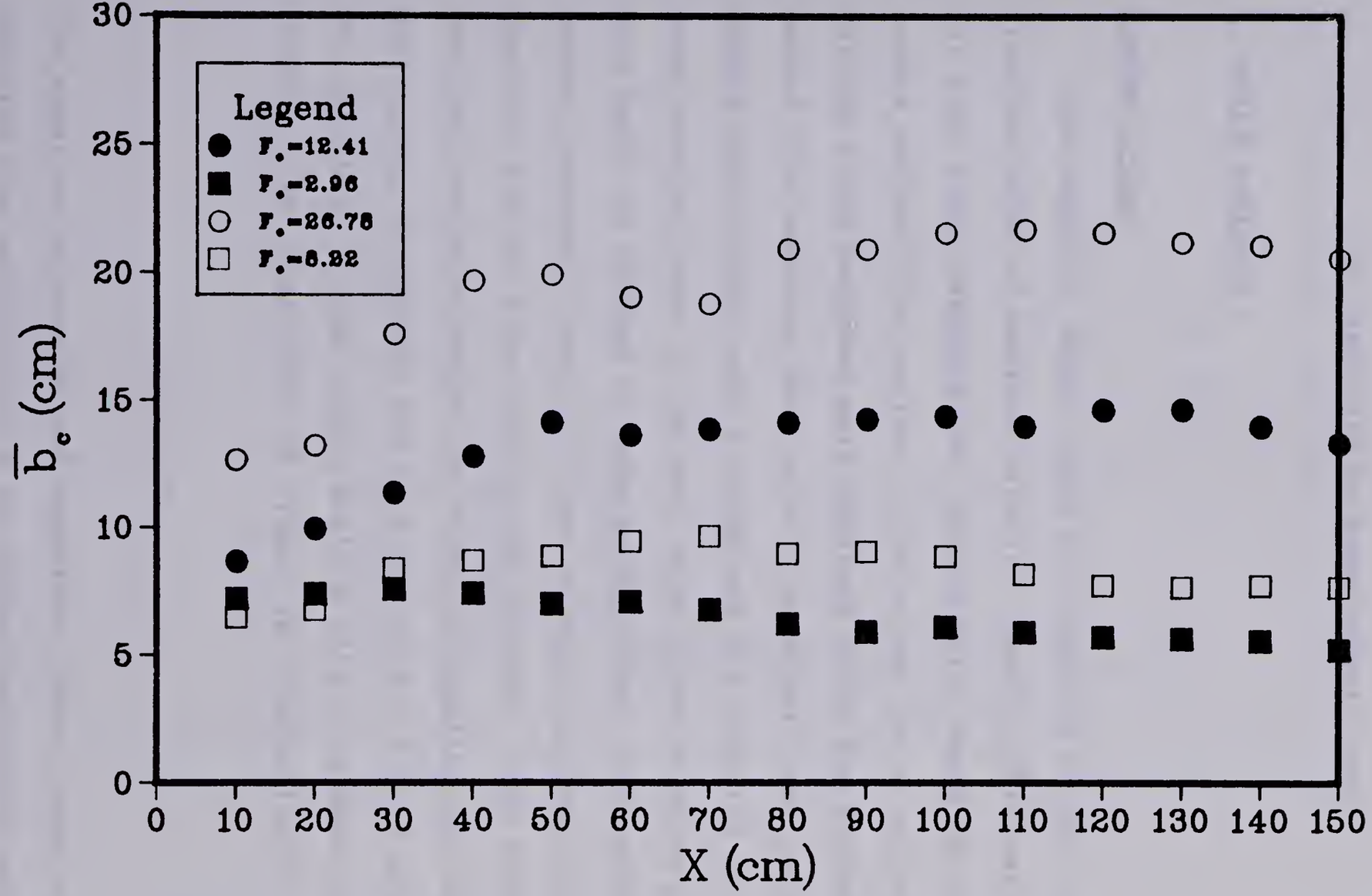

FIGURE 25. The variation of the pollutant width for 4 of the supplementary runs.

IV. ANALYSIS OF EXPERIMENTAL DATA

A. SCALE ANALYSIS

LENGTH SCALES

The velocity length scale b is defined as the distance from the point of maximum velocity, usually the free surface for this flow configuration, to the point where the velocity equals one half the maximum . The values for b at the various cross sections were obtained using the following method. The velocity data points, measured from the hydrogen bubble photographs, were plotted and the profiles for each cross section drawn in by hand. Hand drawn velocity profiles were used, as opposed to some mathematical interpolation scheme, because it was felt that a purely mathematical approach did not allow for enough judgment. From these profiles the point where the velocity equalled one half the maximum was determined and thus values for b were obtained. The variation of the length scale b with x is shown plotted in Figure 26. Also shown in Figure 26 is equation 83,

$$b = 0.07\ x \tag{83}$$

the equation Rajaratnam and Humphries (1984) found to describe the variation of b for plane non-buoyant surface jets. There is considerable scatter in the data but b for

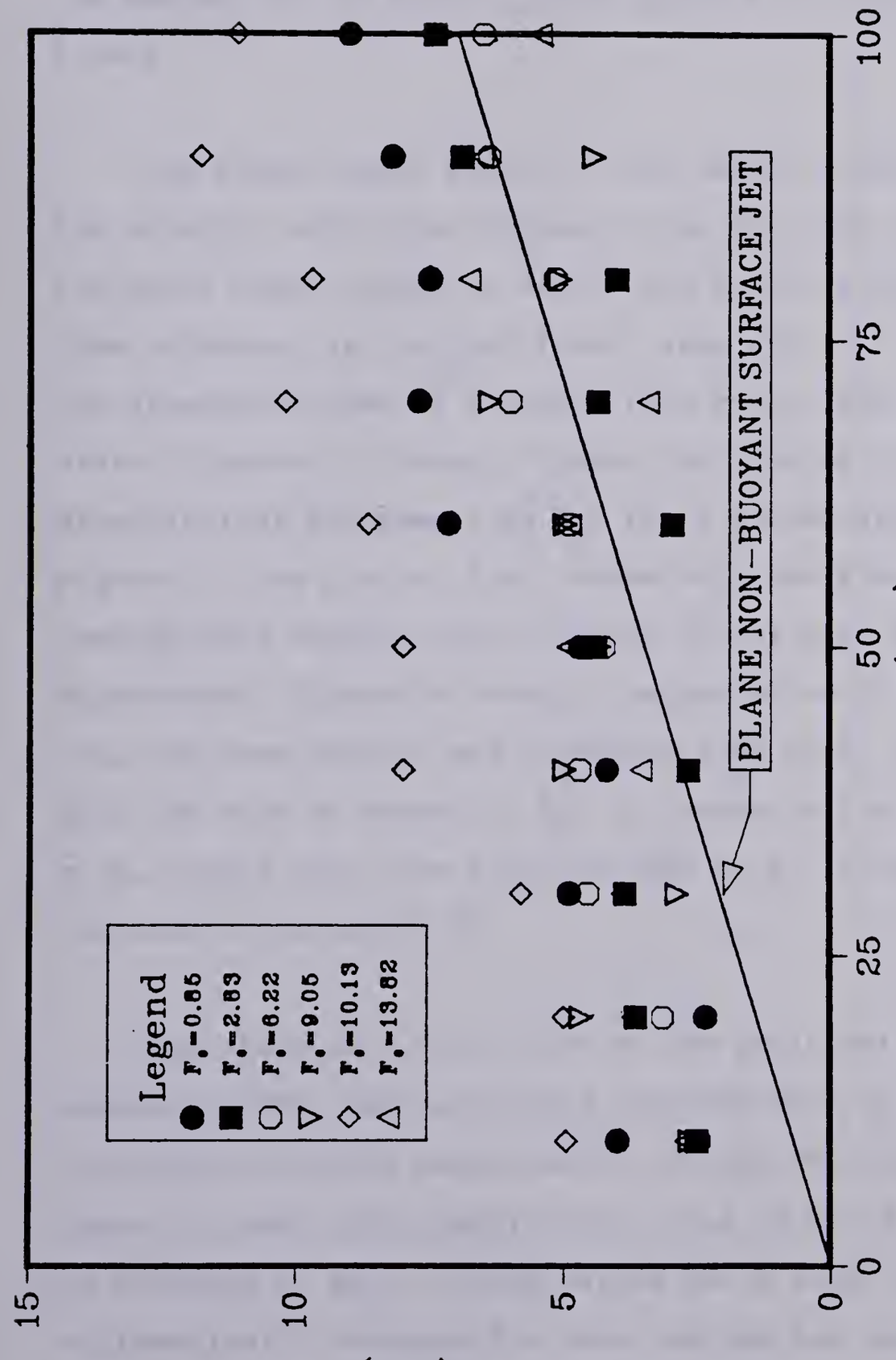

FIGURE 26. The variation of the velocity half width for the 6 complete runs.

the buoyant jet in shallow water appears to increase more slowly.

The three length scales, b the velocity half-width, $\overline{b_u}$ the velocity width (the distance from the free surface to the point where u goes to zero), and $\overline{b_c}$ the pollutant width (the thickness of the dyed flow), were all non-dimensionalized by dividing them by b_o, the outlet width. Figures 27 through 29 show their variation with the dimensionless distance x/b_o for the six complete runs. Figure 27, the plot of b/b_o versus x/b_o contains considerable scatter and no trends in the data are discernable. Figure 28 showing the variation of $\overline{b_u}/b_o$ with x/b_o has less scatter and indicates that as F_o increases so does the rate of spread of $\overline{b_u}$. In Figure 29 the plot of $\overline{b_c}/b_o$ versus x/b_o, the trend is that as F_o increases so does the rate of spread of $\overline{b_c}$.

The value of K, the ratio of the pollutant width to the velocity width, was calculated from the data of the five runs where velocity measurements and dye photographs were taken. At each cross section the value of K was determined by dividing $\overline{b_c}$ by $\overline{b_u}$. These values for K were then arithmetically averaged for each run and are presented in Table 3. The 5 values were then arithmetically averaged again to provide a final value for K as shown in

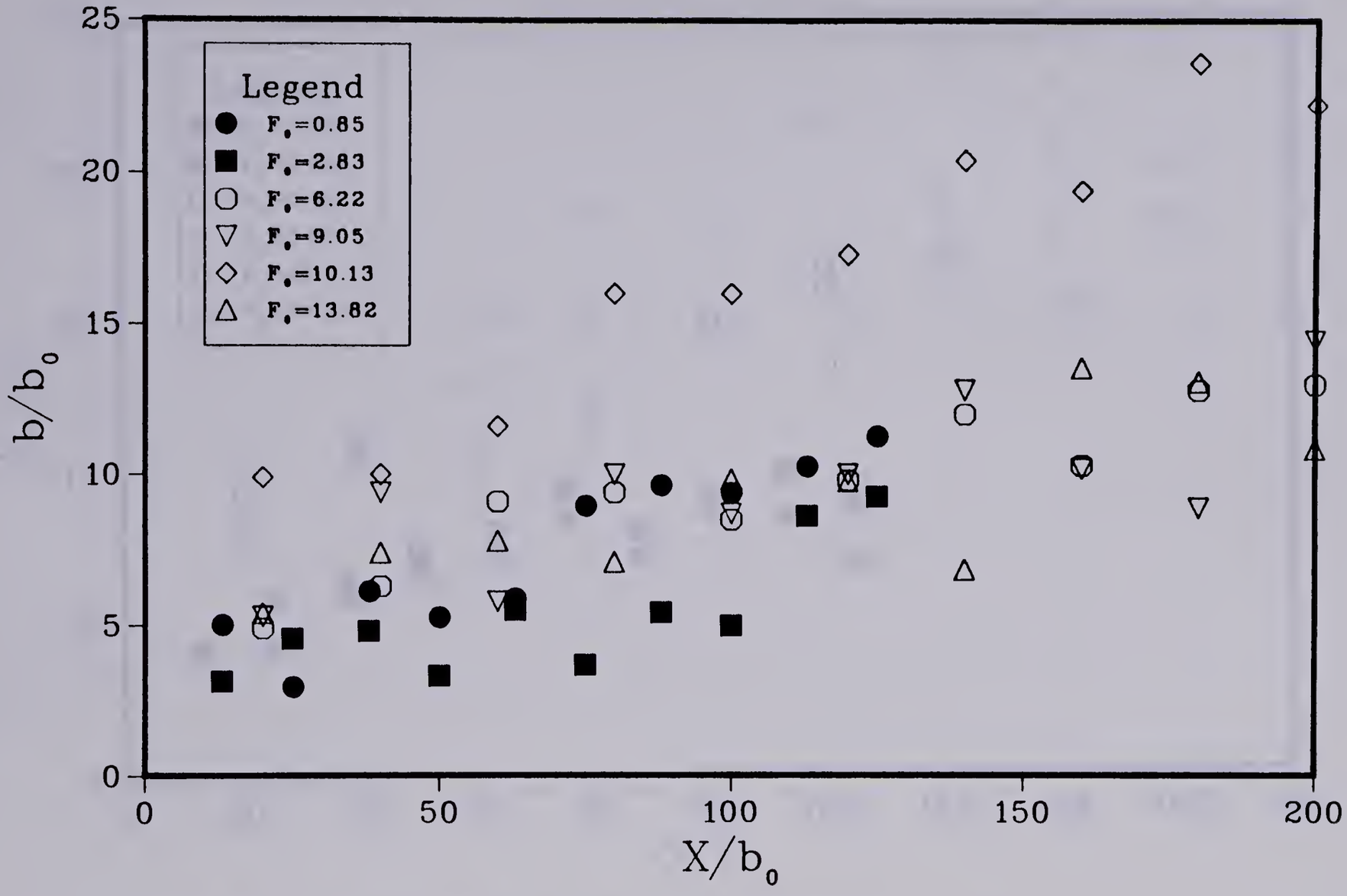

FIGURE 27. The variation of the dimensionless velocity half width for the 6 complete runs.

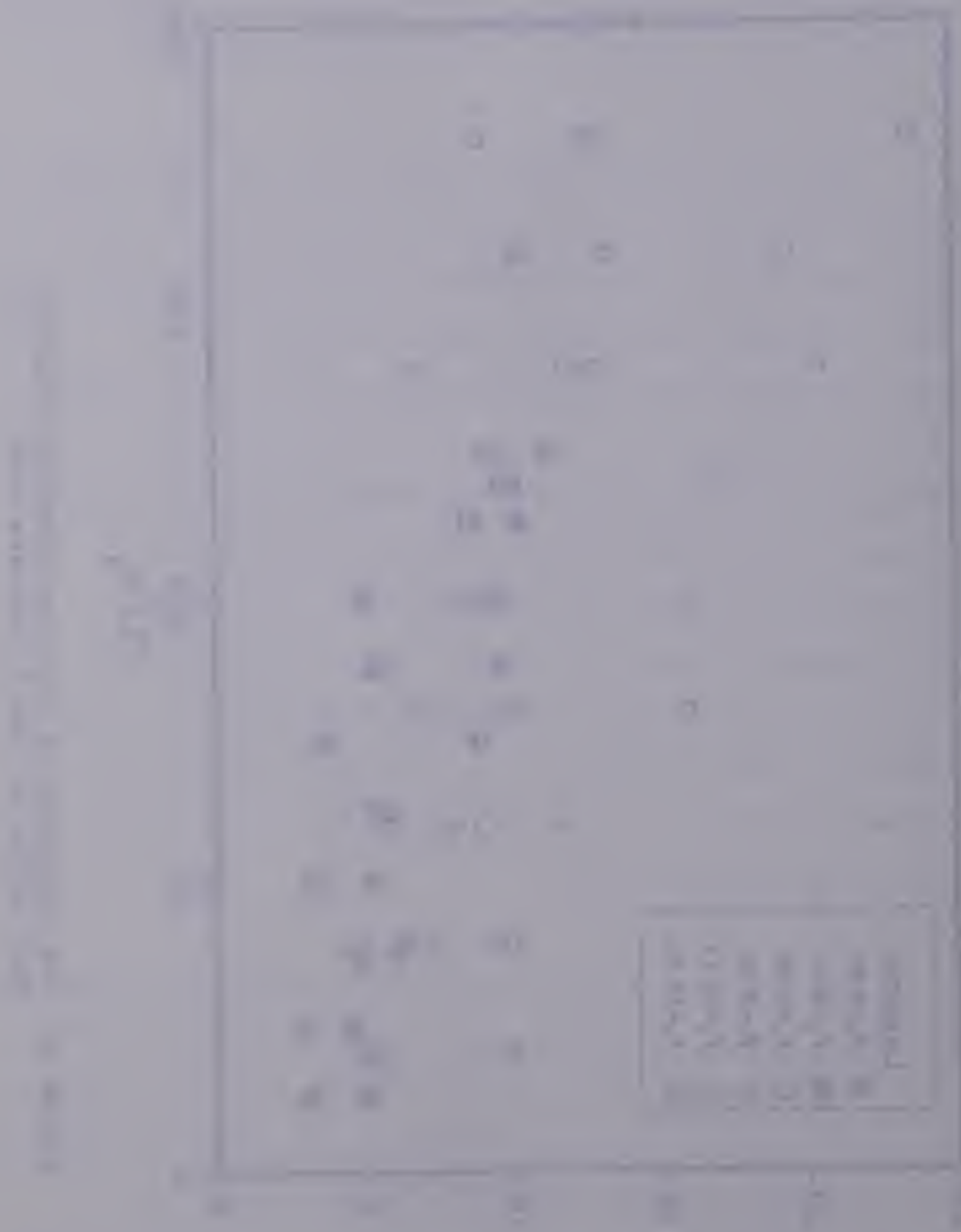

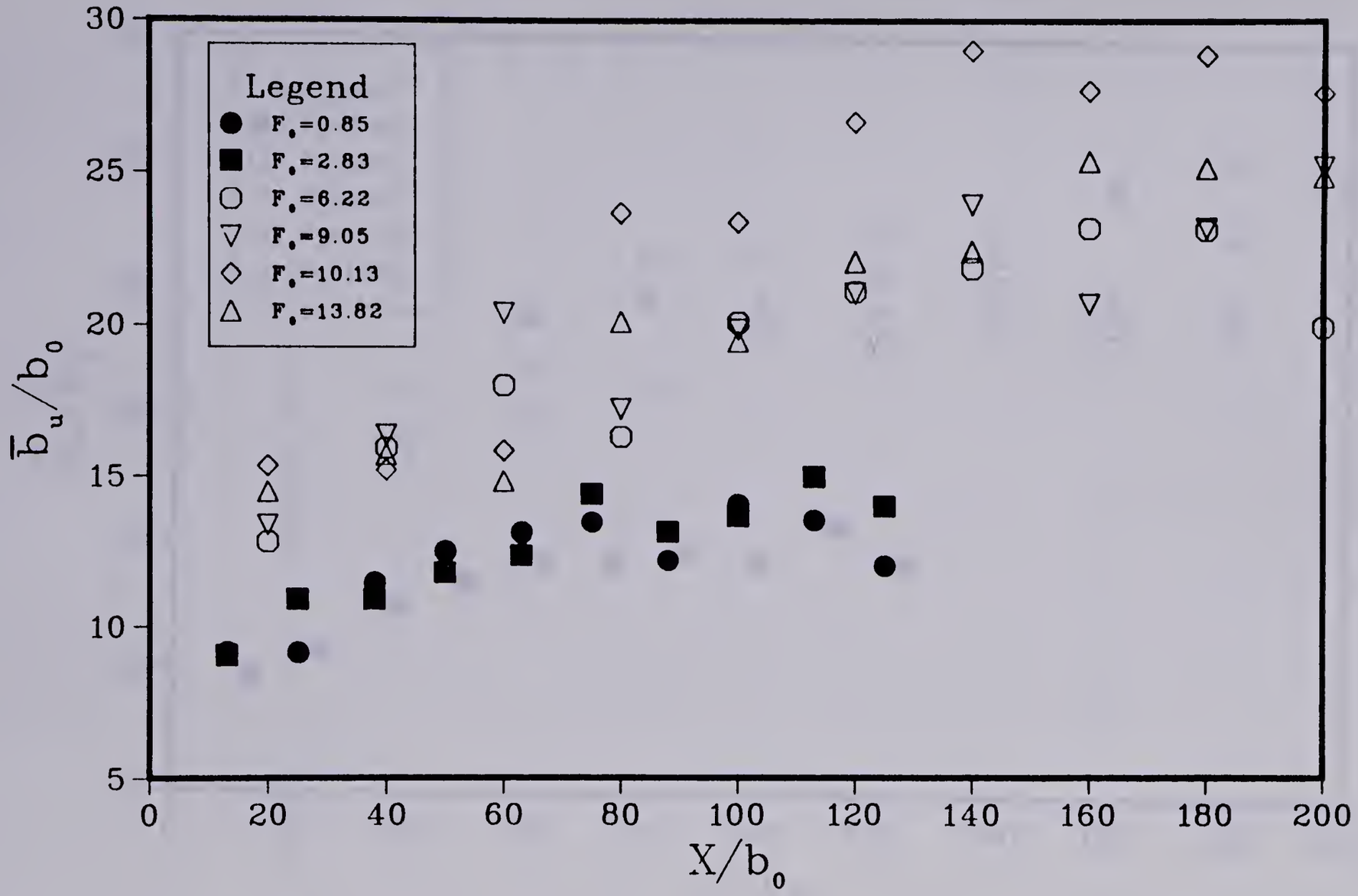

FIGURE 28. The variation of the dimensionless velocity width for the 6 complete runs.

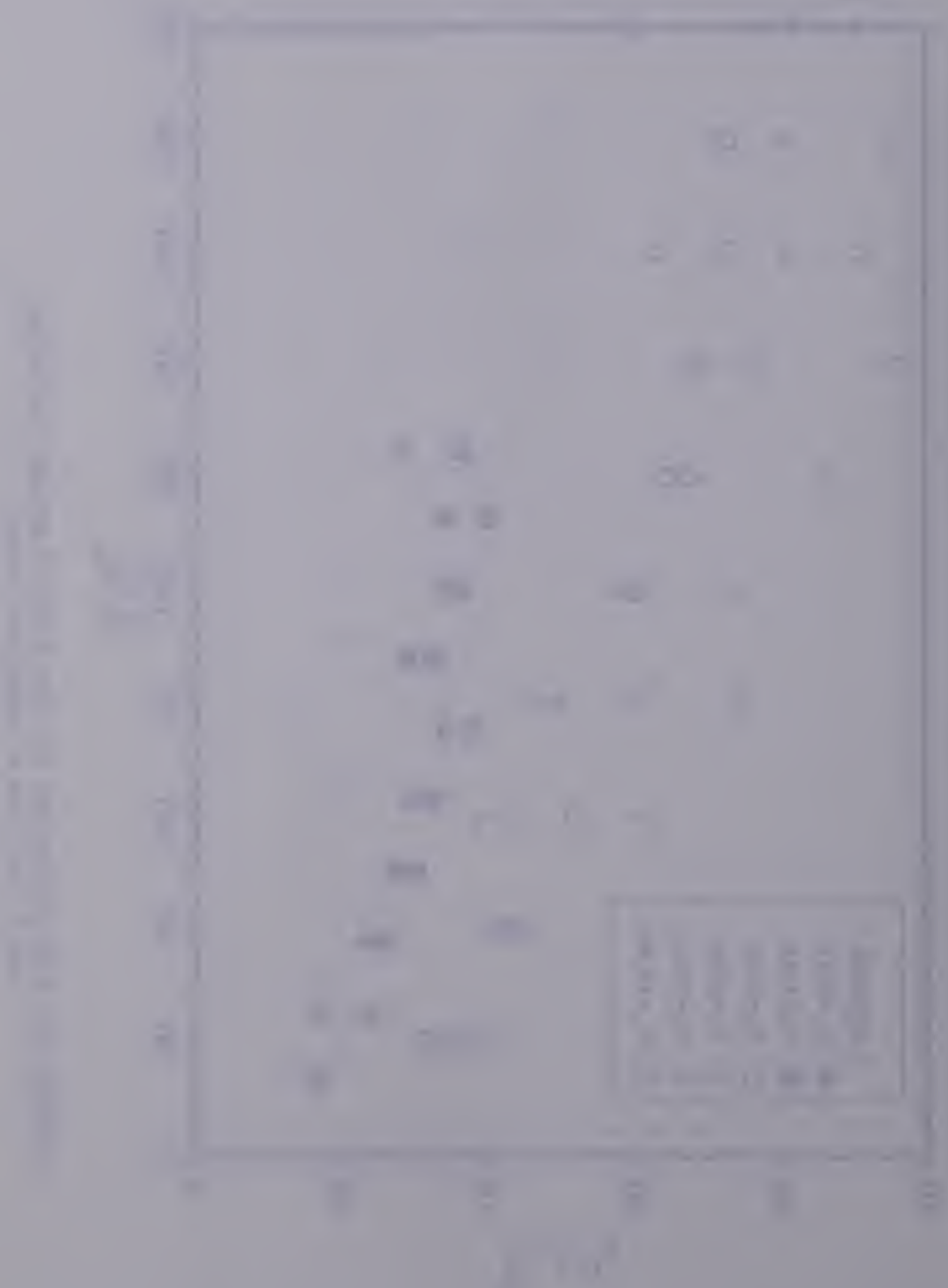

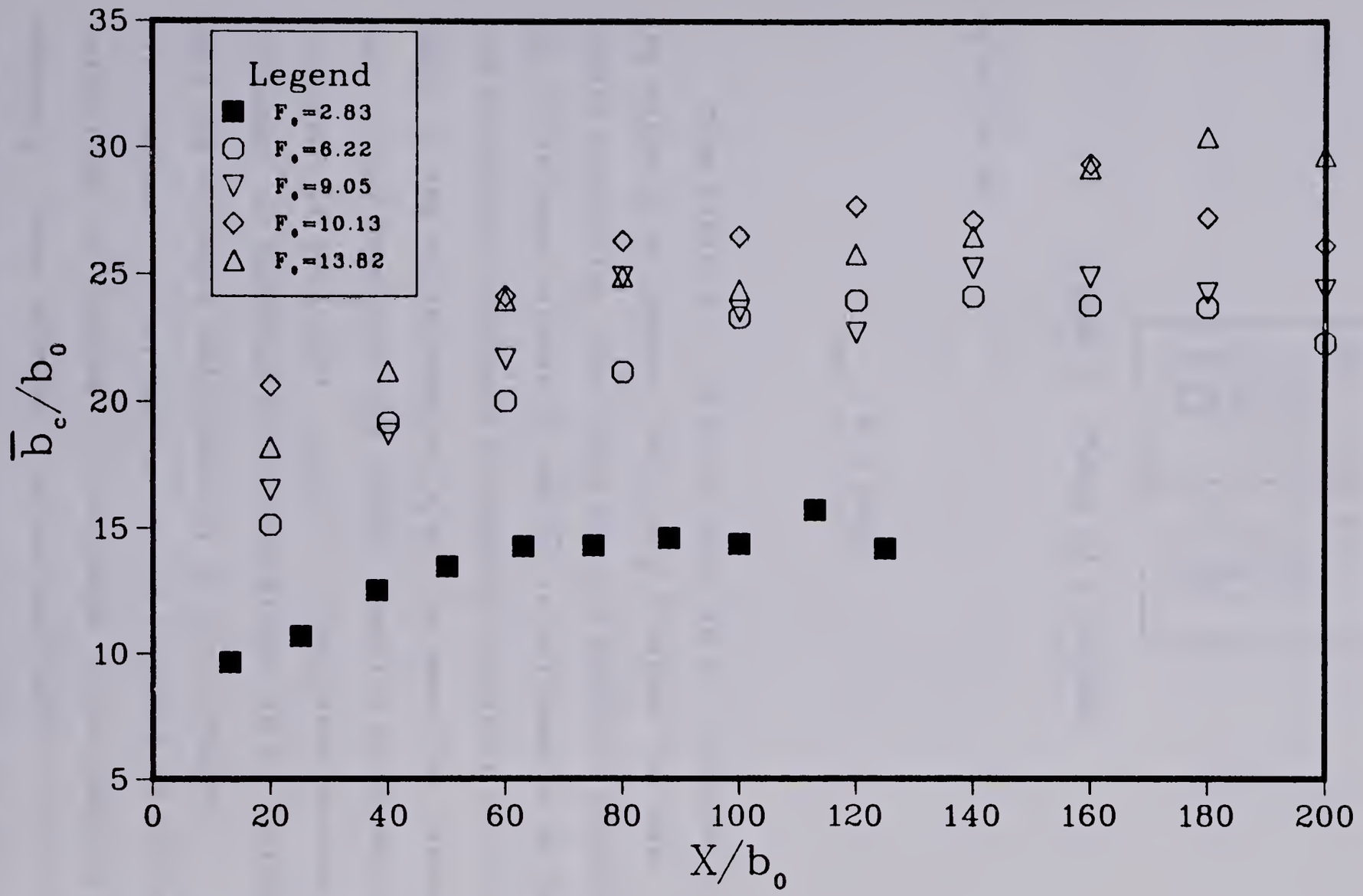

FIGURE 29. The variation of the dimensionless pollutant width for the 6 complete runs.

F_o	K
13.82	1.263
10.13	1.170
9.05	1.143
6.22	1.137
2.83	1.072

TABLE 3. Table of K values.

equation 84.

$$K = 1.16 \tag{84}$$

From Table 3 it is clear that as F_o increases so does the value of K, however with only 5 values the data is hardly conclusive. The trend has one possible explanation. The difference between $\overline{b}_u$ and $\overline{b}_c$ is believed to be due to the fact that turbulence transports pollutant out from the edges of the mainstream while at the same time transporting very little momentum. The little momentum accompanying the transport of pollutant is quickly dissipated because the transport of momentum is not sustained. As F_o increases so does the strength and intensity of the turbulent fluctuations, either because of an increase in the mean velocities, or because of a decrease in the damping due to buoyancy. These stronger fluctuations have the ability to transport the pollutant, further away from the mainstream

than the weaker fluctuations, characteristic of lower F_o values. Therefore the difference between the spreading rates of pollutant and velocity increases with increasing F_o.

VELOCITY SCALE

The velocity scale u_m, the maximum value of u at a cross-section, was made dimensionless by dividing by U_o, the outlet velocity, and plotted against dimensionless distance x/b_o in Figure 30. There was only one discernible trend in the data, that u_m decreased with distance downstream, and it was obviously expected. Therefore u_m was non-dimensionalized again, this time by dividing by u_{mo}, the maximum velocity at the cross section where x=10cm for a given F_o. Figure 31 shows u_m/u_{mo} plotted against x/bo, and the data, while not falling on a single curve, is more tightly grouped. Also shown on Figure 31 is equation 85

$$\frac{u_m}{U_o} = \frac{3.1}{\sqrt{x/b_o}} \qquad (85)$$

which was developed by Rajaratnam and Humphries (1984) and describes the variation of the velocity scale for a non-buoyant surface jet. This equation underestimates the experimental data but is of the correct form. If the coefficient 3.1 in equation 85 is increased to 6.0 the resulting equation more closely describes the data.

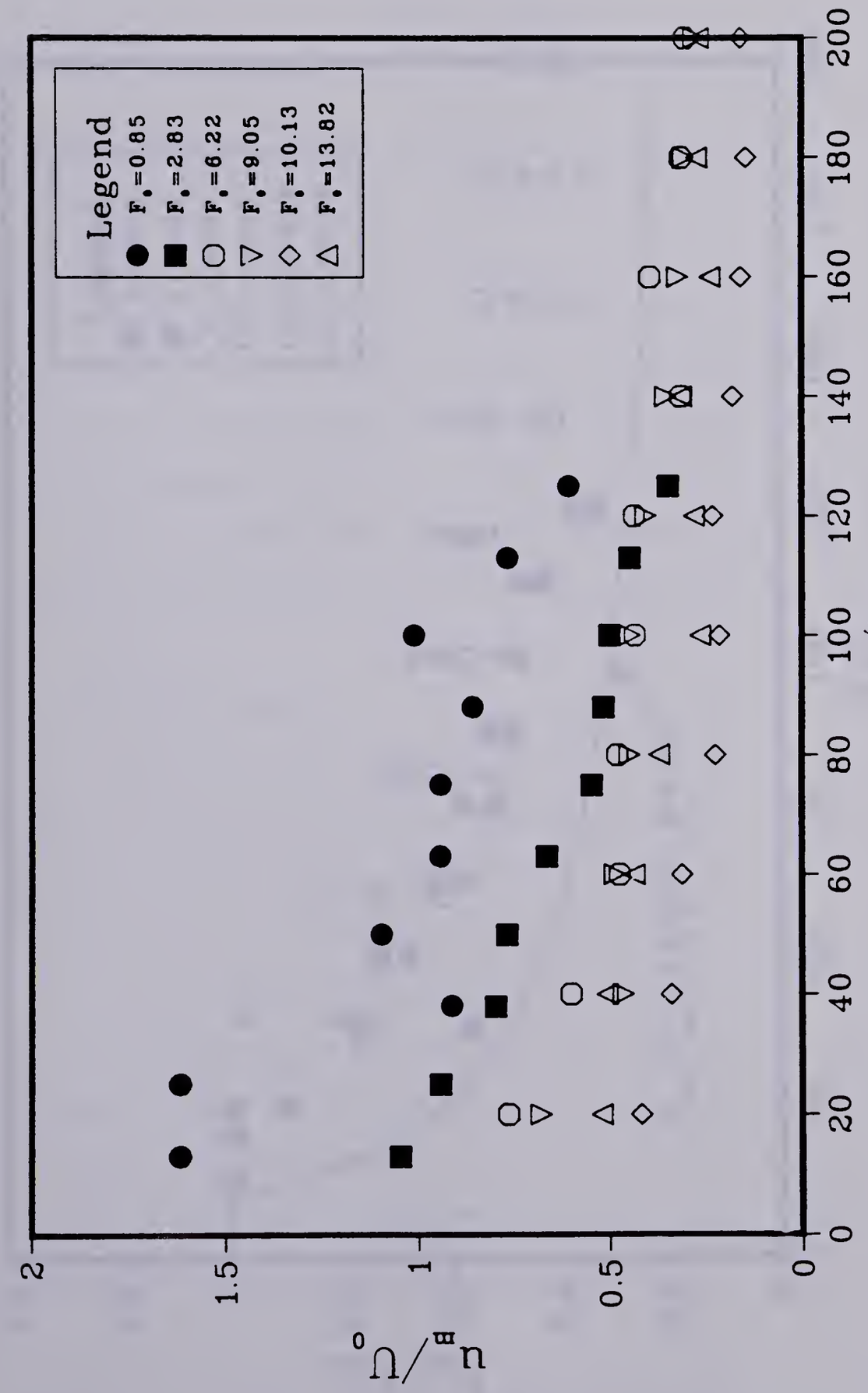

FIGURE 30. The variation of u_m/U_o for the 6 complete runs.

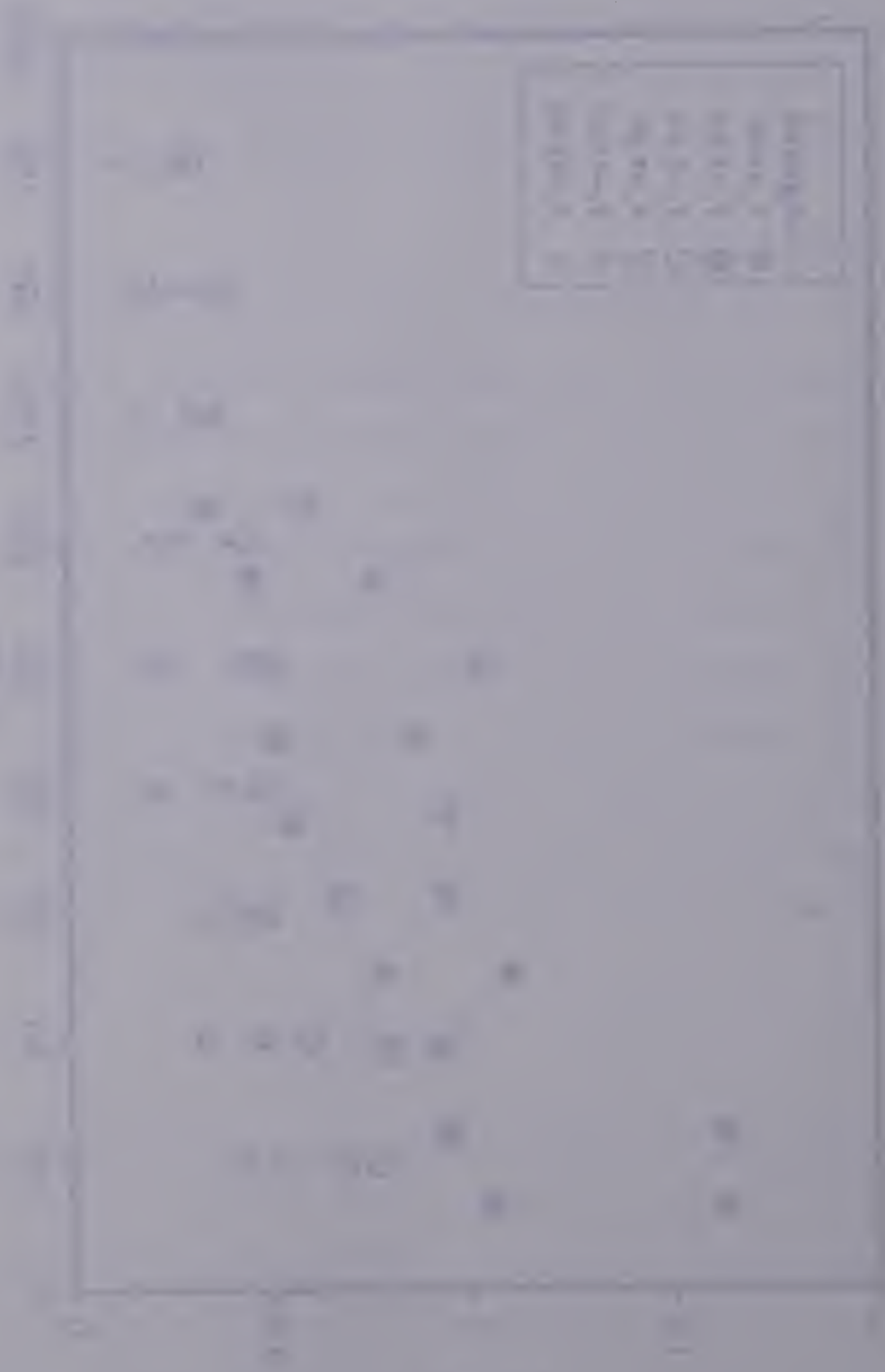

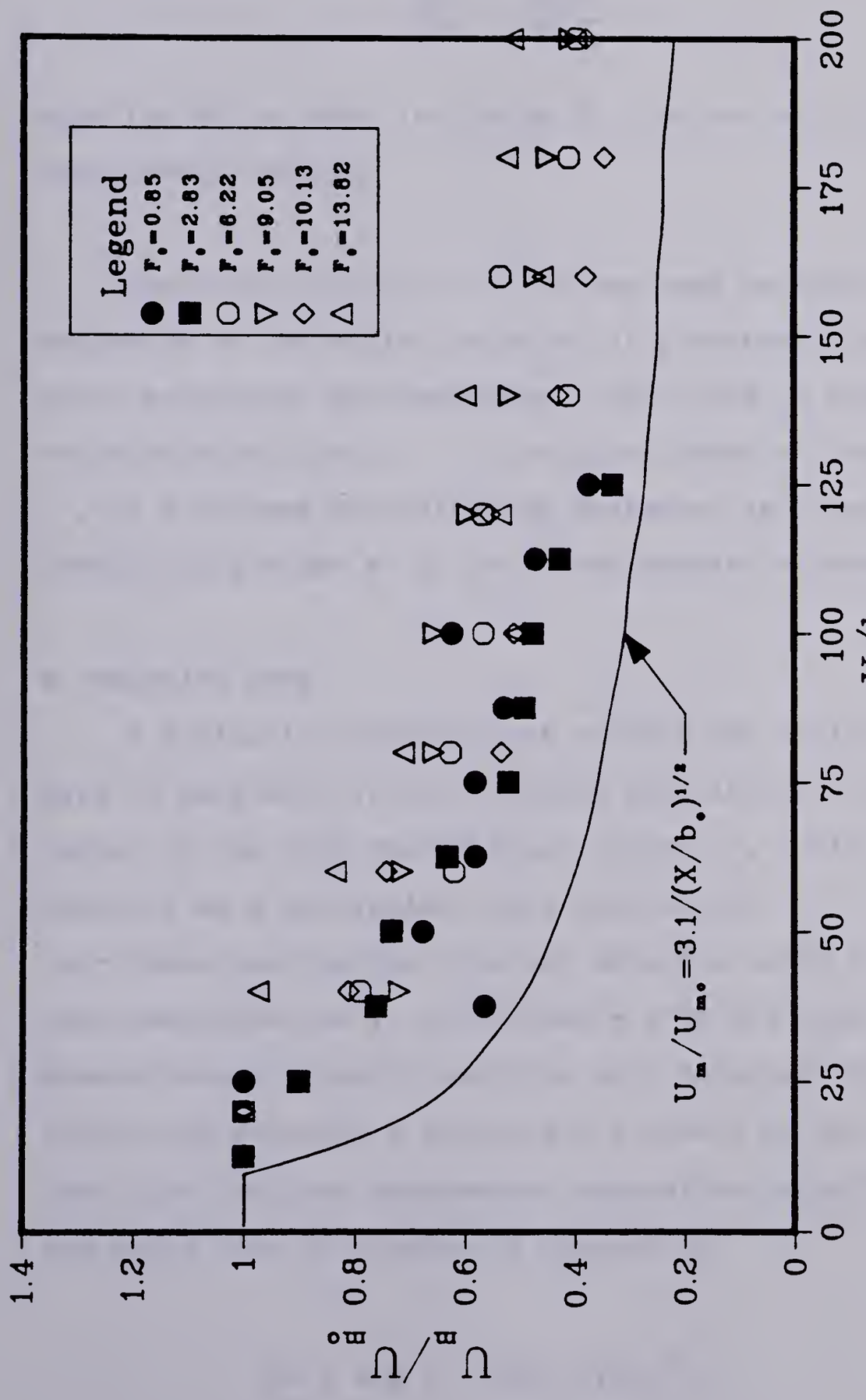

FIGURE 31. The variation of u_m/u_{m_o} for the 6 complete runs, equation 85 is also included.

$$\frac{u_m}{u_{mo}} = \frac{6.0}{\sqrt{x/b_o}} \qquad (86)$$

Equation 86 is shown in Figure 32 together with the experimental points.

The value of u_m at x=10cm was used because it is analogous to the outlet velocity of a surface discharge which Rajaratnam and Humphries (1984) used in their study to non-dimensionalize u_m. It was considered analogous because u_m is a maximum at x=10cm and decreases as x increases downstream similar to U_o for a non-buoyant discharge.

B. VELOCITY DATA

A similarity analysis was carried out on the velocity data to determine if the velocity profiles in the horizontal region of the flow were similar. Using u_m, the maximum velocity at a particular cross section, to non-dimensionalize the velocity data and using b to non-dimensionalize y, the distance from the free surface the dimensionless velocity profiles were obtained. Figures 33 through 38 show u/u_m versus y/b for each of the 6 complete runs. The familiar exponential expression, equation 87, is the solid line in Figures 33 through 38.

$$\frac{u}{u_m} = \exp\left(-0.693\ (y/b)^2\right) \qquad (87)$$

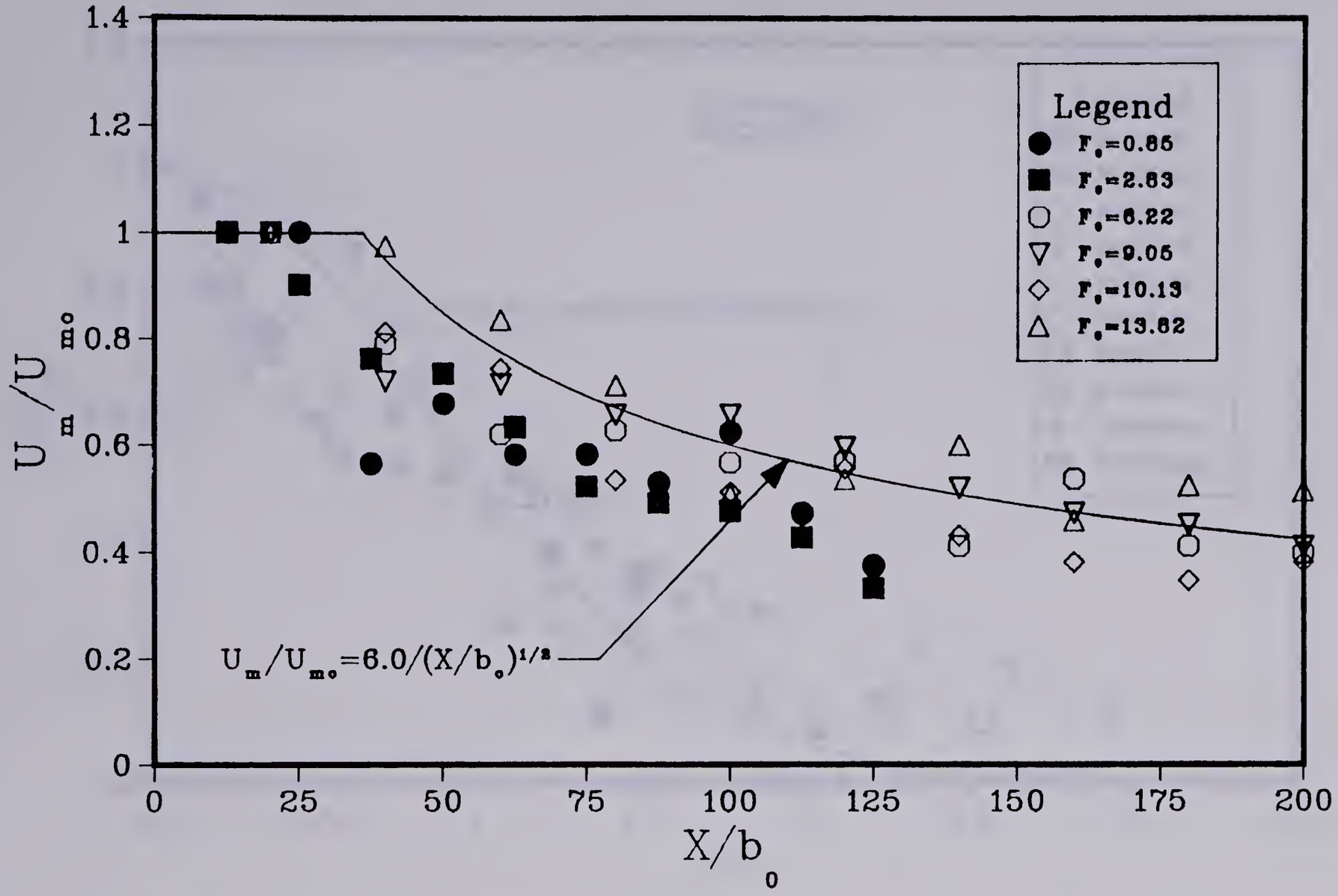

FIGURE 32. The variation of u_m/u_{mo} for the 6 complete runs, equation 86 is also included.

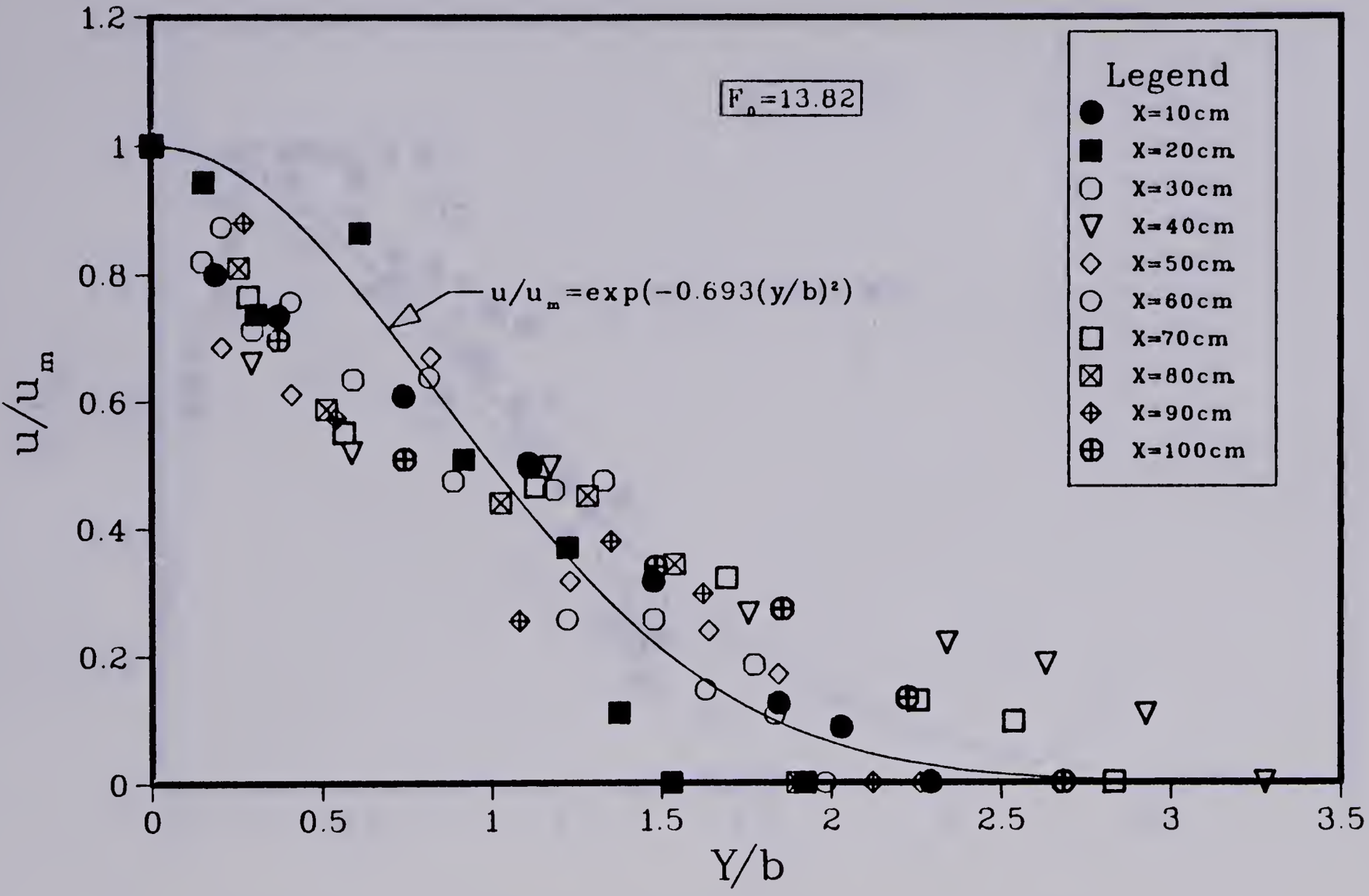

FIGURE 33. Dimensionless velocity profile for the run where F_o=13.82

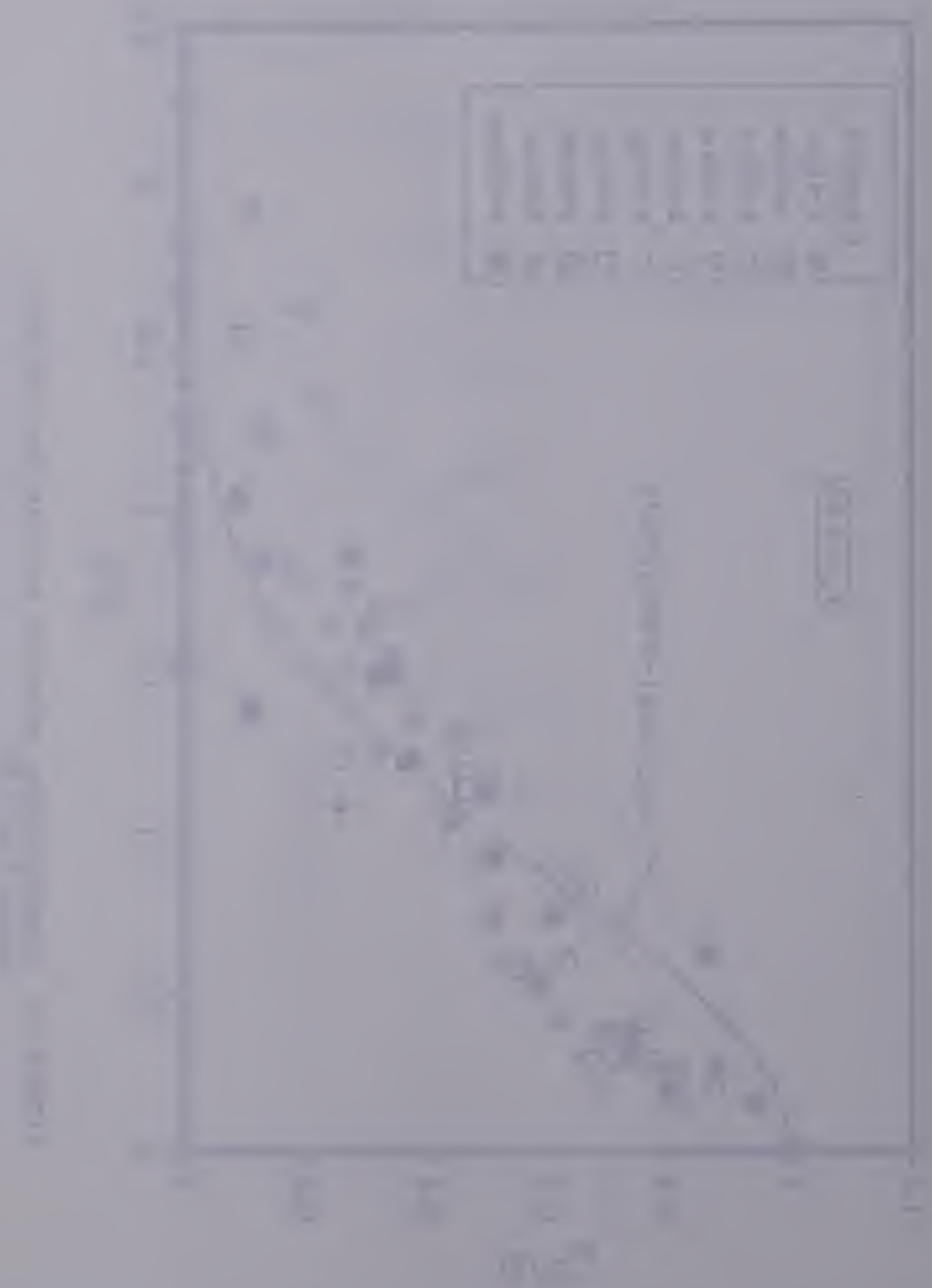

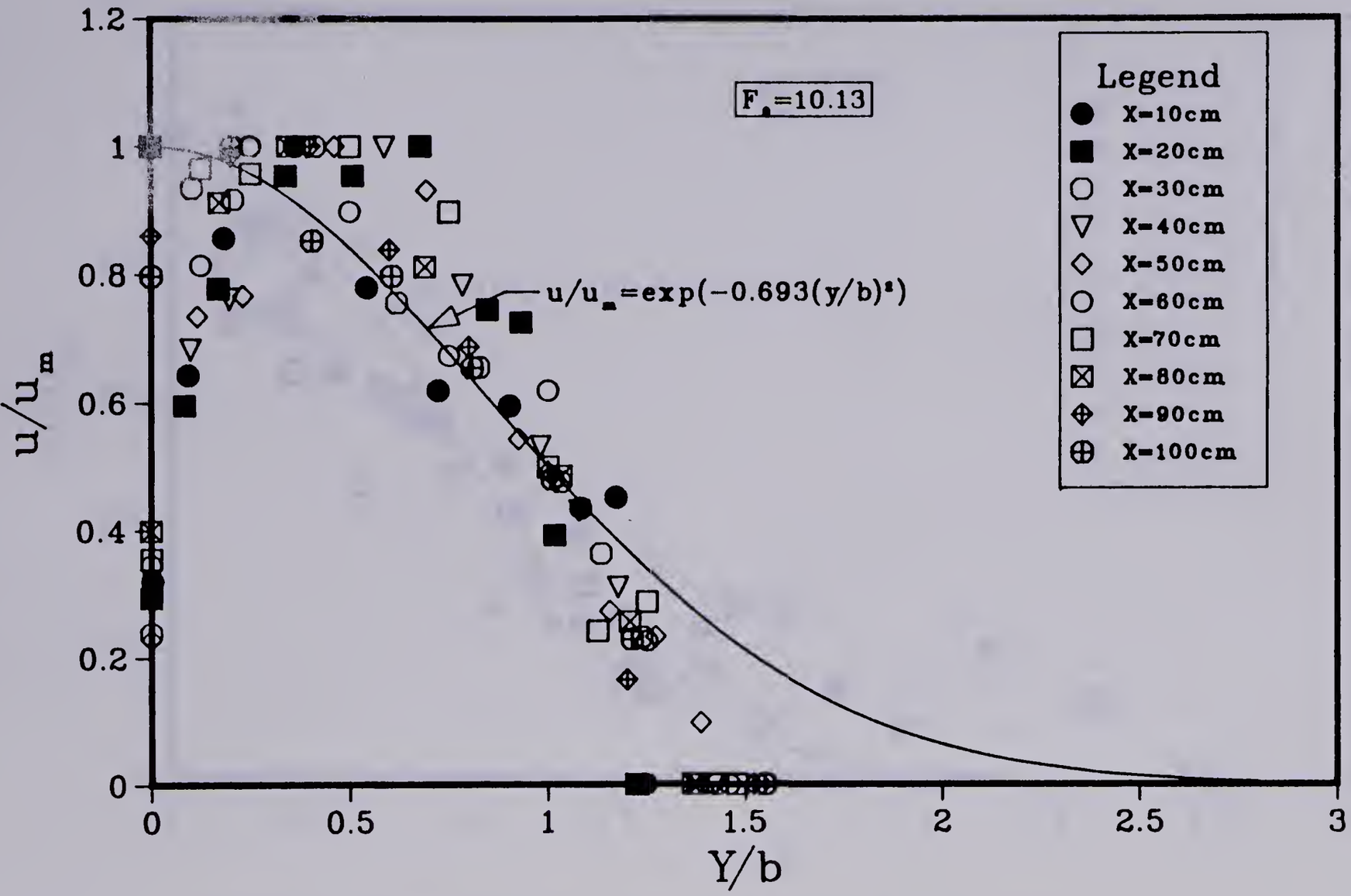

FIGURE 34. Dimensionless velocity profile for the run where F_o=10.13

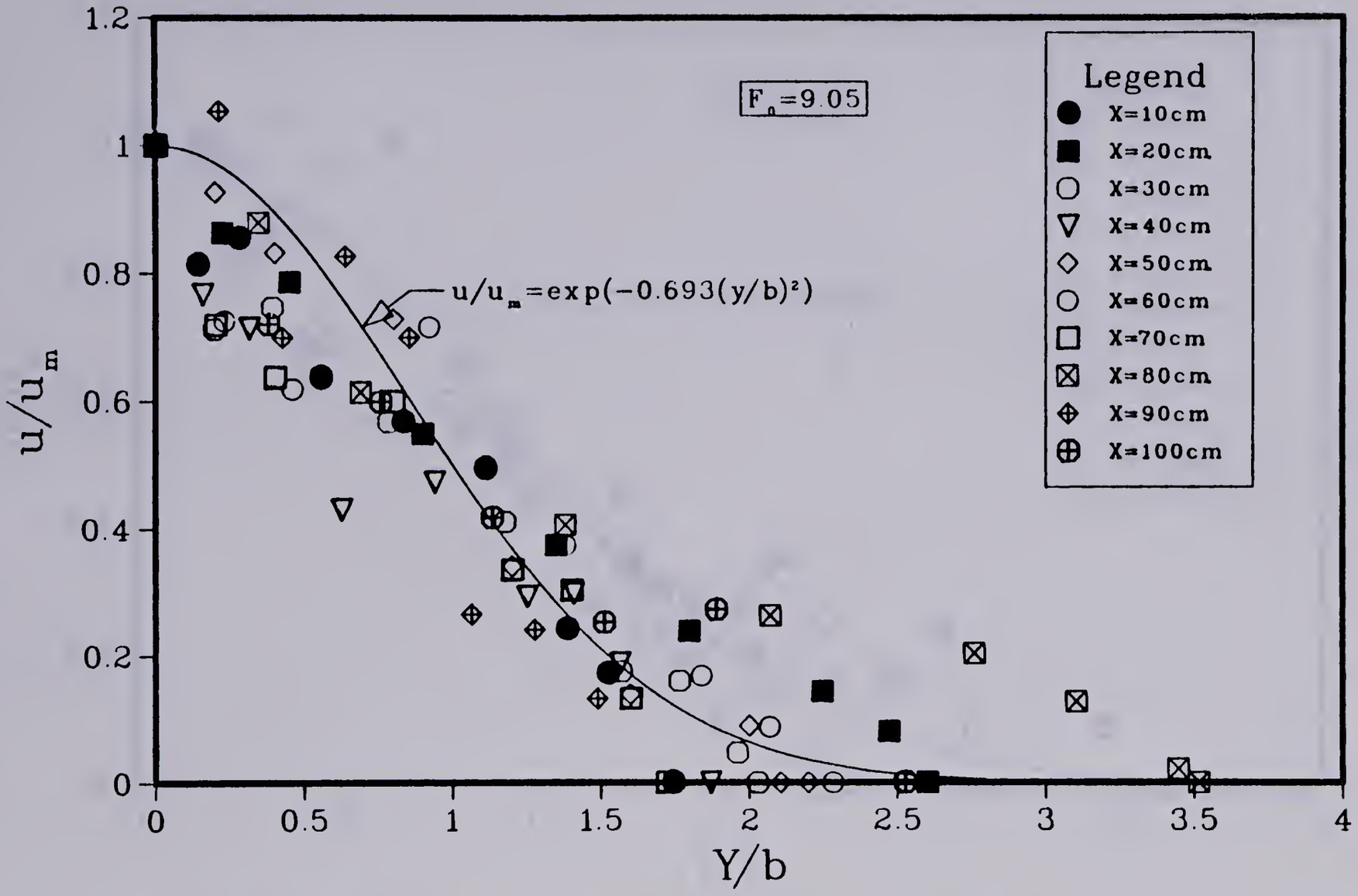

FIGURE 35. Dimensionless velocity profile for the run where F_o=9.05

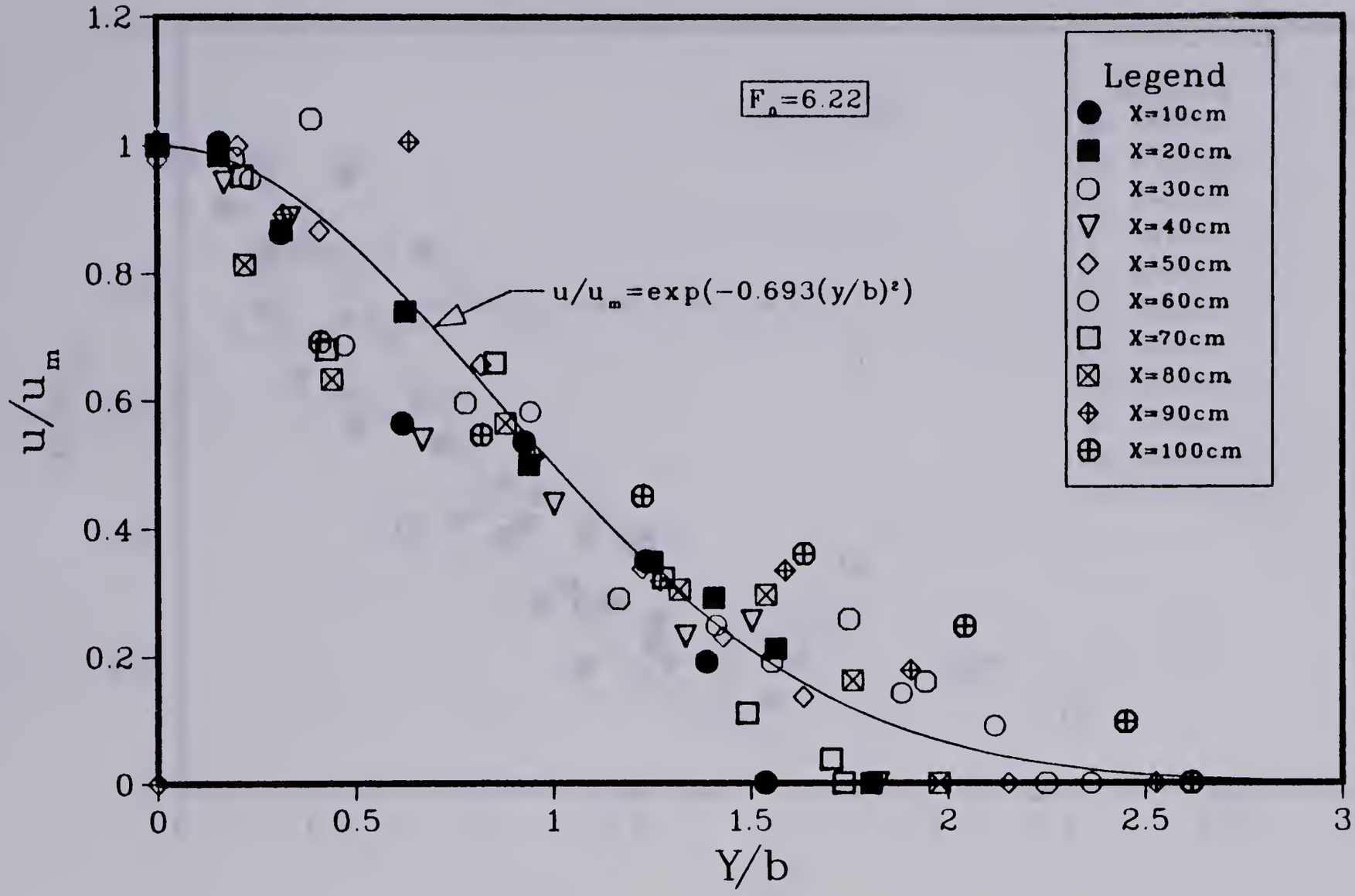

FIGURE 36. Dimensionless velocity profile for the run where F_o=6.22

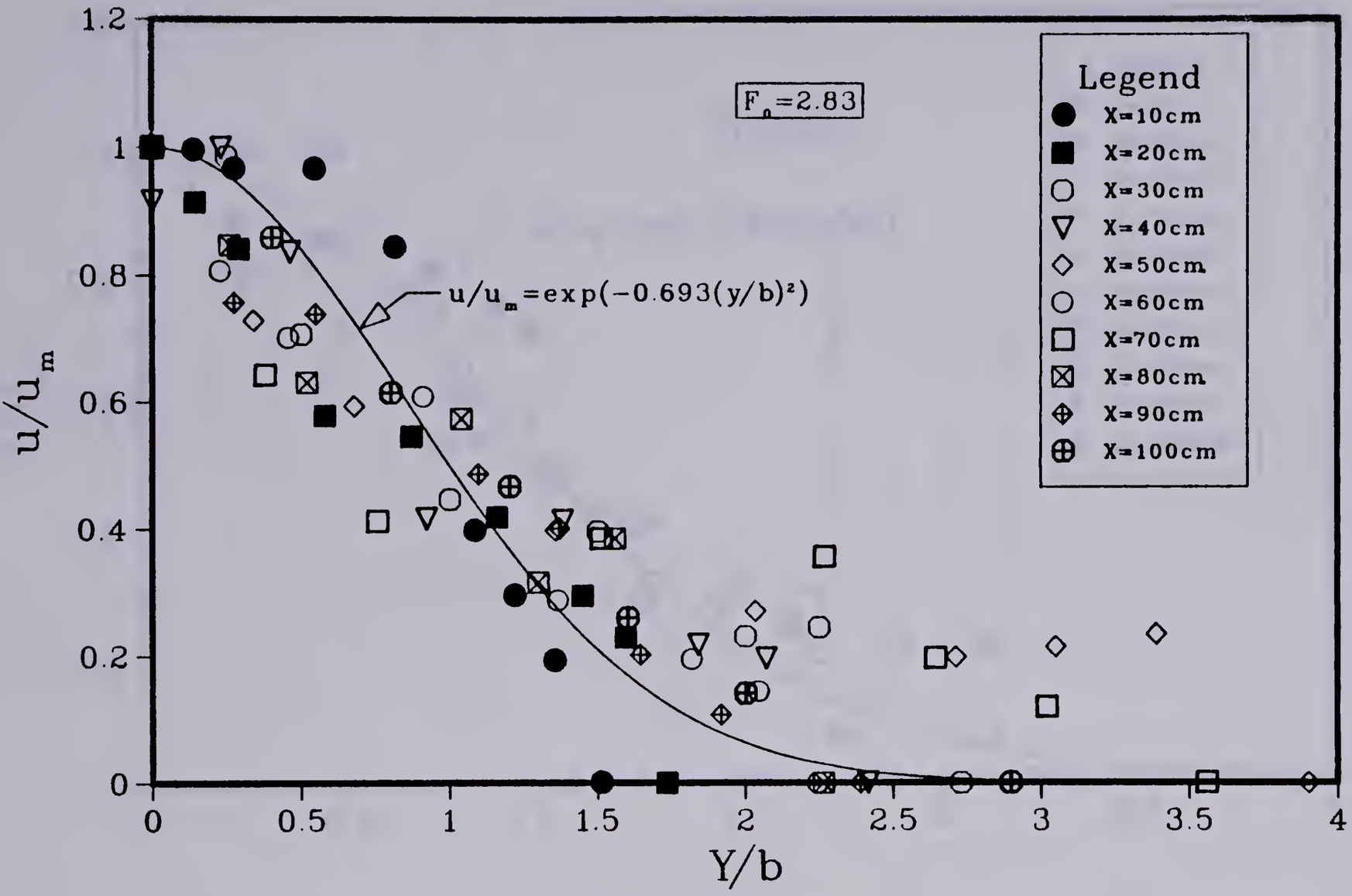

FIGURE 37. Dimensionless velocity profile for the run where F_o=2.83

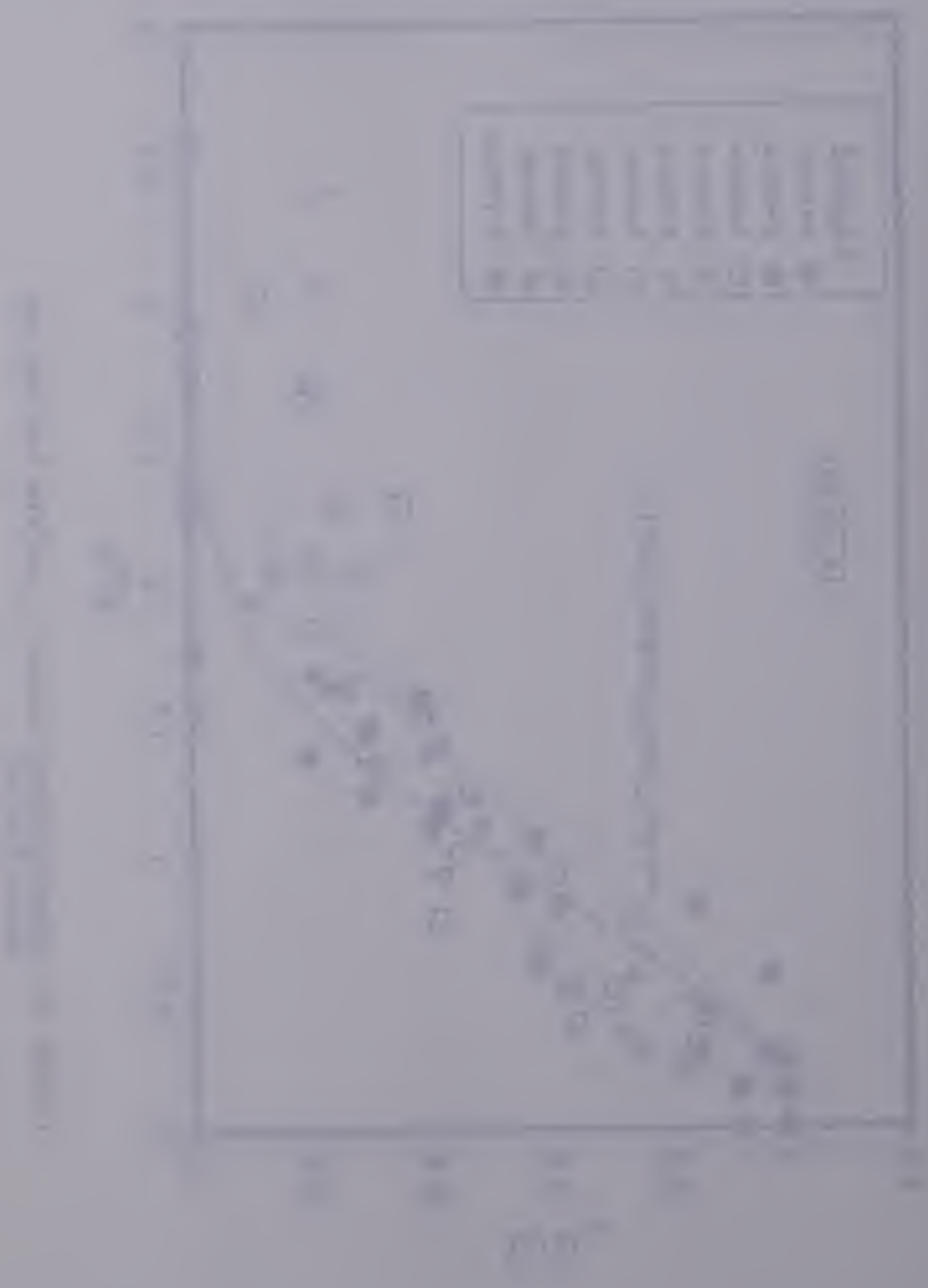

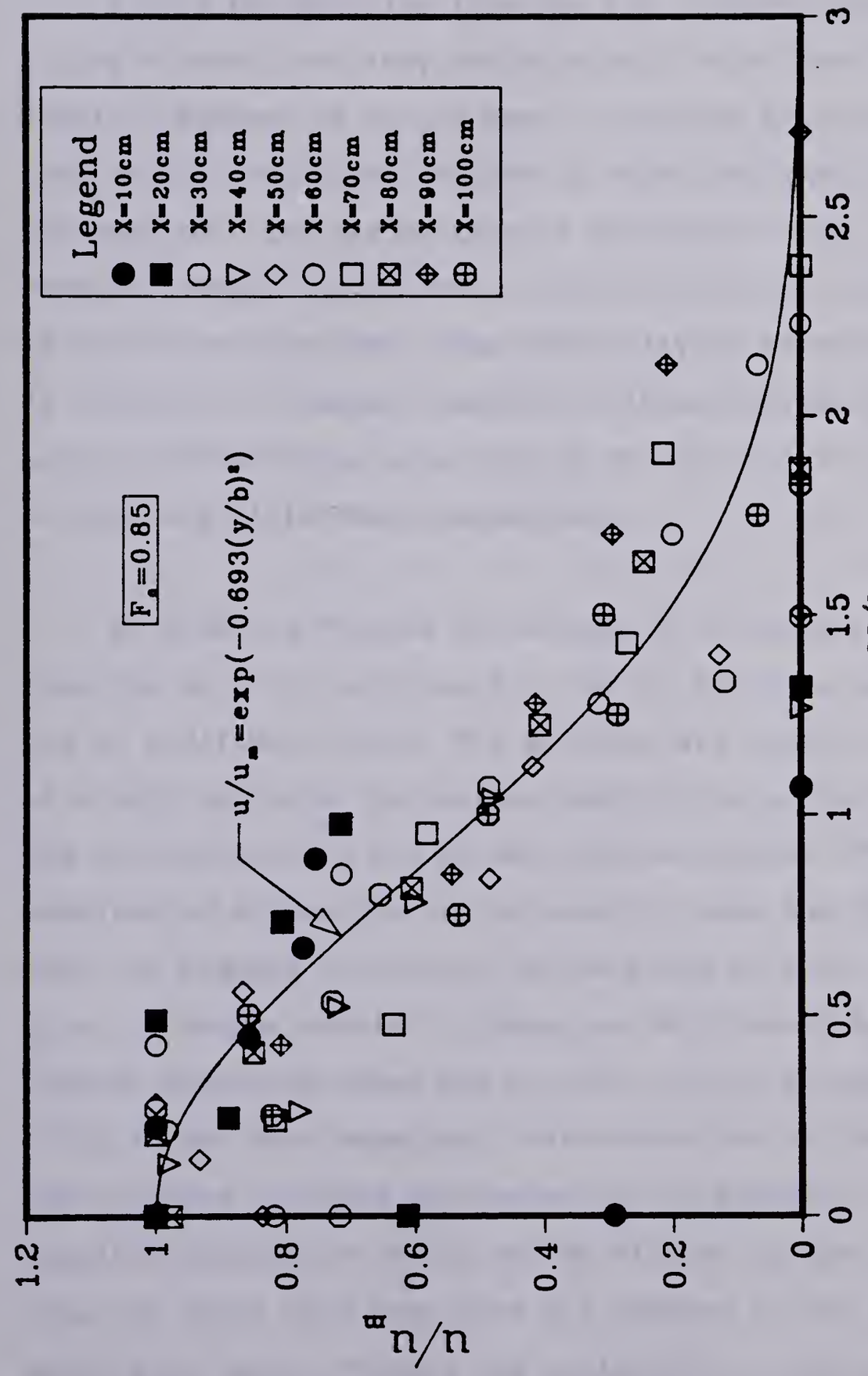

FIGURE 38. Dimensionless velocity profile for the run where F_o=0.85

If all the profiles from the ten cross-sections fell on a single curve then they could be said to be exactly similar. However as can be seen in Figures 33 through 38, they do not. The plots indicate a weak similarity between the profiles. The strong type of similarity which exists in vertical buoyant jet-plumes, as found by Kotsovinos (1975), is not in evidence here. The similarity of velocity profiles is the key to integral analysis. Without similarity the partial differential equations of motion will not simplify to ordinary differential equations.

By studying Figures 33 through 38 it becomes evident that the velocity profiles for the run where F_o equals 10.13 are of a different form. The profiles are similar to those of a wall jet with the maximum velocity occurring not at the bed or free surface but at some distance below. This resulted in distortion of the velocity data and the scale data. In Figures 27 through 29 the plots of b/b_o, $\bar{b}_u/b_o$ and $\bar{b}_c/b_o$ it is the run for F_o equal to 10.13 which has the largest spreading rates and not the run for F_o equal to 13.82 as had been expected. This alteration of the shape of the profiles for this particular run is puzzling. The only possible explanation which can be offered is that during this run there were many more air bubbles in the ambient water than usual. Perhaps the collection of these bubbles at the free surface was the cause of the distortion.

ENTRAINMENT ANALYSIS

To determine if the assumption of negligible entrainment in the internal hydraulic jump was justified the discharge was calculated along the length of the jet. At each section where velocity data was gathered the discharge was calculated. The discharge was calculated by using a computer program to integrate the velocity data at each cross section. A comparison of the results using Simpson's rule and the Trapezoidal rule showed negligible difference between the two methods and therefore the simpler Trapezoidal rule was used. The discharge per unit width Q plotted against x/b_o for the 6 runs is shown in Figures 39 through 44.

The discharge was not completely invariant with x/b_o in any of the runs. However there is no consistent increasing trend in the discharge with increasing x/b_o, as would be expected if ambient fluid were being entrained. For all six runs the data scattered about a mean value, indicated by the solid lines in Figures 39 through 44. This supports the claims that the discharge is constant along the jet and that there is negligible entrainment as assumed.

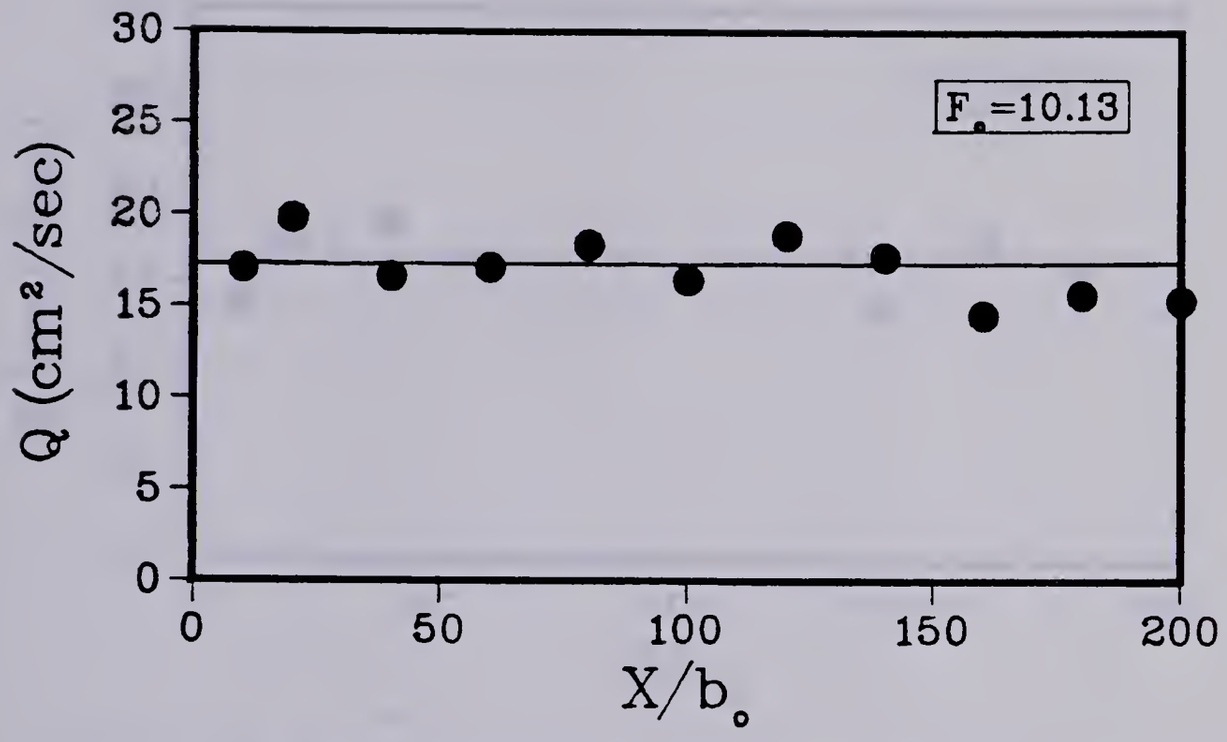

FIGURE 39. The variation of discharge for the run where F_o=10.13

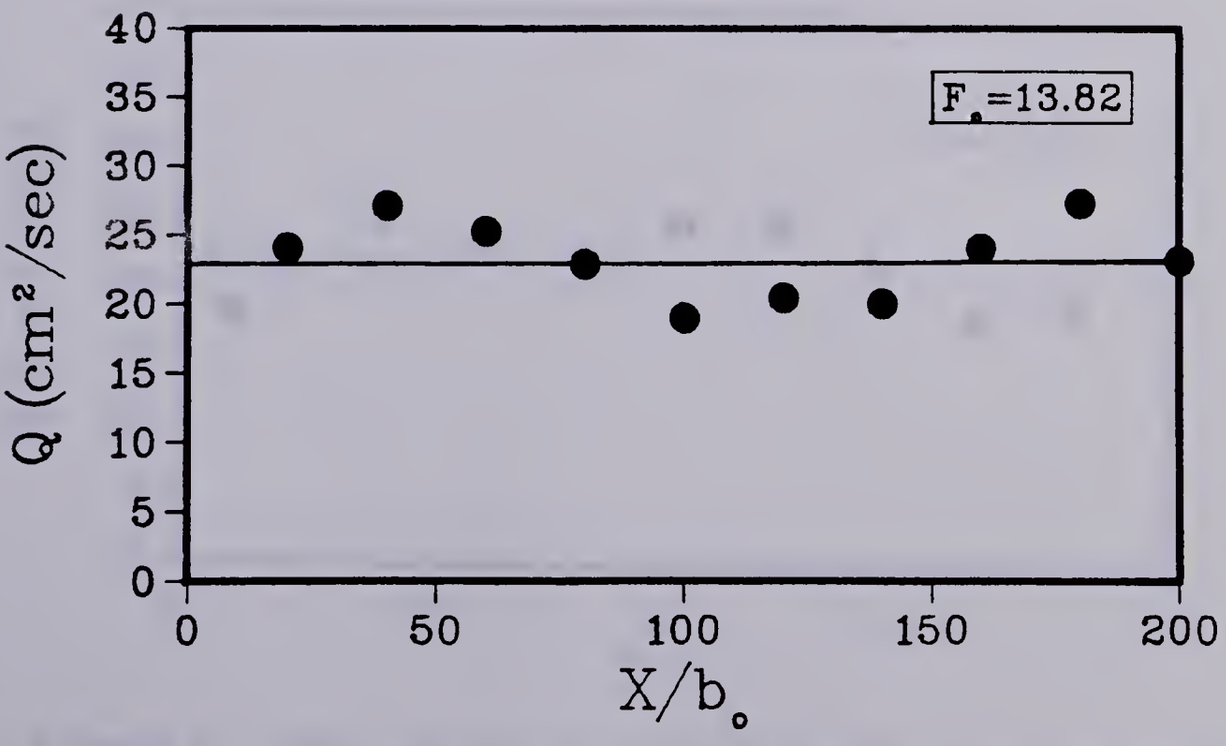

FIGURE 40. The variation of discharge for the run where F_o=13.82

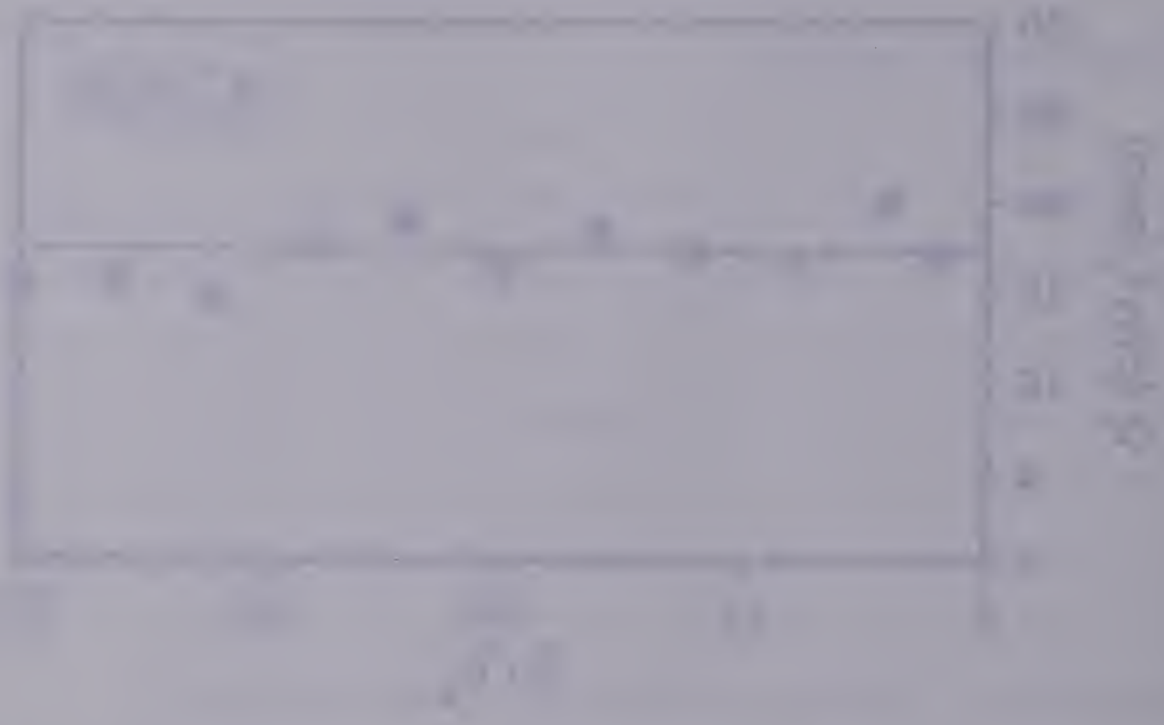

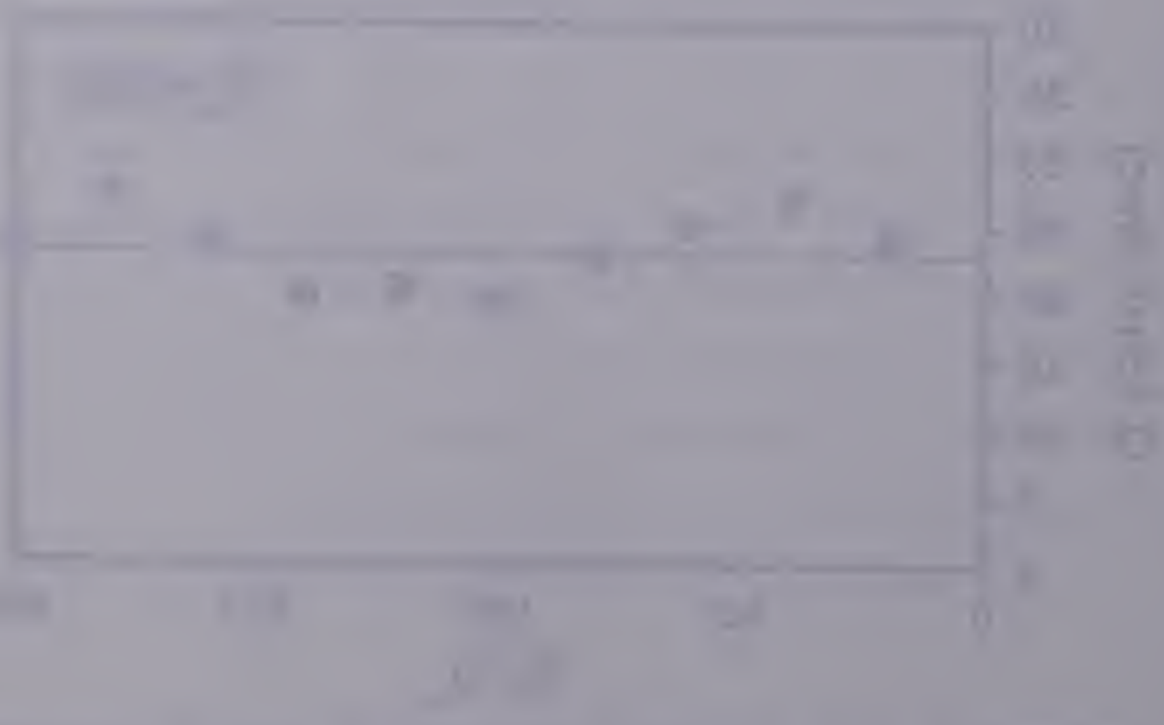

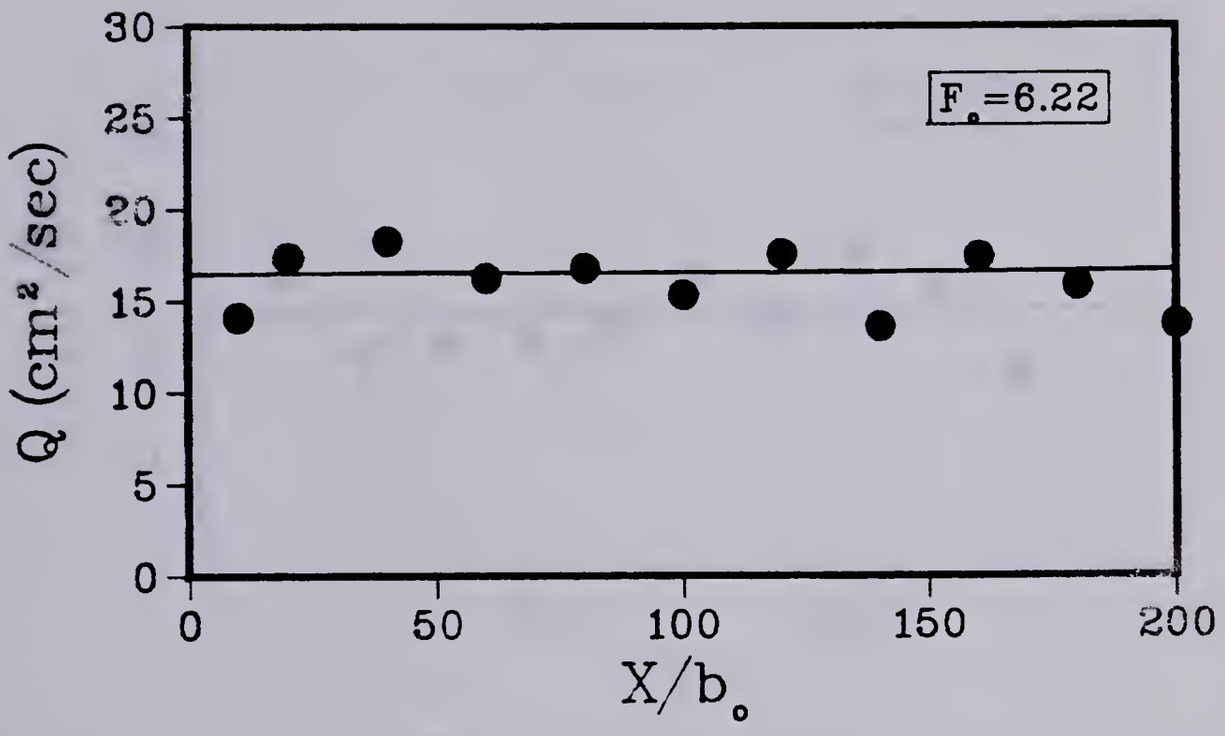

FIGURE 41. The variation of discharge for the run where F_o=6.22

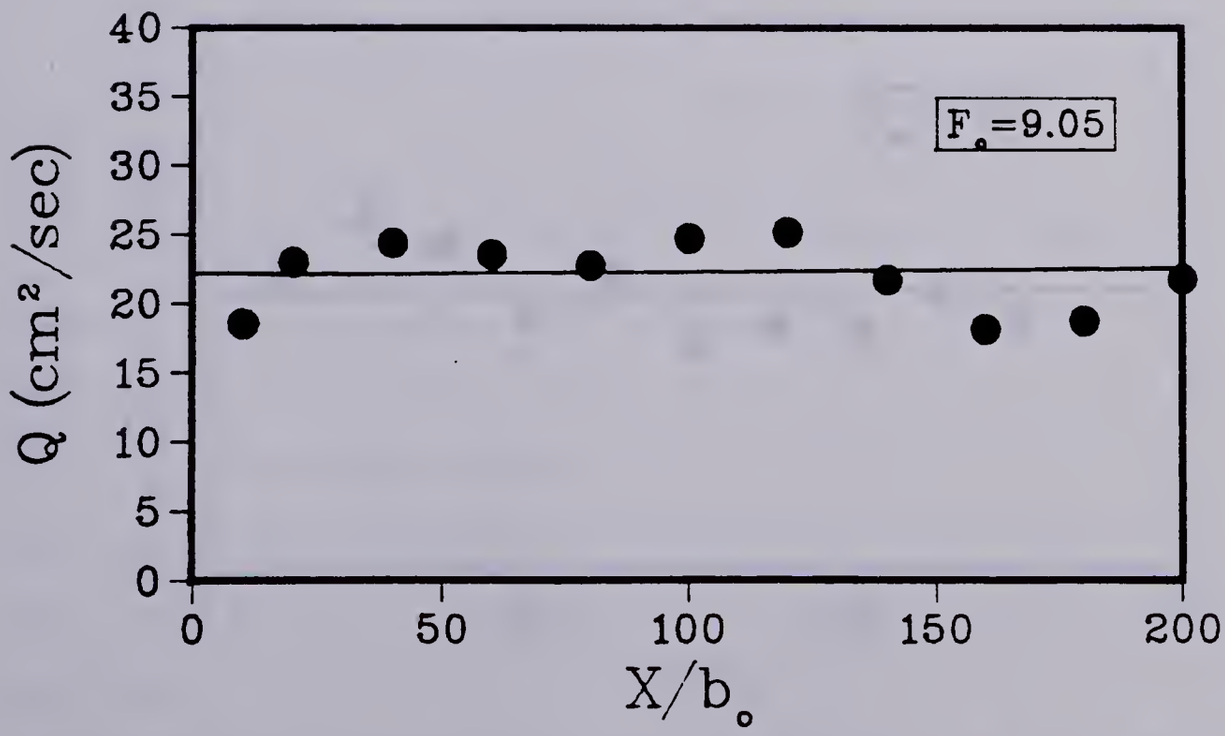

FIGURE 42. The variation of discharge for the run where F_o=9.05

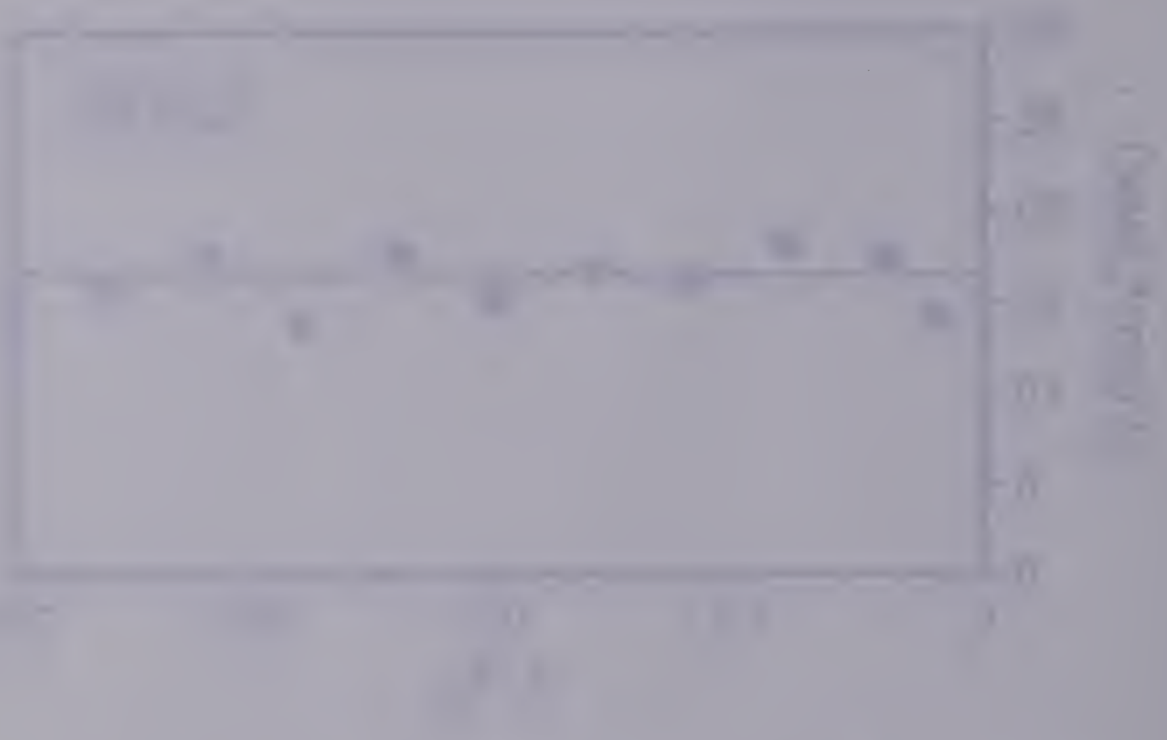

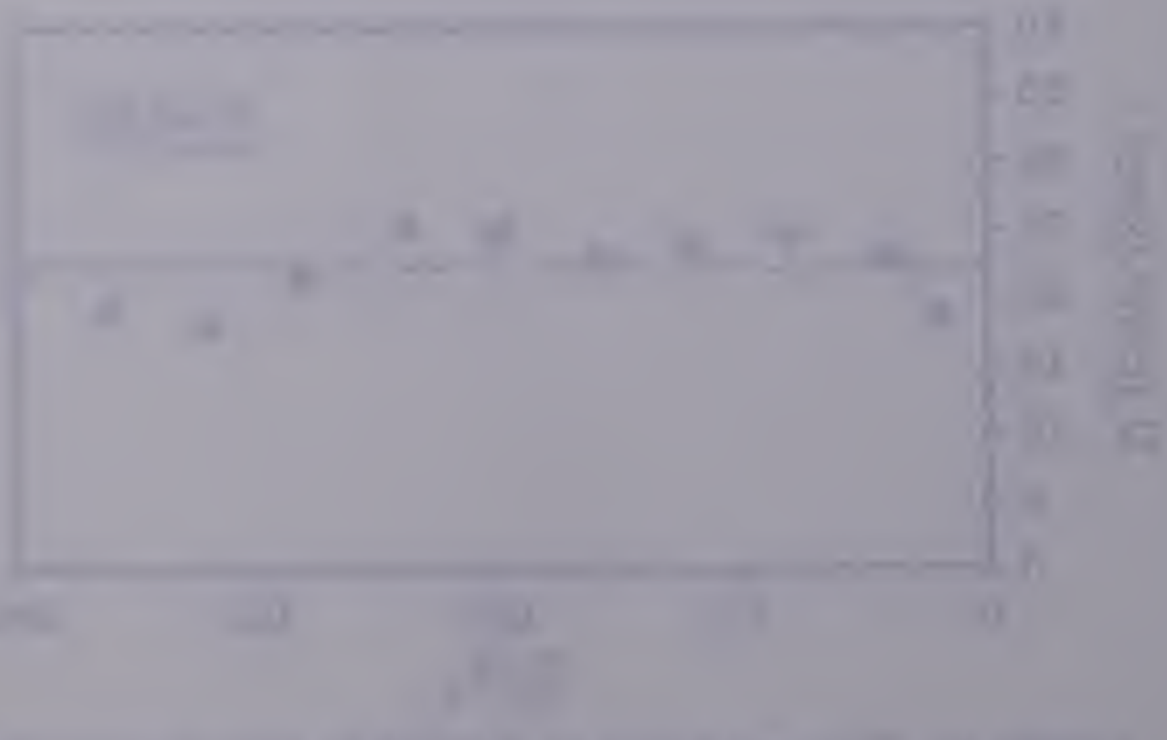

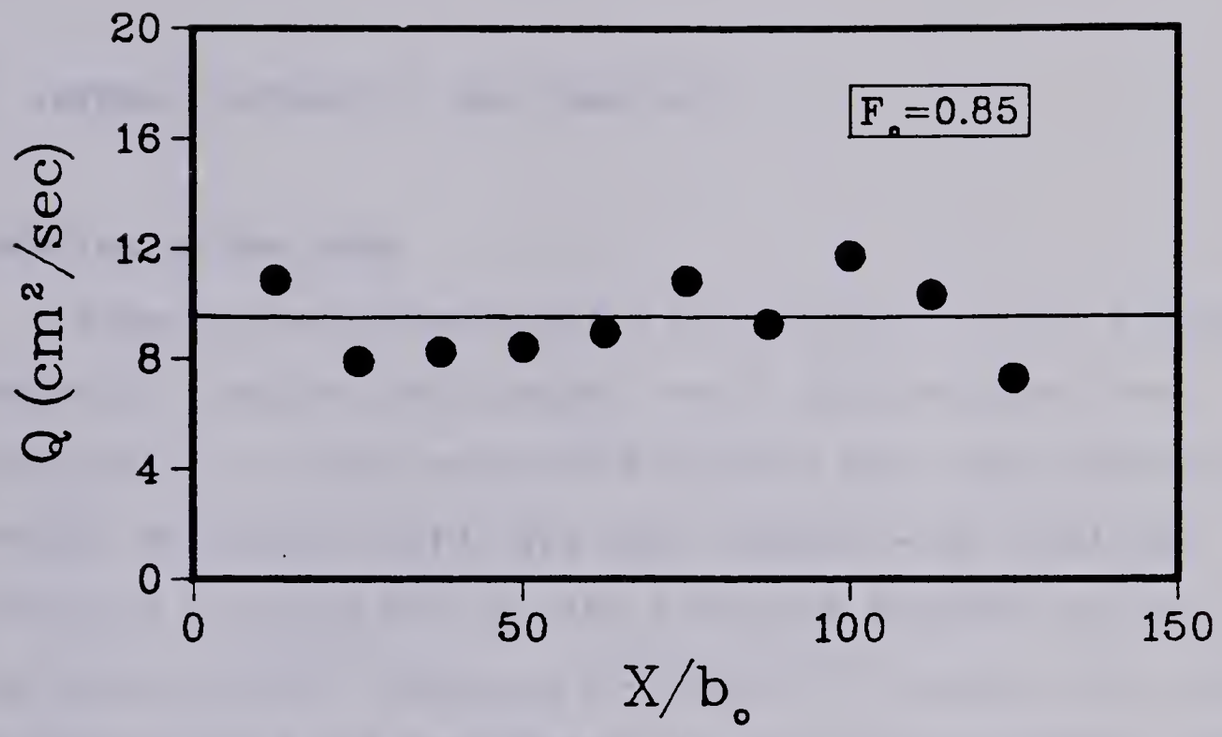

FIGURE 43. The variation of discharge for the run where F_o=0.85

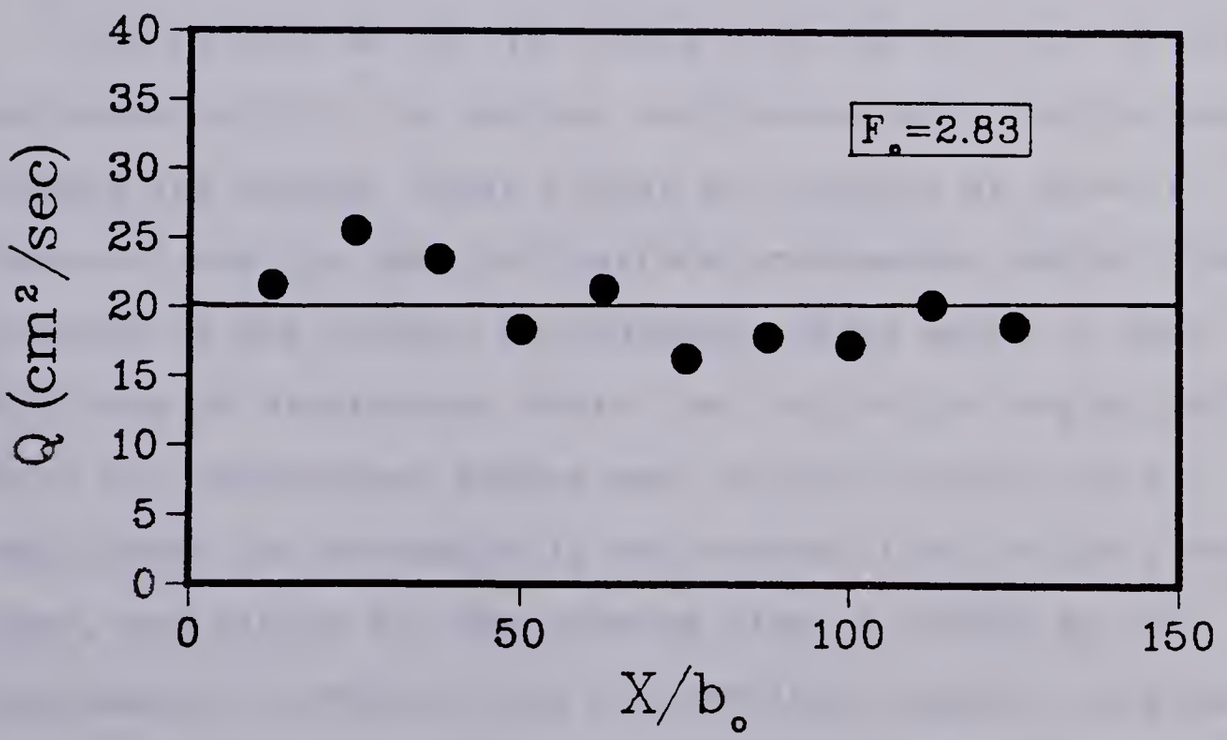

FIGURE 44. The variation of discharge for the run where F_o=2.83

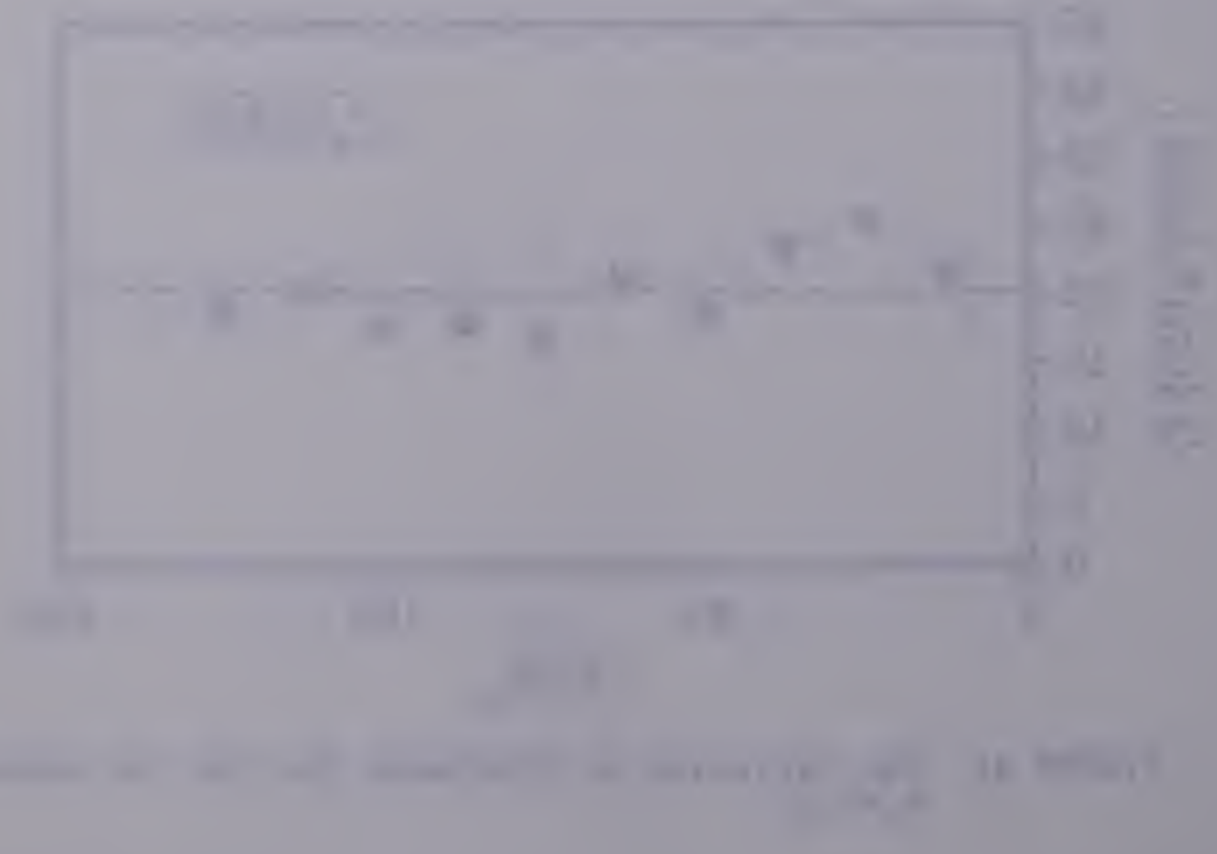

C. INTERNAL HYDRAULIC JUMP ANALYSIS

LOCATION OF THE JUMP

Experimentally determining the location of the internal hydraulic jump for the buoyant jet in shallow water was difficult. It is not possible to locate the jump visually so another method was used. Dye was injected with a syringe carefully into the flow at the interface between the jet and the ambient fluid. Studying the motion of the dye one could determine where the characteristic jump roller begins, and thus where the jump itself begins. However there are several factors which complicate this procedure for the case of the buoyant jet in shallow water.

One is that as the jet turns from the vertical to the horizontal within the surface impingement zone, eddies and rollers are formed. These eddies are located as shown in Figure 45 and are labelled surface impingement eddies. The presence of the surface impingement eddies makes it very difficult to distinguish where the jump roller begins and where the impingement eddies end. Another factor which complicates the procedure is the reverse flow in the lower layer, see Figure 45. The reverse flow is caused by the entrainment of ambient into the vertical buoyant jet-plume region. It is very difficult to distinguish between the reverse flow caused by the entrainment and the reverse flow

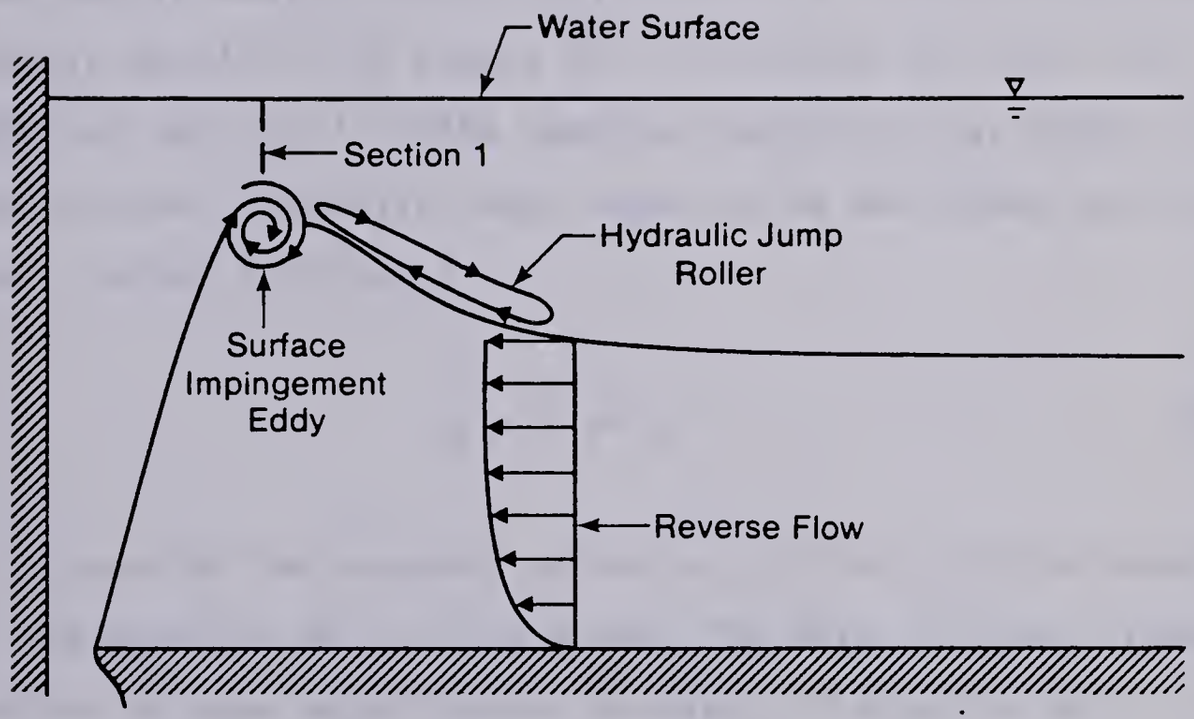

FIGURE 45. Sketch of the surface impingement eddy, internal hydraulic jump and the entrainment reverse flow.

in the roller of the jump.

After studying the motion of the dye injected at the interface for a wide range of F_o it was concluded that the jump always begins immediately after the surface impingement zone at section 1 in Figure 45. It follows then that the depth at section 1 is the upstream supercritical depth for the internal hydraulic jump. Equation 88 developed earlier for y_1 gives this depth.

$$y_1 = 0.20\ H \tag{88}$$

In Figure 46 the measured values of y_1/H are plotted against F_o and equation 88 is also shown. The data conforms closely, subject to some experimental scatter, to equation 88.

CONJUGATE DEPTH ANALYSIS

The Belanger type of equation developed earlier:

$$\frac{y_2}{y_1} = \frac{\sqrt{1 + 8\ \beta\ F_1^{\,2}} - 1}{2} \tag{89}$$

was evaluated for β equal to 1.00, 1.33 and 1.66 and is shown plotted in Figure 47. Also shown is the experimental data from the six complete runs and thirteen supplementary runs. In the ratio y_2/y_1 the value of y_1 was the measured

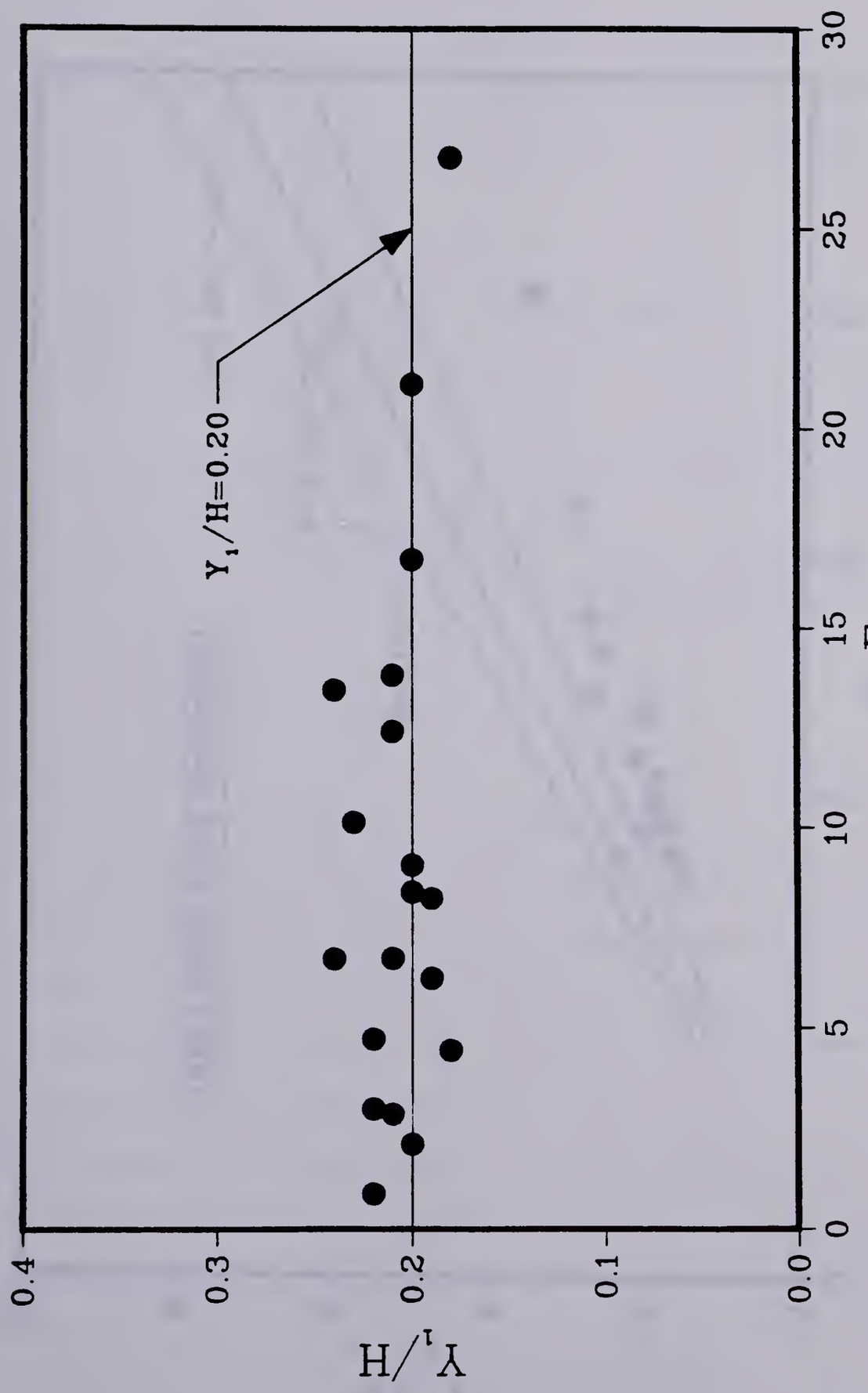

FIGURE 46. The dimensionless impingement height compared to equation 88.

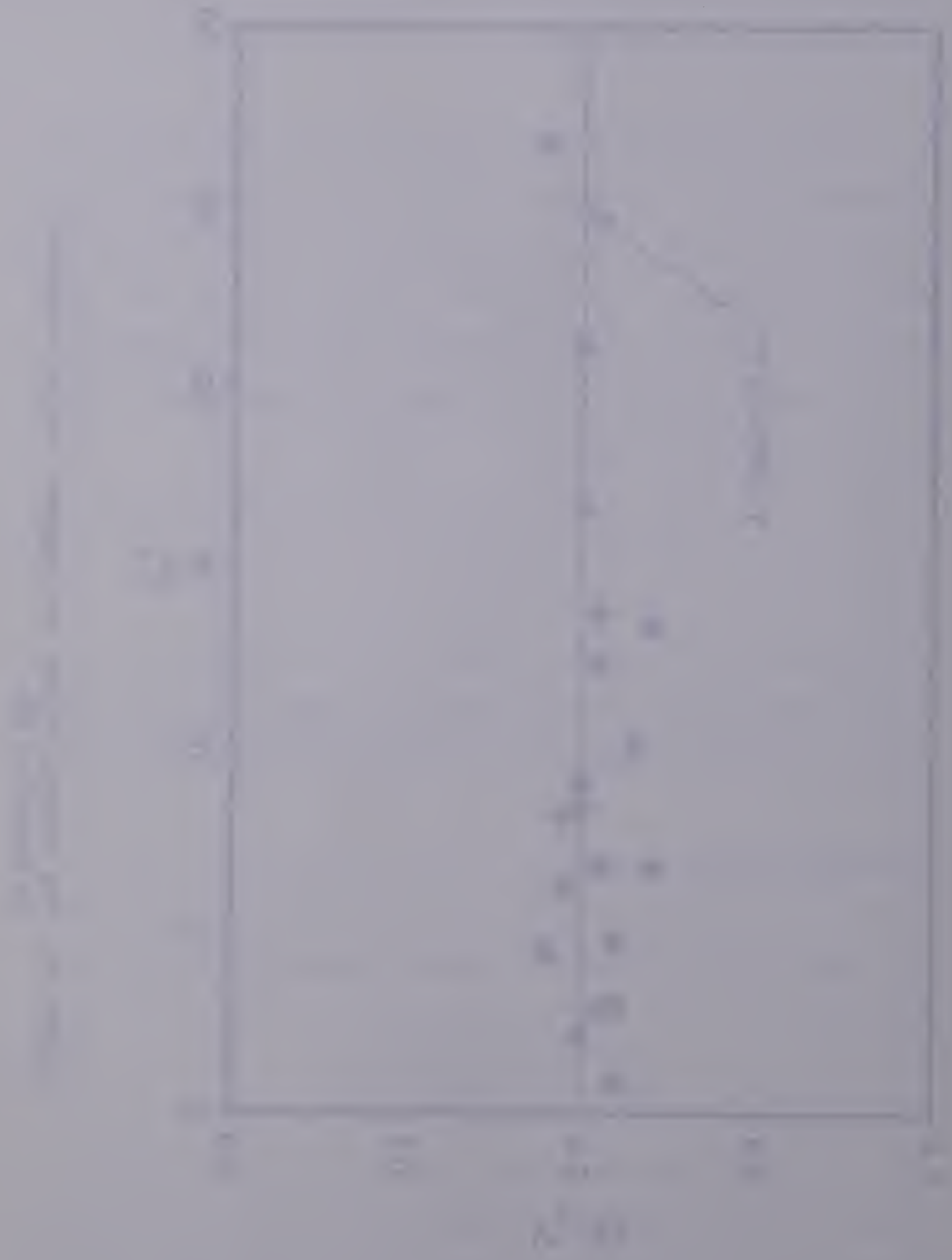

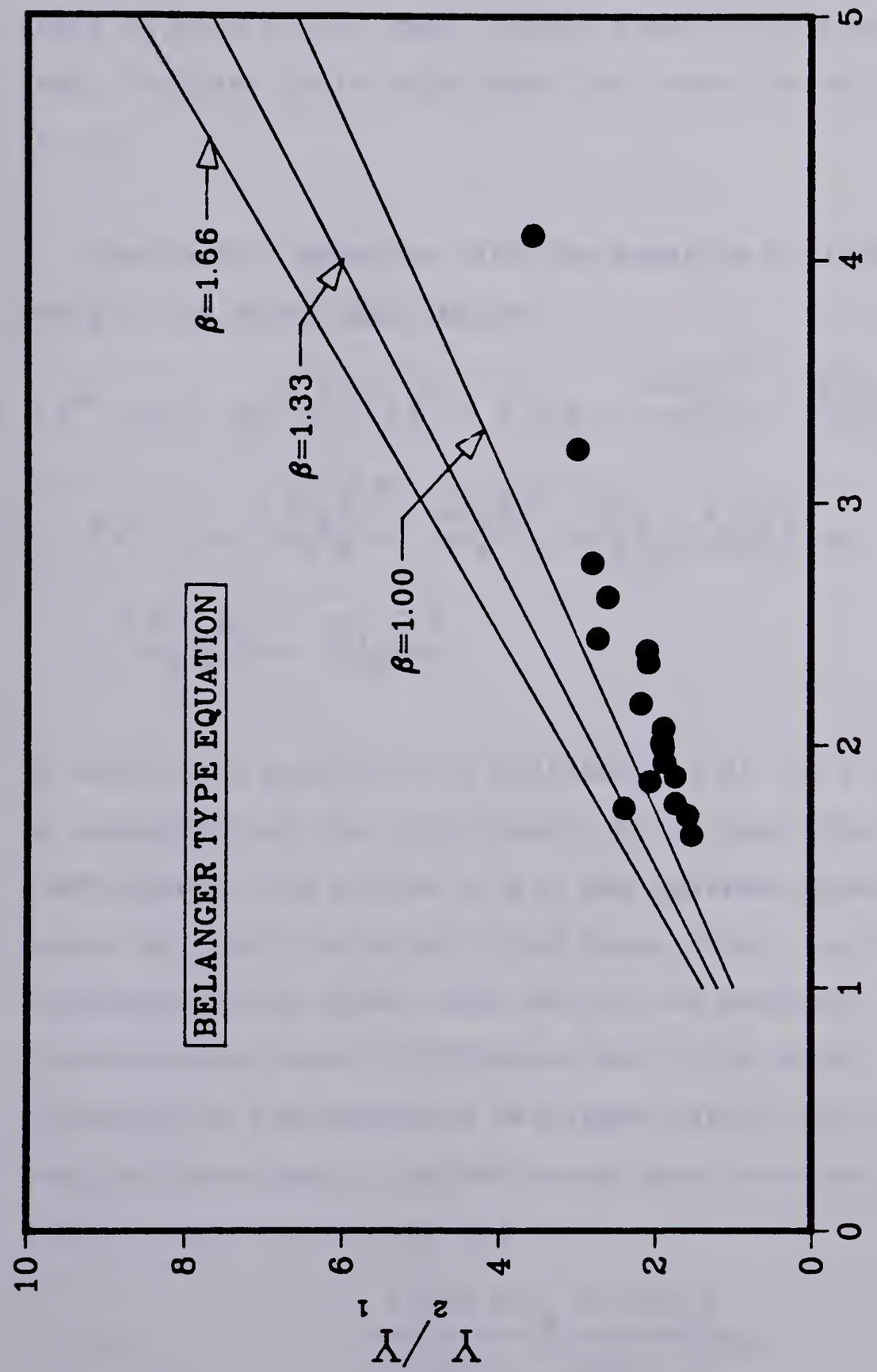

FIGURE 47. Belanger equation plotted for 3 values of β along with the experimental data.

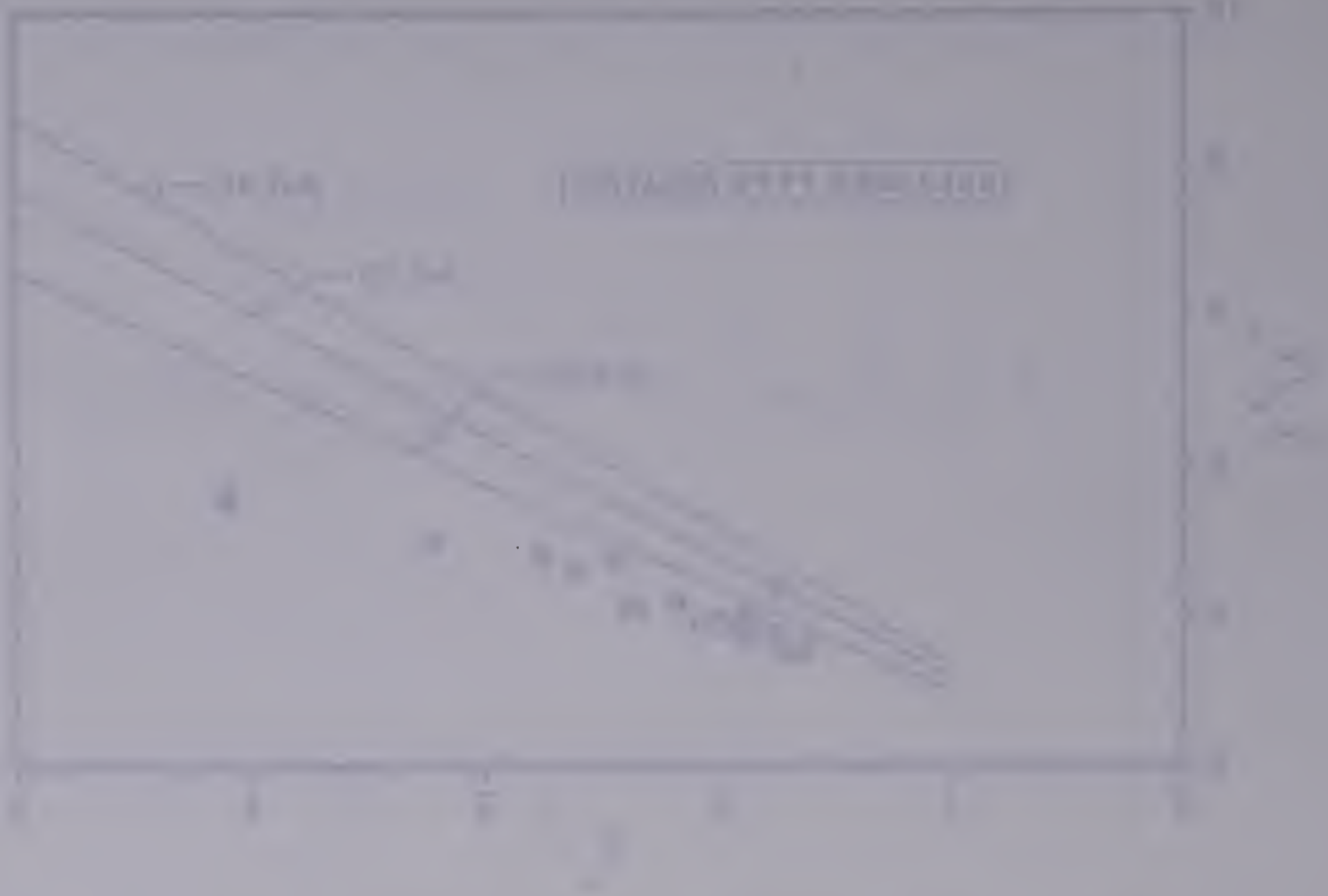

depth at section 1 and the value for y_2 was the greatest depth of flow of the upper layer, measured downstream of the jump. The data falls below even the lowest curve for β equal to 1.0.

Mehrotra's equation with the momentum coefficients β_1 and β_2, is shown again below.

$$0 = \psi^4 - (3 - 2\alpha)\,\psi^3 + \left[\alpha^2 + 2 - 4\alpha + \frac{2\beta_1 \bar{q}_1^{\,2}}{\alpha\, s} - \frac{2\beta_2 \bar{q}_2^{\,2}}{s(1-\alpha)}\right] \psi^2 \qquad (90)$$

$$- \left[\alpha^2 - 2\alpha + \frac{6\beta_1 \bar{q}_1^{\,2}}{s\,\alpha} - \frac{2\beta_1 \bar{q}_1^{\,2}}{s} + \frac{2\beta_2\, r\, \alpha\, \bar{q}_2^{\,2}}{s\,(1-\alpha)}\right] \psi$$

$$+ \frac{4\beta_1\, \bar{q}_1^{\,2}}{s\,\alpha} - \frac{2\beta_1\, \bar{q}_1^{\,2}}{s}$$

To solve this equation the coefficients of the ψ terms must be evaluated and the roots found. To evaluate the coefficients, the values of y_1, the upstream supercritical depth, q_1, the discharge in the lower layer, q_2, the discharge in the upper layer and s, the average dimensionless density difference had to be known. Manipulating the equations developed earlier for the vertical jet-plume , the following equations were derived in order to calculate s, q_2 and q_1.

$$s = \frac{6.763\ \Delta\ \rho_o\ /\ (H/b_o)}{\left[\dfrac{21.18}{F_o^{\,2}} + \dfrac{70.8}{(H/b_o)^{3/2}}\right]^{1/3}} \qquad (91)$$

$$q_2 = 0.0852\ H\ U_o \left[\frac{21.18}{F_o^2} + \frac{70.8}{(H/b_o)^{3/2}}\right]^{1/3} \qquad (92)$$

$$q_1 = q_2 - q_o \qquad (93)$$

y_1 was calculated using equation 88. In the derivation of equation 91 it was assumed that the total density deficiency at section 2 equaled that at section 1. This means that heat loss in the surface impingement zone was neglected. In deriving equation 92 it was assumed that the discharge at section 2 equaled that at section 1, or that entrainment into the surface impingement zone was negligible. Equation 93 is simply an application of the continuity equation.

A computer program using the method of bisection calculated the coefficients and solved for the roots of equation 90. In all cases there was only one root within the physically meaningful range of 0 to 1.0. The equation was solved for β_2, the upper layer momentum coefficient equal to 1.0, 1.33 and 1.66, for β_1, the lower layer momentum coefficient equal to 1.0 and for H/b_o, the submergence ratio equal to 20, 50 and 100. β_1 was assigned the value 1.0 because the velocity distribution in the lower layer was uniform. Figures 48 through 50 show the 3 plots and again the experimental data fall below all of the curves.

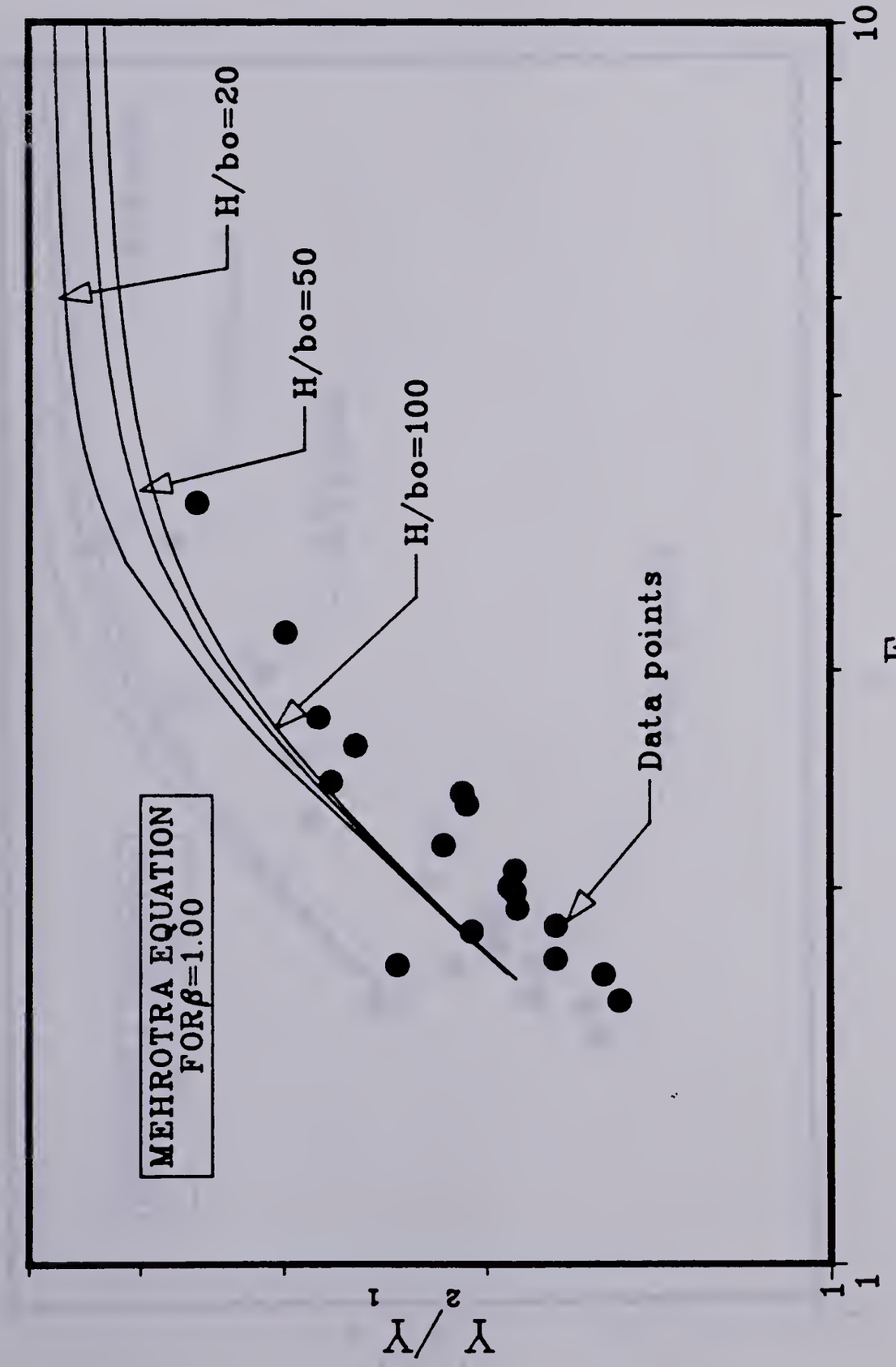

FIGURE 48. Mehrotra's equation with β =1.00 and the experimental data.

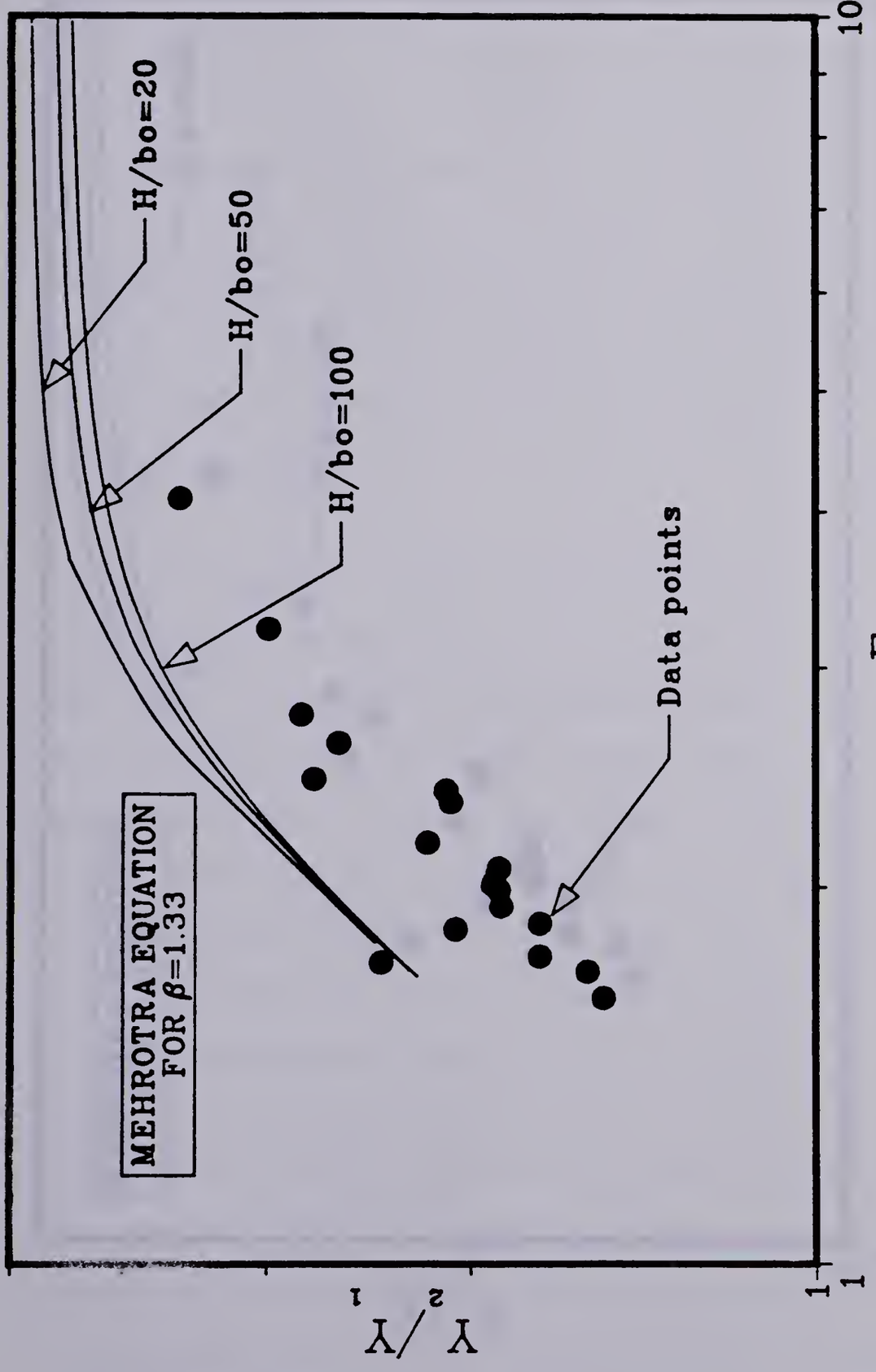

FIGURE 49. Mehrotra's equation with β =1.33 and the experimental data.

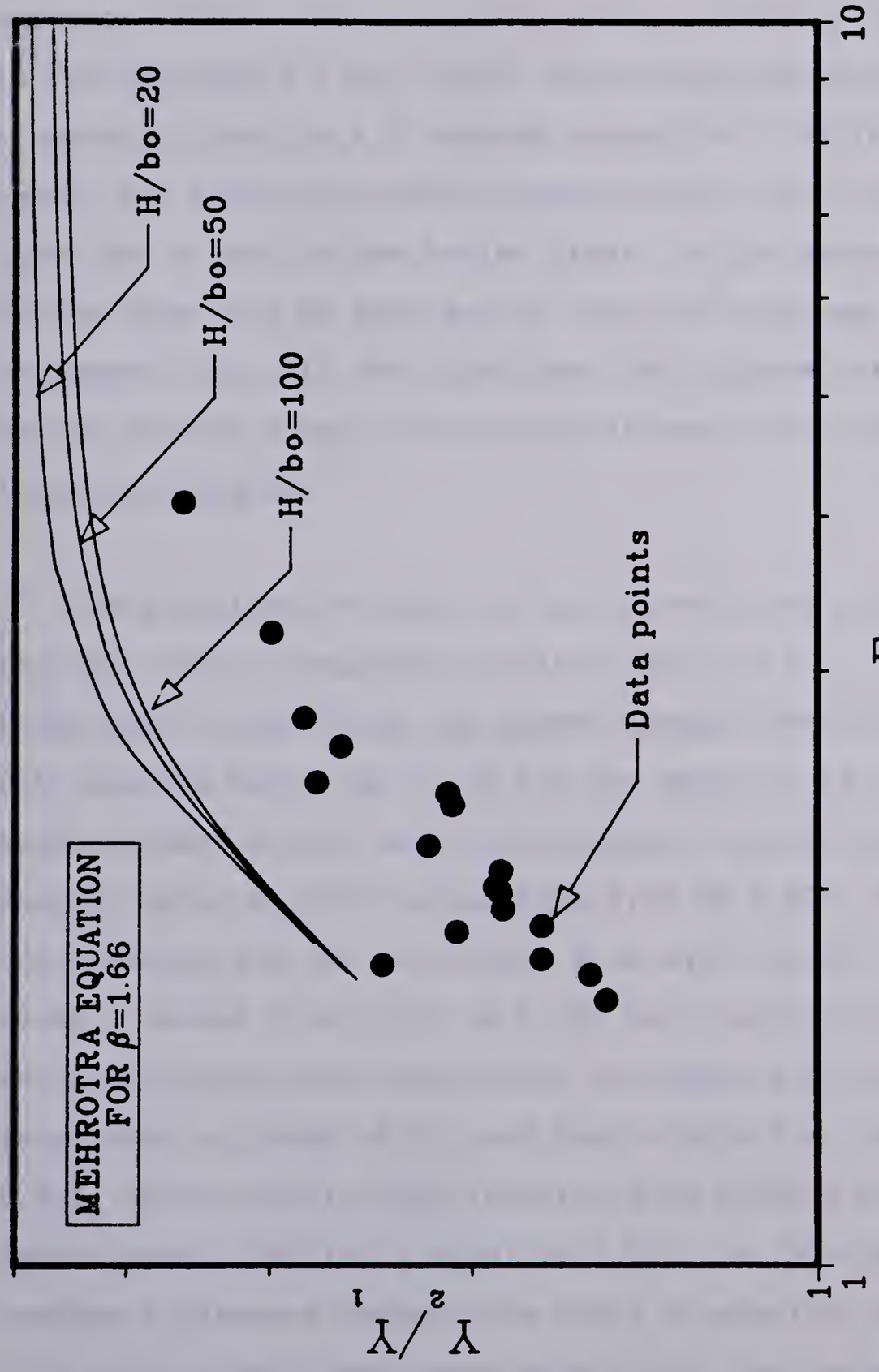

FIGURE 50. Mehrotra's equation with β =1.66 and the experimental data.

There are several explanations as to why the equations and data differ. One explanation can be found by referring to Yih and Guha's (1955) work. They conducted experiments on a hydraulic jump in a 2 layered system for 3 different cases. For the first case the upper layer was at rest and there was a jump in the bottom layer. In the second case the bottom layer was at rest and an inverted jump was formed in the upper layer. In the third case both layers were in motion in such a way that the downstream velocities of both layers were equal.

They plotted the data for all cases along with the Belanger type of equation, equation 89, for β =1.00. They found that in the first and second cases almost all of the data plotted below the curve for the equation as in this study. However their data was dispersed according to the density ratio r which varied from 0.78 to 0.975. As r increased so did the deviations from equation 66. In this study r varied from 0.993 to 0.998 and therefore the deviations from the theory would be expected to be of the same order as those of Yih and Guha's data for r equal to 0.975. Their data for the inverted jump differs by approximately 25% for r equal to 0.975. In this study the average difference between the curve of equation 66 for β =1.0 and the data was approximately 20%. The deviations are of the same order. For the third case in Yih and Guha's

study the data corresponded closely to the theory.

Yih and Guha claim that the neglect of the interfacial shear is responsible for the differences. In the first and second cases there was violent interfacial mixing and thus high interfacial shear, and therefore large differences between the theory and the data. For the third case the interfacial shear and mixing were negligible because the layers were co-flowing. Therefore the theory and data matched closely.

In the present study the two layers are flowing in opposite directions and therefore one would expect the interfacial shear to be high. The interfacial shear was neglected in the development of both equations 89 and 90 and the evidence of this oversimplification can be seen in Figures 47 through 50. The data all falls below the curves for both equations.

Another explanation for the discrepancies between the theory and the experimental data is that the jump does not occur where it was assumed to occur. As explained earlier , it was assumed that the supercritical upstream depth y_1 was found to occur at section 1. If the jump actually occurs further downstream, then the data would correspond more closely to the theory. This is because F_1 is proportional to

$y_1^{-3/2}$ and y_2/y_1 is proportional to y_1^{-1} . If the jump occurred further downstream, the ratio y_2/y_1 would decrease in proportion to y_1^{-1} and F_1 would decrease in proportion to $y_1^{-3/2}$. The data points would move down and to the left in Figures 47 through 50, more in line with the computed curves.

There is another explanation as to why the theory so consistently overestimates the ratio of the conjugate depths. No temperature data other than T_o and T_a was gathered in this study. As well, no velocity data was collected for the thirteen supplementary runs. The ramification of this is that the values for F_1 could not be obtained by using measured values. The equations developed for the plane vertical jet-plume had to be relied on to predict the density, at section 1 for all the runs and to predict the velocity for the thirteen supplementary runs. In order to be consistent the equations were also used to predict the velocity at section 1 for the six complete runs even though velocity data was available. Thus the data points shown on the conjugate depth versus F_1 plots are only quasi-experimental points. Some of the error in the data may then be due to approximations in the jet-plume equations.

V. CONCLUSIONS AND RECOMMENDATIONS

A. CONCLUSIONS

This study was an experimental and theoretical investigation of a plane jet-plume in shallow water. It was thought that since previous investigators had concentrated so heavily on the temperature field and the engineering aspects that a greater contribution could be made by using a more fundamental approach. For this reason the experimental work concentrated on the velocity field. The complete set of velocity profiles gathered in this study should contribute significantly towards the understanding of the physics of the problem.

It was demonstrated that the velocity profiles in the horizontal region of flow are only weakly similar and that the dimensionless velocity profiles contained considerable scatter. Some of this scatter was due to inaccuracies in the hydrogen bubble method of velocity measurement. Pande (1975) carried out an extensive analysis on the accuracy of hydrogen bubble velocity measurements and determined that the total uncertainty was approximately 7%. Therefore there must be another explanation as to why the velocity profiles are not strongly similar.

Near the surface impingement zone, following the turning of the jet-plume, the velocity profiles are jet-like and exponential in form. Within the stratified counterflow region far downstream the velocity profiles are uniform. Therefore there must be a transition from the jet-like exponential velocity profiles to a uniform profile as x increases downstream. Clearly then the profiles will not be similar if profiles from too far downstream are included. Some of the scatter in the dimensionless velocity profiles could then be attributed to this transition from exponential to uniform.

The similarity of velocity profiles is a critical assumption if integral analysis is to be used. Without the assumption of similar velocity and temperature profiles the governing equations will not reduce to a solvable form. This study has shown that because of the weak similarity of the velocity profiles in the horizontal region of flow, integral analysis may be applied. However the results obtained from such an analysis should be used only within the near-field and should be viewed as an engineering approximation only.

Determining the height y_1 of the spreading layer beyond the surface impingement region is important. This height provides the coupling between the surface impingement region and the internal hydraulic jump region. The equation

developed in this study for y_1 is based on sound principles and provides an extremely easy method of obtaining this height. The comparison with the experimental data was good and therefore it is believed that this equation is accurate within the ranges of F_o and H/b_o covered in this investigation.

The growth rate of b, the velocity half width, was compared to that of a plane non-buoyant surface jet. It was found that b for the jet-plume in shallow water increased at a slower rate than for the plane non-buoyant surface jet. The variation of the velocity scale u_m was also compared to the plane non-buoyant surface jet. When u_m was non-dimensionalized by u_{mo}, the maximum velocity at x=10cm, the data were closely grouped. It was found that the dimensionless velocity scale decreased at half the rate as that of the plane non-buoyant surface jet.

The analysis performed on the internal hydraulic jump region demonstrated clearly that the present approaches to this problem are inadequate. The predicted conjugate depths did not agree closely with the experimental results. The neglect of the interfacial shear stresses was the source of some of the error between the theory and the data. The difficulty in locating the start of the internal hydraulic jump is also presented as a possible source of error. The

calculation of F_1 involved relying on the jet-plume theory to predict the density at section 1. This also introduced error into the analysis.

B. RECOMMENDATIONS FOR FURTHER RESEARCH

The behavior of a vertical jet-plume in shallow water should continue to be investigated. A study similar to Kotsovinos'study on plane jet-plumes would provide the solid experimental data required for the complete understanding of the problem. The velocity field would need to be studied in detail with a laser and the temperature field with a system of thermistors. A tank of sufficient dimensions to allow investigation of the far-field as well as the near-field would be required.

Further investigation of the internal hydraulic jump is recommended. The confusion over entrainment into internal hydraulic jumps has been cleared up by Rajaratnam and Subramanyan (1984) but other problems remain unsolved. For example, the importance of the interfacial shear in the calculation of the conjugate depths is still unknown. The effect of various downstream controls on the size and location of the jump also needs to be studied.

A study to examine the depth of the spreading layer y_1 is also recommended. The depth should be measured over a wide range of F_o and H/b_o for plane and round discharges in order to establish conclusively the relationship between y_1, F_o and H/b_o.

Research on the subject of the far-field boundary conditions for surface layers is also recommended. The magnitude and role of the surface heat exchange in determining the far field boundary conditions should be studied. The effect of different far-field geometries on the spreading of the surface layer should be investigated. A check on the validity of data gathered in studies where the far field boundary condition was modelled by a critical control section, as in this study, should be carried out.

I. REFERENCES

Albertson, M.L., Dai, Y.B., Jensen, R.A. and Rouse, H., ' Diffusion of Submerged Jets', Transactions, A.S.C.E., Vol. 115, 1950.

Beltaos, S., 'Normal Impingement of Plane Turbulent Jets on Smooth Walls', M.Sc. Thesis, Department of Civil Engineering, University of Alberta, Edmonton, Canada, 1972.

Chu, V.H. and Vanvari, M.R., 'Experimental Study of Turbulent Stratified Shearing Flow', A.S.C.E., Journal of the Hydraulics Division, Vol. 102, 1976.

Henderson, F.M., 'Open Channel Flow', MacMillan Publishing Co., Inc., New York, 1966.

Jirka, G.H. and Harleman, D.R.F., 'Stability and Mixing of a Vertical Plane Buoyant Jet in Confined Depth', Journal of Fluid Mechanics, Vol. 94, 1979.

Kotsovinos, N.E., 'A Study of the Entrainment and Turbulence in a Plane Buoyant Jet', W.M. Keck Laboratory of Hydraulics and Water Resources, Report No. KH-R-32, California Institute of Technology, Pasadena,

California, 1975.

Lee, J.H.W. and Jirka, G.H., 'Vertical Round Buoyant Jet in Shallow Water', A.S.C.E., Journal of the Hydraulics Division, Dec. 1981.

Mehrotra, S.C. and Kelly, R.E., 'On the Question of Non-uniqueness of Internal Hydraulic Jumps and Drops in a Two-fluid System', International Symposium on Stratified Flows, Novosibirsk.

Mehrotra, S.C., 'Limitations on the Existence of Shock Solutions in a Two-fluid System', Tellus, Vol. XXV, 1973.

Morton, B.R., Taylor, G.I. and Turner, J.S., ' Turbulent Gravitational Convection from Maintained and Instantaneous Sources', Proceedings of the Royal Society of London, Series A, Vol. 234, 1956.

Pande, B.B. Lal, 'A Theoretical and Experimental Study of Heated Surface Discharges Into Quiescent Ambients', Ph.D. Thesis, Department of Civil Engineering, University of Alberta, Edmonton, Canada, 1975.

Pryputniewicz, R.J. and Bowley, W.W., 'An Experimental Study of Vertical Buoyant Jets Discharged Into Water of Finite

Depth', A.S.M.E., Journal of Heat Transfer, No. 75-HT-RR, 1975.

Rajaratnam, N., 'Turbulent Jets', Developments in Water Science 5, Elsevier Publishing Co., 1976.

Rajaratnam, N. and Subramanyan, S., 'An Experimental Study of Plane Turbulent Buoyant Surface Jets and Jumps', Water Resources Engineering Report 83-3, Department of Civil Engineering, University of Alberta, Edmonton, Canada, 1983.

Rajaratnam, N. and Humphries, J.A., 'Turbulent Non-buoyant Surface Jets', Journal of Hydraulic Research, Vol. 22, 1984.

Roberson, J.A. and Crowe, C.T., 'Engineering Fluid Mechanics', Houghton Mifflin Company, Boston, 1980.

Rouse, H., Yih, C.S . and Humphreys, H.W., ' Gravitational Convection From a Boundary Source', Tellus, Vol. 4, 1952.

Sarma, K.V.N., Lakshminarayana, P. and Lakshmana, R., 'Velocity Distribution in Smooth Rectangular Channels ', A.S.C.E., Journal of the Hydraulics Division, Feb. 1983.

Schijf, J.B. and Schonfeld, J.C., 'Theoretical Considerations on the Motion of Salt and Freshwater', Proceedings of the Minnesota International Hydraulics Convention, I.A.H.R. and A.S.C.E., 1953.

Streeter, V.L., 'Handbook of Fluid Dynamics', McGraw-Hill Book Company, Inc., New York, 1961.

Yih, C.S. and Guha, C.R., 'Hydraulic Jump in a Fluid System of Two Layers', Tellus, Vol. 7, 1955.